Characterizing, modeling, and predicting the external ground reaction forces of legged movement

by

Paweł Kudzia

M.A.Sc., Queen's University, 2015

B.Eng., Queen's University, 2013

Thesis Submitted in Partial Fulfillment of the
Requirements for the Degree of
Doctor of Philosophy

in the
School of Engineering Science
Faculty of Applied Sciences

SIMON FRASER UNIVERSITY

Fall 2023

Declaration of Committee

Name:	**Paweł Kudzia**
Degree:	**Doctor of Philosophy (Engineering Science)**
Title:	**Characterizing, modeling, and predicting the external ground reaction forces of legged movement**
Committee:	**Chair:** **Edward Jung Wook Park** Professor, Mechatronic Systems Engineering
	Max Donelan Supervisor Professor, Biomedical Physiology and Kinesiology
	Ivan Bajic Committee Member Professor, Engineering Science
	James Wakeling Committee Member Professor, Biomedical Physiology and Kinesiology
	Steve Robinovich Committee Member Professor, Biomedical Physiology and Kinesiology
	Carolyn Sparrey Examiner Associate Professor, Mechatronic Systems Engineering
	Amy Wu External Examiner Assistant Professor, Mechanical and Materials Engineering Queen's University

Ethics Statement

The author, whose name appears on the title page of this work, has obtained, for the research described in this work, either:

a. human research ethics approval from the Simon Fraser University Office of Research Ethics

or

b. advance approval of the animal care protocol from the University Animal Care Committee of Simon Fraser University

or has conducted the research

c. as a co-investigator, collaborator, or research assistant in a research project approved in advance.

A copy of the approval letter has been filed with the Theses Office of the University Library at the time of submission of this thesis or project.

The original application for approval and letter of approval are filed with the relevant offices. Inquiries may be directed to those authorities.

Simon Fraser University Library
Burnaby, British Columbia, Canada

Update Spring 2016

Abstract

In this thesis, I explore legged agility with a primary focus on controlling external ground reaction forces produced by our legs. I conduct empirical studies and develop models to understand how we control external forces and develop innovative means to measure them. My research consists of four aims, each contributing to our understanding of human performance and driving potential advancements in sports, robotics, and rehabilitative technologies. In Aim 1, I characterize the control of leg external forces (n=14). To achieve this, I construct a mechanical system and a real-time visual feedback system to capture force magnitudes and positions exerted by my leg. Using system identification, I gain insights into the control of leg external forces across different magnitudes and positions. In Aim 2, I examine the effects of neuromuscular fatigue on our nervous system's capacity to control leg external forces (n=18). I hypothesize that heightened fatigue results in a decrease in both the responsiveness and accuracy of leg force control. My results reveal a significant reduction in mean maximum force production, leading to a substantial decline in my leg force control responsiveness. These findings enhance our understanding of how fatigue influences agility and may guide strategies to sustain performance in the presence of fatigue. In Aim 3, I set out to understand the limit of vertical jumping by studying the external forces generated during jumping (n=10). I develop physics-based models of varying complexity to predict external forces during vertical jumps and identify the simplest model that accurately predicts human-like forces. This model, capable of simulating jumps from different depths, highlights the significance of force-velocity properties and maximal force as limiting factors for jump height. In Aim 4, I develop a novel approach to estimate the external forces generated by each leg during vertical jumps. Using a transformer-based neural network and video data (n=30), I demonstrate that the model accurately predicts each leg's external forces, offering a new tool for measuring jump height and forces from video. My work aims to make biomechanical analysis accessible, a task typically confined to laboratory settings. In summary, this thesis investigates the control of leg external forces, the effects of fatigue, and the development of predictive models. It underscores the potential of machine learning in biomechanical analysis, contributing to a broader understanding of human performance and paving the way for new technological advancements

Keywords: legged agility; ground reaction forces; neuromuscular fatigue; vertical jumping; pose estimation; mathematical modeling; biomechanics

To my parents,

Wanda and Andy

Dziękuję za wszystko.

Acknowledgements

Completing this Ph.D. has been a remarkable adventure, intertwined with various life events, personal challenges, and even a global pandemic. Despite the turmoil, I found comfort and inspiration in embracing nature, logging countless kilometers running in the mountains in Squamish, ski mountaineering, and biking across the province twice. Through these activities, I created cherished memories with the people around me. Enabling the Ph.D. As I reflect on the research outputs I present here, I experience a sense of accomplishment in seeing my work culminate into a final product. Based on my research, the road ahead is full of further exploration and development opportunities.

I want to extend my thanks to my supervisor, Dr. Max Donelan. Max, your guidance has been critical throughout this journey. The time and effort you invested into my projects and my growth as a researcher have not gone unnoticed. You have demonstrated a balance of passion and fun while managing many responsibilities, setting an example for me as I move forward into the big world. You emphasized the need for asking questions and delivering them effectively. Above all, you've highlighted the importance of continual learning and maintaining relationships with colleagues, friends, and family.

I am deeply grateful to my friends, my pillars of support through the highs and lows of my Ph.D. journey and beyond. Your unwavering support has been invaluable, whether accompanying me on cycling routes, ski slopes, running trails, exploratory adventures, or engaging in thoughtful phone calls (T.S.). To James, Jon, Erin, Taylor, Josh, Anna, and Silian, among others, your camaraderie has been my anchor and inspiration. Even though the chapter of my Ph.D. has concluded, our shared adventures will continue to be woven into the ongoing narrative of life. Life's journey, an endless voyage, is made richer by the companionship of friends like you. Standing as the best man at your wedding, Jon, and being the witness at your wedding Elizabeth, are memories that profoundly enriched my journey.

I deeply thank Dr. Andy Hoffer for embracing me into his team and offering me countless opportunities. His work ethic and tenacity will forever serve as an inspiration to me. I owe a debt of gratitude to Dr. Lou Awad, my mentor and friend. You opened doors for me, leading me to places I never imagined. Your kindness and patience consistently inspire me. To my committee members, I thank you for your time, energy, and commitment throughout this journey. James, Steve, and Ivan, you have each taught me invaluable lessons and provided a beacon of hope during challenging times. Thank you to all my lab mates, past and present. Travelling together and hanging in/out of the office was so fun. Thank you, Dr. Sina Mehdizadeh, for your patience, feedback, and good laughs.

A special nod of appreciation goes to the volunteers who graciously participated in my experiments. Your contribution forms the bedrock of this research, and without you, it simply wouldn't have been possible. Thank you, Anna (and Maisy), for your patience and understanding as I navigated the final stages of this thesis. The process was grueling, filled with long hours of me at my desk, moments of frustration, and for sure, some grumpiness. Yet, through it all, you stood by me, bearing the brunt of the pressures. I can't express enough my gratitude for your unwavering support.

In the words of Christopher McCandless, "*I now walk into the wild*," ready to embark on the next chapter of life's journey.

Table of Contents

List of Tables

List of Figures

List of Acronyms

m	body mass (normalized by body weights)
H	jump height.
g	gravitational acceleration
Y_{opt}	optimal contractile element length of the muscle
y_{ground}	distance extended pushing against the ground
w	contractile element force-length width of the muscle
v_{to}	take-off velocity.
v_{peak}	peak vertical velocity of center of mass
V_{max}	maximum contractile element shortening velocity of the muscle
t_{to}	take-off time
F_{vGRF}	vertical ground reaction force
F_{max}	maximum contractile element force of the muscle
v_i	initial velocity
L_{slack}	series elastic element slack length of the muscle
K_s	series elastic element stiffness of the muscle

Published Studies

Research contained in this thesis has been published, or is in revision, in the following peer-reviewed journals:

Chapter 2

P. Kudzia, S. N. Robinovich, and J. M. Donelan, “Characterizing the performance of human leg external force control,” Sci. Rep., vol. 12, no. 1, p. 4935, Mar. 2022.

https://doi.org/10.1038/s41598-022-08755-3

Chapter 3

P. Kudzia, J. M. Wakeling, S. N. Robinovitch, and J. Maxwell Donelan, “Neuromuscular fatigue reduces responsiveness when controlling leg external forces,” bioRxiv, p. 2023.05.24.541485, May 25, 2023. doi: 10.1101/2023.05.24.541485.

https://www.biorxiv.org/content/10.1101/2023.05.24.541485v1

Chapter 1.

Introduction

1.1. Agility

Our bipedal capabilities are remarkable. The ability to execute a jump, maneuver a swift pivot, or tackle an obstacle displays the intricacy of our movement. We thrive in diverse environments like bustling city sidewalks and rugged mountain trails. This versatility is a testament to our evolution as a species and the biomechanics and neurophysiology that underpin our movement.

The Oxford Dictionary defines agility as the ability to “move quickly and easily” but leaves ‘quickly’ and ‘easily’ undefined [1]. Sports scientists define agility as the ‘ability to change direction rapidly,’ a definition criticized for omitting crucial aspects of agile performance [2]. Such elements include swift motor control in response to stimuli, cognitive abilities like visual scanning and decision-making, physical strength and conditioning, and biomechanical skills necessary for quick changes in direction across various terrains [2]–[4]. A more comprehensive definition may be: “a rapid whole-body movement with change of velocity or direction in response to a stimulus” [2]. In this thesis, I frame agility as swift, controlled, and deliberate redirection or reorientation of the body in response to an environmental trigger.

Agility is integral to movement-based excellence. It forms a key aspect of numerous athletic events and team sports, including badminton, squash, basketball, soccer, and rugby. Players demonstrate rapid footwork and abrupt directional changes in these contexts while maintaining balance on the court or field [5]. Coaches often assess an athlete’s agility using specific movement tasks, such as the Four Corners, Hexagon, and 5-0-5 Agility Test [6]. These tasks demand quick, accurate navigation around lines or pylons. Speedier completion signals higher agility [5]. Athletes are also judged on their sprint speed on a track [7], jumping ability [4], and time-constrained navigation of obstacle courses [8]. These assessments hint at an individual’s agility.

Excelling in sprinting, high jumping, and quick direction changes requires our legs to generate controlled external ground reaction forces within a specified time frame. Our

nervous system must control leg external forces under environmental and physiological factors, including fatigue. Specifically, our nervous system must control the external forces' magnitude and positions. This control of external forces is a critical component of agility, illustrating the vital role of forces in physical performance.

The li'its of our nervous systems' control of leg external forces (Aim 1) and the changes in control when our muscles become fatigued (Aim 2) are questions I explore in this thesis. Another aspect of my research is studying what restricts our ability to generate larger magnitude external forces in constrained time frames when jumping (Aim 3). Finally, developing new technologies that leverage machine learning to estimate external forces (Aim 4) is my final avenue of investigation.

This thesis begins a journey where I explore the subtle interplay of forces and control that underpin our visible agility. In the process, I develop mathematical models and novel machine-learning tools that enable an intimate exploration of kinetics. As I unveil the mechanisms that transform our bodies into skillful performers, I aim to provide insights into the extraordinary capabilities of the human body and showcase technologies that can help us measure movement and improve our lives. By studying leg external force control, my research strives to contribute to the broader understanding of human performance and pave the way for advancements in sports, robotics, and rehabilitative technologies.

1.2. Leg external ground reaction forces

Our legs often play the role of a primary interface with the ground in our engagement with the environment, generating external forces that dictate our movements. The forces that our feet apply to the ground are reciprocated back, pushing against our bodies and propelling our center of mass (Figure 1-1) [9]. Control of this reciprocating external force is vital in agility-demanding activities such as high jumps [10], fast running [11], or quick alterations in movement direction [12]. These external forces are vector quantities, requiring meticulous control for agile performance. Throughout this thesis, I will use the term 'force-magnitude' to refer to the control of the magnitude of the vertical external ground reaction force and 'force-position' to denote the location where this force is applied to the ground via the foot contact point or center of pressure. Generating a larger vertical force magnitude within a specific timeframe can augment performance in certain movement activities. Concurrently, a rapid shift in force position can modify the resultant

external force vector acting on our bodies, facilitating longer jumps [13] or faster body reorientations in gymnastic maneuvers [14].

Effective control of both force magnitude and force position is critical to agile performance [15]. Our nervous system controls muscle forces, which, in turn, controls the resultant external force vector under our legs. However, before the nervous system comes into play, our body's inherent mechanical properties, or preflexes, provide an initial response to changes in force or position [16]. These preflexes, found in our muscles and tendons, react within a few milliseconds, an order of magnitude faster than neural reflexes, serving as our body's first line of control against unexpected changes [17]. While preflexes are faster than the reflexes controlled by our nervous system, they are less adaptable, responding in a fixed way based on the physical properties of the muscle or tendon. In contrast, reflexes can be adjusted based on the specific situation or task.

The crucial role in governing the external forces generated by our legs falls to our nervous system, working in tandem with preflexes. This collaboration operates through an intricate network of sensors and feedback mechanisms that align our limb positions and manage the forces our muscles generate. How our body interacts with its environment is informed by exteroception, our sensitivity to external stimuli, and proprioception, our self-awareness of body and joint movements and positions. Combined with the swift response of preflexes and the adaptable nature of reflexes, this understanding empowers our nervous system to form suitable forces for various movements [16]. Acting as our body's central controller, the nervous system collaborates with preflexes to guarantee quick and effective responses, significantly enhancing agility [18].

In any leg configuration, the muscles and the resultant joint torques in our legs control the external forces generated on the ground [19]. When our muscles contract and generate force, the force acting on a moment arm results in a joint torque. When our foot makes contact with the ground, this gives rise to external force vectors at the point of contact with our foot and the ground. For instance, in a static posture like standing upright, our feet exert force against the ground to maintain balance, with the external force vector manipulated to help support this equilibrium [20], [21]. To enable dynamic movement, the nervous system uses feedback mechanisms to generate suitable muscle forces and joint torques with appropriate external forces to allow desired movements.

Feedback serves as a crucial component of the central and peripheral nervous system. Sensory signals originate from muscle spindles and force sensing from Golgi tendon organs [22], [23]. Activated during muscle contraction or passive stretching, these sensory receptors, including muscle spindles and Golgi tendon organs, transmit feedback signals via spinal mono-and polysynaptic pathways. This process modulates the commanded neural activity and the mechanical output of the muscle, such as force, stiffness, impedance, and work [24]. One can perceive this control process as a closed-loop control system [25]–[27]. However, inherent delays in the sensorimotor control system may limit the speed at which an individual can sense and respond to a stimulus, potentially curtailing the speed and accuracy of leg external force control.

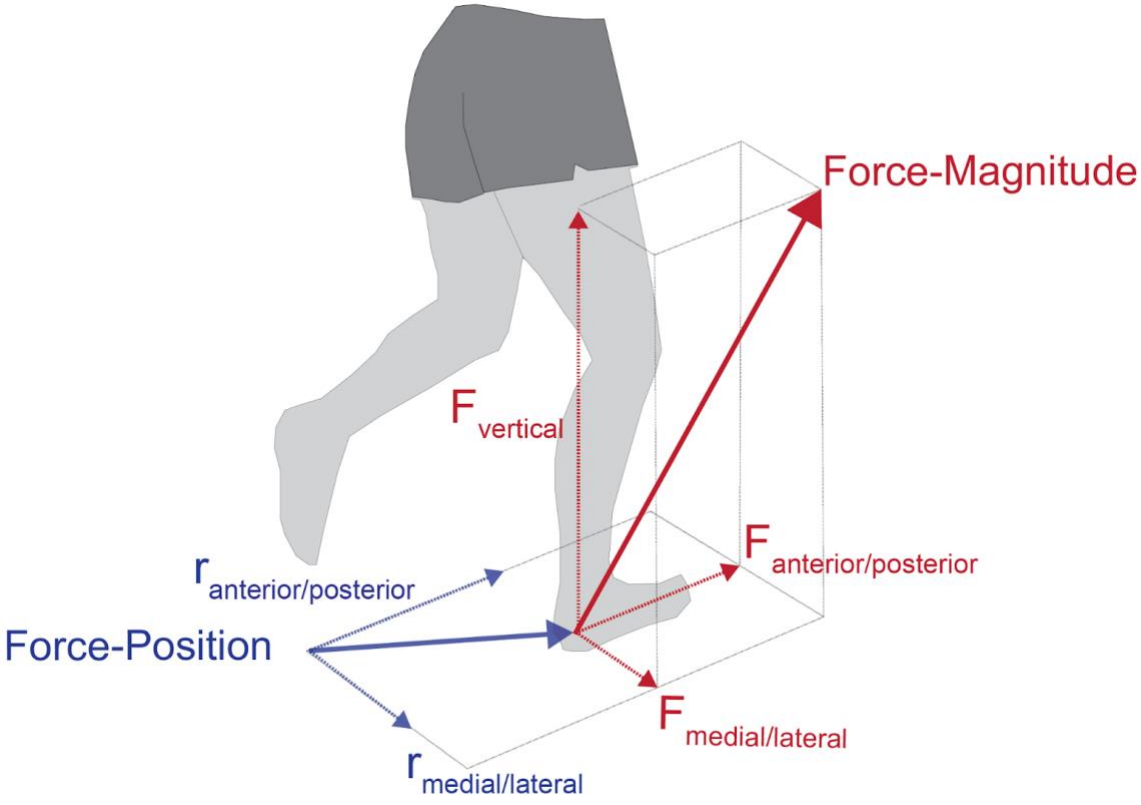

Figure 1-1. Illustration of the external ground reaction force vector and its components. The diagram highlights three orthogonal force magnitudes moving in vertical, anterior/posterior, and medial/lateral directions, complemented by two perpendicular force positions oriented in anterior/posterior and medial/lateral axes.

1.3. Limits to agility imposed by our motor control system

Information transmission in nerves and muscles is slow, limited by a maximum conduction velocity [28]. For instance, when you push your foot against the ground, the cutaneous afferents from the leg provide exteroceptive information about the onset of stimuli, such as ground pressure. This triggers a feedback response from the sensorimotor system (Figure 1-2). The minimum time required to generate peak muscle force at the ankle between the stimulus and response is around 120ms, equivalent to when your foot is in contact with the ground while sprinting [9]. The conduction velocity in muscle fibres depends on several factors, such as the diameter of the fibre, the temperature, and the type of muscle (fast twitch or slow twitch). On average, the conduction velocity in human skeletal muscle fibres ranges from about 3 to 5 meters per second. However, in larger motor neurons that innervate muscles, the conduction velocity can be much faster, up to 70-120 m/s, due to myelination, which speeds up the conduction of the electrical signals along the neuron. [29], [30]

Sensorimotor delays can significantly impact the control of leg external forces. In a muscle, the response time between the onset of a stimulus and the peak muscle force is known as the total delay, which comprises several component delays. These component delays include sensing delay, nerve conduction delay, synaptic delay, neuromuscular junction delay, electromechanical delay, and muscle force generation delay [31], [32].

The sensing delay, the first component delay, is the time from the onset of the stimulus to the generation of an action potential in a sensory receptor at the foot. The action potential is transmitted along the sensory and motor nerve fibres, known as the nerve conduction delay, which is proportional to the signal's travel distance [31]. The signal then transfers from the sensory nerve fibre to the motor nerve fibre at the synapse in the spinal cord, referred to as the synaptic delay. From the motor nerve fibre, the signal transfers to the muscle fibre at the neuromuscular junction in the muscle, known as the neuromuscular junction delay. Upon reaching the muscle, the time taken for the action potential to be conducted along muscle fibres and to activate molecular mechanisms involved in cross-bridge formation is called the electromechanical delay. Once the muscle begins to contract, a force generation delay is associated with the time to peak force. Muscle force generation delay can be attributed to several factors. This includes the time it takes for the action potential (nerve signal) to propagate along the motor neurons, the time it takes for

calcium ions to be released and bind to the contractile proteins within the muscle fibres, and the time it takes for the cross-bridges between actin and myosin filaments to form and generate force [31]–[33].

Component delays play a crucial role in constraining the speed of muscle force generation, while intrinsic muscle properties can constrain the magnitude of force produced. The primary function of a muscle is to generate force, serving as an actuator. Ideally, an actuator should be capable of producing variable force magnitudes and seamlessly transitioning between different force levels, irrespective of its state. However, muscles deviate from this ideal scenario as they possess intrinsic properties that, alongside sensorimotor delays, introduce and limit the instantaneous generation of force, depending on the muscle's state. These intrinsic properties include the force dependency of the muscle on properties such as excitation and kinematic variables like muscle velocity and length [34]–[36]. Additionally, muscle-tendon characteristics and the physiological properties of the muscle itself further contribute to the limitations in force generation.

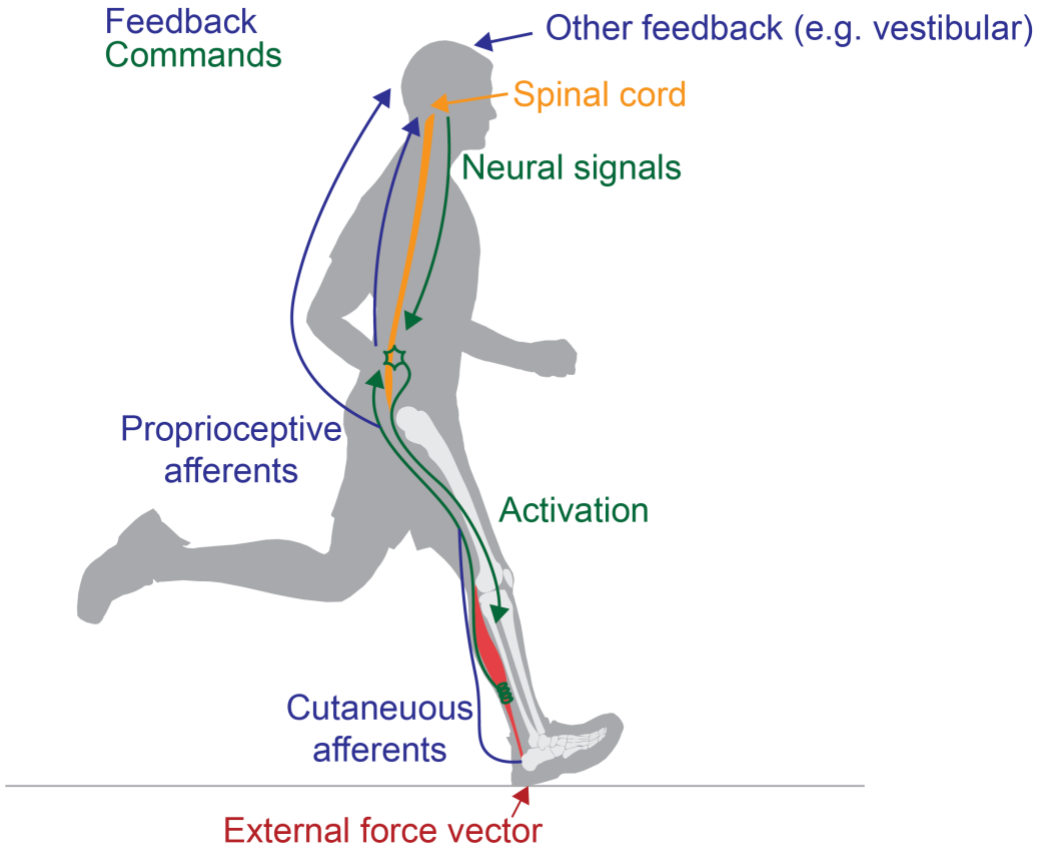

Figure 1-2 The nervous system plays a crucial role in controlling the leg's external ground reaction force vector by forming a closed-loop control system. This system involves transmitting commands to muscles and receiving feedback from sensors. Feedback mechanisms include force feedback from the Golgi tendon organ and length and velocity feedback from muscle spindles, which travel along the peripheral and central nervous systems. Subsequently, appropriate neural commands are sent to activate the muscles, producing torques and generating external force vectors. The capability to control and generate these external force vectors is constrained by the functional capacities of the nervous system and the muscle actuators that generate joint torques.

Muscle is composed of muscle fibres, and a bundle of these fibres innervated by a single motor neuron is known as a motor unit. When a motor unit receives a neural signal resulting in an action potential (depolarization of the cell membrane), all muscle fibres within the motor unit become excited (depending on the external load, the muscle may shorten). Muscle force depends on the number of excited motor units. Maximal contraction occurs when all motor units are excited, realizing the muscle's maximum force potential

[37]. Motor units can be large, containing many muscle fibres, or small, with few fibres. Small motor units tend to be composed of slow-twitch fibres (designed for long-duration motion and slow to fatigue), and large motor units consist of fast-twitch fibres (for quick, powerful movements but prone to rapid fatigue) [37].

The proportion of slow and fast-twitch motor units determines muscle force dependence on muscle velocity. As the muscle shortens and the shortening velocity varies, the muscle's force depends on this velocity. As muscle velocity increases, the muscle produces less force until it reaches a maximal velocity (V_{max}), generating no force [37].

The force a muscle can generate also depends on its length. Experiments on isolated muscles suggest a parabolic relationship between force and muscle length; an optimal muscle length maximizes the force, and deviating from this optimal length results in a decline in muscle force [37], [38]. Muscles connect to bones via a spring-like tendon, which, like a spring, exerts more force as its length increases. The tendon's force-length relationship is commonly considered first-order [39]. Lastly, muscle force depends on the muscle's material properties, with passive force produced as the muscle progressively stiffens when it lengthens [37]. This passive stiffness can increase exponentially as the muscle lengthens, but the passive properties of the muscle can vary depending on its function [38], [40]. Taken together, these intrinsic properties of muscles limit the force a muscle can generate and slow the rate at which muscle force is generated, as it cannot be generated instantaneously.

1.4. Neuromuscular fatigue

Muscle fatigue is a type of perturbation to the nervous system that can impact force control and lead to widespread changes in movement performance. When someone is fatigued, sensorimotor control is temporarily impaired, often resulting in modifications in leg stiffness and step characteristics [41]. This fatigued state may also prolong muscle reaction time, slowing the response to stimuli [42]. At the same time, muscular activation tends to decrease, undermining the overall strength and reactivity of the muscles [43]. Changes such as altered proprioception, distorting the body's perception of self-movement and position [44], as well as challenges in maintaining specific positions or executing precision-required movements, are often observed with fatigue [45], [46]. Body balance might also be compromised, increasing the risk of instability and potential falls that lead to injury [47].

Fatigue significantly disrupts force control, affecting many motor skills and physical functions.

Exercise-induced fatigue falls into two categories: central fatigue and peripheral fatigue. The former originates in the central nervous system (CNS) and reduces the neural drive to the muscle, lowering voluntary activation [48]. Peripheral fatigue, often called muscle or neuromuscular fatigue, originates from the neuromuscular junction and beyond, impacting neuromuscular transmission, excitation-contraction coupling, or muscle bioenergetics [49]. This often results in decreased muscle force or power output [50]. The duration and intensity of exercise can determine the balance between central and peripheral fatigue. Short, high-intensity exercises result in peripheral fatigue reducing the maximum voluntary contraction (MVC), while longer, moderate-intensity exercises tend to lead to central fatigue [51]. The type and intensity of the exercise can also influence the proportion of central and peripheral fatigue experienced [49]. Low-force, prolonged isometric contractions likely induce central fatigue, while short, high-force contractions tend toward peripheral fatigue [48]. Illustrating a complex and often difficult-to-objectively-measure interplay between central and peripheral factors during various muscle contractions. As in this thesis, I am interested in how fatigue affects leg external force control. I focus primarily on peripheral fatigue and will refer to it throughout the remainder of this thesis as neuromuscular fatigue or just fatigue.

Fatigue can impact athletic performance, affecting muscle function and neuromuscular control. Fatigue leads to decreased muscle force generation, slower muscle contraction, and reduced mechanical power output [52]. This power decrease hinders athletic performance, especially in activities requiring high forces over short durations, such as vertical jumping, where athletes jump to lower heights or shorter distances when fatigued [53]–[55]. Fatigue slows muscle reaction time [42], alters proprioception [44], and delays neuromuscular control, potentially compromising the body's center of mass stability [56]. For instance, sprinters often show speed reductions in the final meters of a race [57]. In sports like soccer, where players frequently transition between jumping, sprinting, and tackling, fast-twitch muscle fibre fatigue can lower muscle activations and performance [58]–[60]. Fatigued soccer players also struggle to maintain balance on unstable surfaces [61].

These fatigue-induced performance changes, impacting the control of the center of mass through external leg forces, have widespread implications for various sports. Sports like cross-country skiing [62], long-distance running [63], and basketball, requiring quick changes of direction, are particularly susceptible to fatigue-related agility reductions [12], [64], [65]. One mechanism that may explain the decline in agility post-fatigue could be a deterioration in the nervous system's control of external ground reaction forces.

1.5. Mathematical models to study leg external forces

Mathematical models and simulations provide practical tools for studying legged movement, allowing biomechanists to explore areas that are challenging or impossible to investigate with human subjects. These models typically incorporate link segments, joints, and Hill-type muscle actuators to form mathematical representations of the human legs and other body segments [10], [66]–[68]. By hand or using computer software, equations of motion can be derived to mathematically capture the system's behaviour. With computational complexity quickly becoming overwhelming with increases in segments or features in multibody dynamic systems, computers are commonly the primary tool for deriving equations of motion.

Mathematical models frequently utilize optimal control, which determines an optimal set of model parameters that minimize an objective function over time. In biomechanics, a common objective function aims to minimize the squared difference between an empirically observed, physiologically meaningful variable and the equivalent variable determined by the model. This approach is often referred to as least-squares optimization. For instance, one might compare the external ground reaction force generated by a model with the same force empirically determined by a human. Without empirical signals from physiology, an objective function can simulate the goal of the nervous system in the task. For example, in walking, the objective function might aim to optimize energy usage [69]. In contrast, in jumping, the objective function might focus on maximizing the model's take-off velocity [10].

Phenomenological models often estimate the forces a muscle actuator generates during contraction. A popular mechanical model, the Hill-based muscle model, aptly represents the intrinsic force properties of muscles and is widely employed in biomechanics to actuate

biomechanical models simulating human movement. A typical 3-element Hill-type muscle model comprises a parallel contractile element (CE), a parallel elastic element (PE), and a series elastic element (SEE) [37], [40] (Figure 1-3).

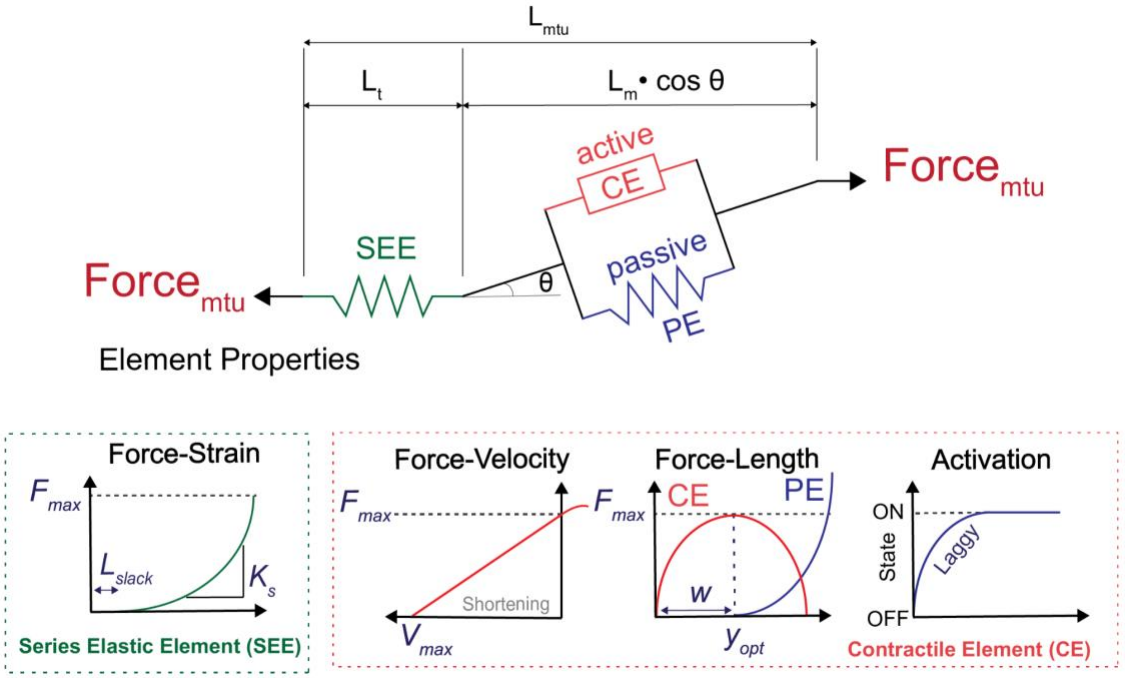

Figure 1-3 An example Hill-type muscle model illustrating the series elastic element ($\boldsymbol{SEE}$), contractile element ($\boldsymbol{CE}$), parallel elastic element ($\boldsymbol{PE}$), muscle-tendon unit length ($\boldsymbol{L_{MTU}}$), and total muscle length ($\boldsymbol{L_T}$). This model represents the mechanical behaviour of skeletal muscles and provides insights into muscle force generation. The force generated by the muscle-tendon unit ($\boldsymbol{F_{mtu}}$) can be calculated using the equation $\boldsymbol{F_{mtu} = F_{max}\,[\,a(t)\,F_v(v_m)\,F_L(L_m) + F_p(L_m)] * cos(\theta)}$, where $\boldsymbol{a}$ represent the activation of the muscle from 0 (inactive) to 1 (fully active), $\boldsymbol{F_{max}}$ represents the maximal force of the contractile element ($\boldsymbol{CE}$) and theta is the pennation angle of the muscle. The series elastic element ($\boldsymbol{SEE}$) represents tendons and other compliant structures that store and release energy during muscle contraction. It exhibits properties where the tension increases as length extends beyond a predefined slack length ($\boldsymbol{L_{slack}}$). The contractile element ($\boldsymbol{CE}$) generates force and has force-length and force-velocity properties. Force declines when muscle length deviates from an optimal length ($\boldsymbol{y_{opt}}$), and force decreases with increasing shortening velocities up to $\boldsymbol{V_{max}}$. The parallel elastic element ($\boldsymbol{PE}$) represents the passive elastic component contributing to muscle stiffness. It stiffens as muscle lengthens away from $\boldsymbol{y_{opt}}$. The Hill-type muscle model enables simulations and analysis of muscle function by capturing the essential characteristics of muscle behaviour, including force production, energy storage, and mechanical properties. Understanding the interplay between the $\boldsymbol{SEE}$, $\boldsymbol{CE}$, and $\boldsymbol{PE}$ is crucial for studying muscle function, biomechanics, and optimizing performance. Figure adapted and modified from [70].

The model's Contractile Element (CE) represents the force dependency of muscle fibres on their kinematic state. For instance, as a muscle actuator shortens rapidly, the force it generates declines up to a point at maximum shortening velocity (V_{max}), where force generation ceases. When the muscle actuator is isometric with no velocity, it can theoretically generate maximum force (F_{max}).

The force generation of a muscle actuator depends on its length, with a parabolic relationship indicating an optimal length (y_{opt}) at which maximal force (F_{max}) is generated. Beyond this optimal length, force generation decreases. The parabolic width of this relationship varies among muscles serving different purposes and is determined within the model [37], [40].

Furthermore, the model captures the muscle actuator's force dependence on the degree of muscle contraction, often called 'muscle activation.' This activation level measures how much the muscle fibres contract in response to the nerve signals they have received, termed 'excitation.' Excitation is when a nerve signal or action potential is sent to a muscle fibre, triggering a series of events that lead to muscle contraction. The activation values range from 0, representing a state of no contraction or inactivity, to 1, representing maximum contraction or full activity. This activation value is then multiplied by the output force of the Contractile Element (CE) output force to modify further the force that the CE generates. It is important to note that in this context, 'activation' describes the state of the muscle fibres after they have been excited by a nerve signal, with the degree of activation determining the force of muscle contraction.

The model also considers the passive properties of muscles, represented by the Parallel Elastic Element (PE). The Contractile Element (CE) represents the actual muscle fibres capable of actively generating force and changing length, and the PE change length simultaneously as they are arranged in parallel. The Series Elastic Element (SEE) represents the tendon, which, while not actively contracting, behaves like a spring to store and release energy when stretched. The series tendon length (SEE) is predefined as a proportion of the total muscle length (LTotal), with a force-length curve describing the SEE's behaviour as it stretches. It's important to note that if the length is too short, it could result in a slack muscle and potentially destabilize the mathematical model [36]. In reality, the muscle and the tendon have both passive and active properties, and various factors can influence their behaviour. The Hill-type muscle model is a valuable tool for

understanding and predicting muscle behaviour, but it simplifies the complex reality of muscle and tendon mechanics. Parameters for Hill-type muscle models can be extracted from existing literature [71], or deduced via mathematical optimization, as I will show later in this thesis.

Evaluating a mathematical model's effectiveness requires solving differential equations describing the segment's kinematics actuated by Hill-type muscle actuators. In forward dynamics, these equations are numerically integrated over time, considering environmental factors such as gravity and inertia and optimal muscle actuator properties. This allows for the prediction of the model's behaviour under defined conditions. Simulations of muscle-actuated forward dynamics can highlight relationships between muscles' intrinsic properties and movement performance. For instance, a four-segment, 16-Hill-type muscle actuator model was recently used to explore the constraints on sprinting speeds imposed by muscles' intrinsic properties. The group simulated sprinting behaviour under altered muscle intrinsic properties—a near-impossible experiment to perform on humans. They found that removing muscle force dependence on muscle velocity or length can increase sprinting speed. Their model achieved running speeds up to +15% and +4% faster when leg muscle properties were modified [11], [72].

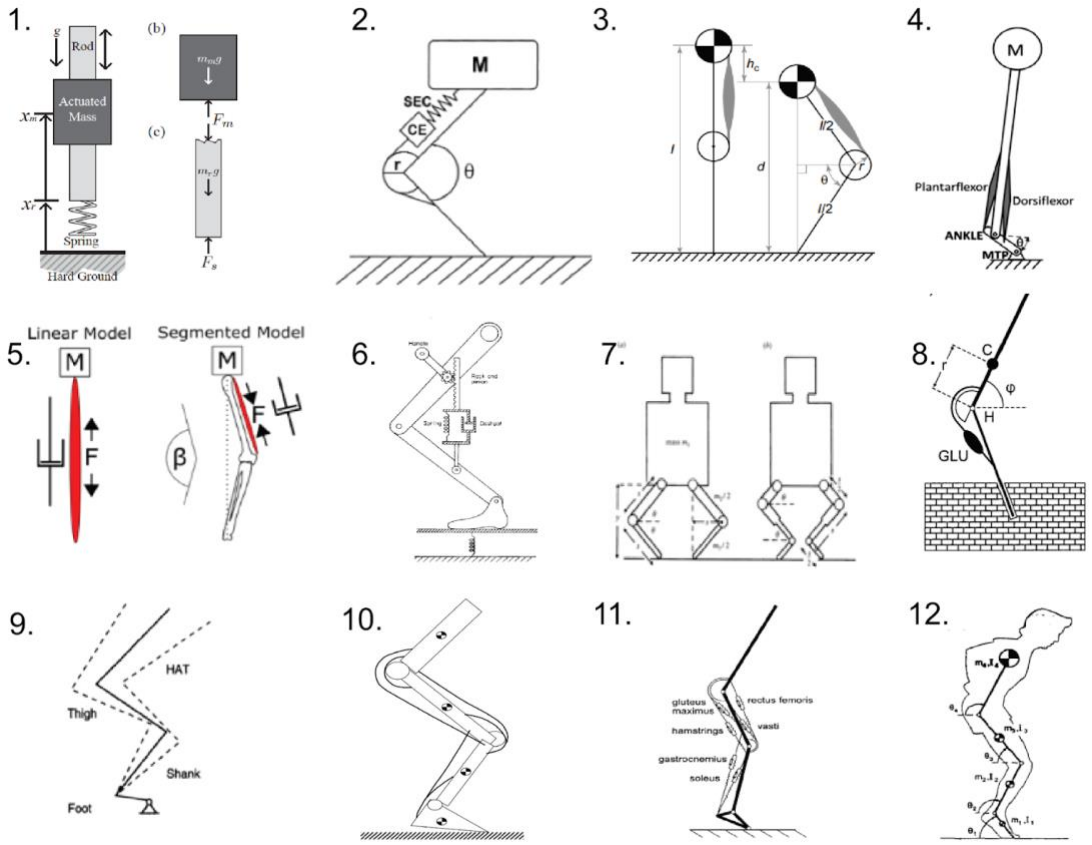

Figure 1-4 Example jumping models from the literature. Jumping is a highly suitable movement task for modelling due to its clear objective of maximizing the take-off velocity of the center of mass, which correlates with other agile movements. Literature on jumping models encompasses a range of approaches, including single-segment and multi-segment models and models utilizing hill-type muscle activation or torque generation. While complex models offer detailed insights, fundamental understanding often arises from simpler models that gradually incorporate complexity when necessary 1. [73] 2. [74] 3. [75] 4. [76] 5. [77] 6.[78] 7. [68] 8. [79] 9. [80] 10. [81] 11. [10] 12. [66]

While simple models contribute valuable insights, they have yet to emphasize accurate estimates of the external forces that humans generate during jumping. Developing a simple model that can jump from many positions and accurately reproduce the external forces developed during jumping can provide insights into developing larger magnitude forces for higher jumping and more agility. Complex models composed of many muscles may be able to reproduce external forces better, but none have focused on this specifically [10], [66], [83].

1.6. Machine learning for biomechanics

The continuous evolution of algorithms and models pave a path toward a more unified understanding of our complex motor control system. Machine learning, a branch of artificial intelligence, concentrates on creating statistical models and algorithms that equip computers to learn and predict autonomously without explicit programming. This process can involve using a specific dataset to train a model, which is then deployed to make predictions or draw inferences from new, unseen data. Human physiological and biomechanical data, often time series in its nature, provides an excellent source of training for machine learning models and may lead to novel discoveries or new tools for sports and medicine to improve our lives. Perhaps such algorithms can even be deployed to progress the estimation of external forces and power tools that are not currently available.

Inspired by the structure and function of the human brain, artificial neural networks are computational models composed of interconnected nodes, or neurons, arranged in layers (Figure 1-5). A branch of machine learning known as deep learning utilizes deep neural networks, which contain multiple hidden layers between the input and output layers. The depth of these networks enables them to discern intricate patterns and learn hierarchical representations. During training, the network adjusts weights assigned to inputs iteratively to minimize a defined loss function. Optimization algorithms, such as stochastic gradient descent, utilize mathematical techniques to update the weights gradually and converge toward an optimal solution. Deep neural networks can incorporate multiple layers, each performing a mathematical transformation on the input data. These transformations are mathematically represented as matrix multiplications followed by applying activation functions. By building a hierarchical structure, artificial neural networks can learn increasingly abstract and intricate representations of the input data through these mathematical operations. Integrating mathematics with the architecture of neural networks is pivotal in leveraging the power of these algorithms. This synergy allows for the development of sophisticated models capable of capturing complex dynamics.

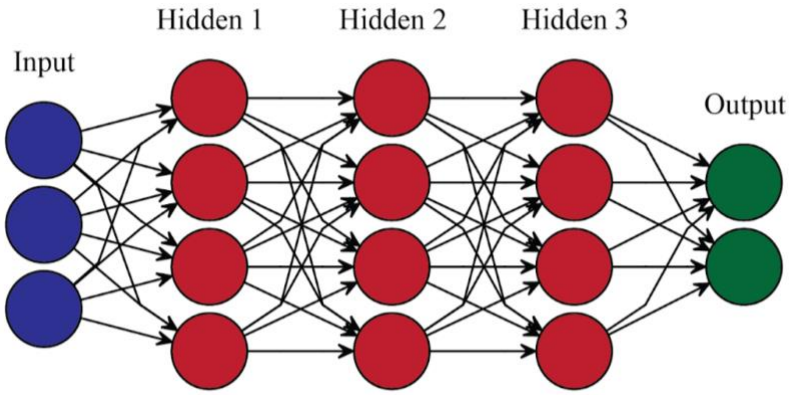

Figure 1-5 : Illustration of a deep neural network architecture inspired by the human brain. The network consists of an input layer (blue), three hidden layers (red), and an output layer (green). Deep neural networks leverage the interconnectedness of neurons in multiple hidden layers to extract intricate patterns and learn hierarchical representations. During the training process, the network iteratively adjusts the weights assigned to inputs to minimize a defined loss function. Deep neural networks can capture complex dynamics and provide accurate estimations by incorporating multiple layers and performing mathematical transformations on the input data.

Enabling computers with the ability to comprehend and analyze visual information from the environment, computer vision is a key subfield of machine learning. Its scope includes image and video recognition, object detection, segmentation, and tracking. Computer vision aims to train computers to process images and videos similarly to human vision. The advent of deep learning has substantially advanced this field, bypassing traditional techniques that relied heavily on hand-crafted features and shallow learning algorithms that operate on a few layers and often struggle to handle the complexity of real-world visual data. Recently, advancements in computer vision are enabling biomechanists to gather data more rapidly and in greater volumes than ever before. In a recent study, biomechanical videos of 405 participants were recorded, analyzed, and studied, with each participant filming themselves sitting and standing up using their smartphones in their homes [84]. One of the major challenges in extracting biomechanical data from videos has always been the time-consuming and inefficient process of manually labelling anatomical landmarks or key points in video frames [85], [86]. By leveraging computer vision to identify these landmarks on the human body, deep neural networks present a practical solution to this problem, reducing the time and effort involved in video analysis.

Key point detection or ‘pose estimation’ is a computer vision tool that detects key features of the human body in video data (Figure 1-6). Algorithms such as DeepLabCut and OpenPose use deep learning to visualize features and predict key landmarks in RGB video frames. For instance, DeepLabCut, an open-source software that employs a pre-trained neural network architecture based on the ImageNet database, is widely used in research and education for its scalable and efficient tools [87]. Tracking movement data from video to study the behaviour and conservation of animals such as cheetahs, spiders, and gazelles enables many scientific and technological advancements from otherwise challenging animals to work with [87]–[89]. Whereas libraries like OpenPose enable the prediction of human poses from video [90]. This is paving a future of markerless motion capture, where kinematic data, typically measured using expensive and constrained motion labs, can now be easily and flexibly collected directly from video [91], [92].

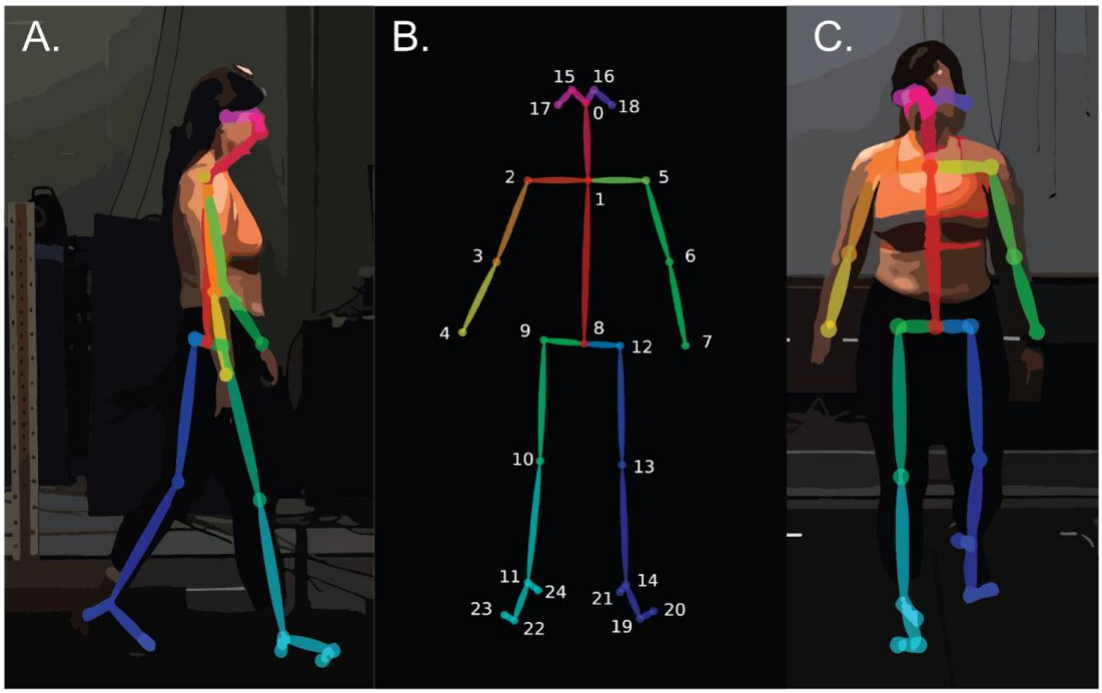

Figure 1-6: Example output of OpenPose, an open-source computer vision tool for human pose estimation [90]. OpenPose detects and tracks key body joints and body parts using computer vision, representing human movement (B.). In this example, the skeletonized representation of a person's pose is shown from the side view (A.) and the frontal view (C.), with key joints and body parts identified and connected by lines. OpenPose enables a markerless approach to studying human movement, offering valuable insights for various applications, including sports science, rehabilitation, and human-computer interaction.

The combination of standard RGB video and deep neural networks holds immense potential for the future of our field. Videos are a low-cost and widely available resource, with smartphones offering easy and broad access. Traditional biomechanical tools like force plates for kinetic measurements and motion capture systems for kinematics are costly and environment-bound. Coupling these tools with machine learning could revolutionize physiological measurements of motion. For example, recent work named OpenCap utilizes two smartphone video cameras, leveraging computer vision and machine learning techniques, to analyze video data and provide insights into movement dynamics [93]. To demonstrate its practical utility, OpenCap was tested in a field study involving 100 subjects to demonstrate its practical utility. The results were promising, as a clinician using OpenCap could estimate movement dynamics 25 times faster than traditional laboratory-based approaches while costing less than 1% of the traditional

methods. As biomechanical variables extracted from human motion are time series data, it is crucial to consider the appropriate machine learning frameworks that could be designed to work with this data. Here I will focus on two neural network architectures: Bidirectional LSTMs and transformer-based models.

LSTM models are widely used for time series analysis because they capture temporal dependencies. Kinematic and kinetic variables often exhibit complex and changing patterns over time; consider joint angles, muscle forces, or ground reaction forces. LSTM models excel at capturing long-term dependencies by utilizing memory cells that store and propagate information across different time steps [94]. This enables such models to learn the relationships and patterns within the time series data, making them practical for tasks like predicting joint angles [95]–[97] and estimating external ground reaction forces from kinematic data [98]. This is possible by leveraging data from wearable sensor data [99], load cells [100], and pressure insoles in shoes [101]. LSTMs can handle variable-length sequences commonly found in biomechanical data, accommodating movements of different durations or sampling rates.

Bidirectional LSTMs extend the capabilities of LSTM models by processing input sequences in both forward and backward directions. By incorporating information from past and future observations simultaneously, Bidirectional LSTMs capture more comprehensive temporal dependencies [102]. In biomechanics, this can be particularly useful for analyzing kinematic and kinetic variables, as both past and future events often influence movements. This suggests that Bidirectional LSTMs may be more powerful in situations where future information is relevant for accurate predictions or analysis. By incorporating future context, Bidirectional LSTMs can better model the dynamics of biomechanical movements and improve the accuracy of predictions. However, it is also essential to consider that Bidirectional LSTMs may introduce some challenges related to real-time prediction or applications where future information is unavailable.

On the other hand, Transformers models, while primarily known for their success in natural language processing, show great use in time series data analysis. Transformers operate on the principle of self-attention, allowing them to capture relationships between different elements within a sequence [103]. This attention mechanism enables the model to focus on relevant patterns and dependencies, making it highly suitable for capturing complex temporal relationships in time series data [104]–[106]. Additionally, Transformers have the

advantage of parallelization. They can process the entire time series sequence in parallel, making them efficient for handling large-scale datasets. This parallel computation across the sequence allows for faster training and inference times, which is particularly beneficial when working with substantial amounts of data. DeepLabCut, for example, utilizes Transformers for its kinematic key point prediction algorithms [107]. A recent study using wearables sensors to estimate vertical ground reaction forces during walking and running showed that a transformer model could reduce prediction errors by 25% compared to an LSTM architecture [108]. Transformers provide an understanding of the data by considering each element in relation to the entire sequence. This holistic approach enables them to capture intricate relationships, potentially revealing hidden patterns in data that may not be readily apparent with other models.

Bidirectional LSTMs and Transformer models offer distinct technical advantages for predicting time series data in biomechanics. Bidirectional LSTMs models excel at capturing long-term dependencies, handling variable-length sequences, and managing time lag. They are beneficial for modelling complex biomechanical patterns that span multiple time steps. On the other hand, Transformers provide parallelization, attention mechanisms, contextual understanding, and the potential for greater transfer learning. They can efficiently capture intricate relationships in biomechanics data and reveal hidden patterns, which may be an appropriate choice for developing new technology to estimate external forces during movement.

1.7. Thesis Aims

In this thesis, my primary goal is to investigate the boundaries of leg external force control and develop technologies that utilize machine learning and computer vision to estimate kinetics from video footage. To accomplish this, I conduct empirical studies involving human participants who exert controlled external force vectors of varying magnitudes and positions. I use system identification to characterize their control performance (Aim 1). I examine the effect of fatigue on the control of external force (Aim 2) and use mathematical models of legs and muscles to gain a deeper understanding of the limitations and capabilities of leg force control (Aim 3). Finally, I developed a machine learning methodology to estimate leg external forces from video data (Aim 4). These four interconnected projects aim to explore the neuromechanical mechanisms that enable

force control and improve our ability to estimate the external ground reaction forces that drive our movements.

Aim 1: To characterize the control of leg external forces. The ability to modulate the force that a leg applies to the ground, and the position of that force, is a crucial factor in agility. My goal is to measure the performance of the human leg in controlling external ground reaction force magnitudes and positions and compare this performance to the control of agile robotic legs. To accomplish this, I designed and constructed a mechanical system restricting the body while allowing one leg to push isometrically on a force plate. I also developed a real-time visual feedback system that provides target force magnitudes or positions the leg should exert against the ground. I recruited 14 participants who tracked step changes in target leg force-magnitude (or force-position). I used system identification to characterize how well participants' leg force control matched the target steps. Finally, I modelled the empirical response using a 2nd order system and found that this model effectively explained leg external force control in humans. The insights gained from this work could potentially inform the design of more agile prosthetics and exoskeletons, improving mobility for individuals with physical disabilities and enhancing performance in athletes.

Aim 2: To determine the effects of neuromuscular fatigue on the nervous system's capacity to rapidly and accurately control leg external forces. Neuromuscular fatigue can impair our agility by inducing physiological changes, such as slowing our muscle reaction time, altering our proprioception, and delaying our neuromuscular control in ways that affect the control of our muscles. I hypothesized that increased leg fatigue would result in a decline in both responsiveness (how quickly a system responds to changes in its inputs) and accuracy of leg force control. To test this, I used the apparatus I previously constructed in Aim 1, which allowed participants to exert controlled vertical external forces using one leg pushing against a force plate while immobilizing the rest of their bodies. I recruited 18 participants and asked them to control their leg external force to best match step targets presented to them on a screen. I then induced fatigue by having participants hold submaximal leg forces at 25% of their maximum voluntary external force and measured their leg force control performance between fatigue trials. Understanding the effects of fatigue on leg force control may help to develop strategies and technologies to maintain agile performance even in the presence of fatigue.

Aim 3: To understand how muscle actuator properties enhance vertical jump height and influence the corresponding external forces. I developed and optimized simple physics-based models that predicted vertical external forces during jumps from various initial starting depths. The optimized model utilized a single set of optimal actuator properties, enabling it to jump from various depths while aligning the external force with empirical data. I recruited 10 participants to perform vertical squat jumps from five different initial starting depths, during which I collected data on their external leg forces using a ground-mounted force platform. Subsequently, I created and evaluated vertical jumping models of increasing complexity. I applied simulation and optimization techniques to align the model's predicted vertical external forces with the empirical data from each jump. Ultimately, I created a model that could jump from various depths and generate vertical external forces that closely aligned with the empirical data, all while using a single set of optimal actuator properties. With this model, I investigated how incremental changes in muscle actuator properties affected the vertical external forces generated and how this impacted the height of a vertical jump. Finally, I aimed to use this model to determine the factors contributing to a jump's preferred depth when jumping maximally. Understanding the biomechanical factors that contributed to vertical jumping performance provided insights into athletic training, rehabilitation programs, and technologies developed to optimize jump height.

Aim 4: To develop a new method for estimating external forces during vertical jumping using video and machine learning. I combined video data with computer vision and machine learning techniques to bring the capabilities of a laboratory into the convenience of a smartphone. I recruited 30 participants to perform a series of vertical jumps while simultaneously capturing their movements through video recording and measuring the external ground reaction forces. I processed the video data using an open-source pose estimation tool to extract kinematic landmarks for each participant's body during each jump. I used these extracted data to train a transformer-based neural network that predicted the external ground reaction forces. Next, I evaluated the model's performance using a leave-one-participant-out cross-validation method. The outcomes of this research potentially eliminated the need for sophisticated equipment in estimating external forces during movement by harnessing the power of readily available technology such as video and machine learning algorithms.

Chapter 2.

Characterizing the performance of human leg external force control

2.1. Abstract

Our legs act as our primary contact with the surrounding environment, generating external forces that enable agile motion. To be agile, the nervous system has to control both the magnitude of the force that the feet apply to the ground and the point of application of this force. The purpose of this study was to characterize the performance of the healthy human neuromechanical system in controlling the force-magnitude and position of an externally applied force. To accomplish this, we built an apparatus that immobilized participants but allowed them to exert variable but controlled external forces with a single leg onto a ground-embedded force plate. We provided real-time visual feedback of either the leg force-magnitude or position that participants were exerting against the force platform and instructed participants to best match their real-time signal to prescribed target step functions. We tested target step functions of a range of sizes and quantified the responsiveness and accuracy of the control. For the control of force-magnitude and for intermediate step sizes of 0.45 bodyweights, we found a bandwidth of 1.8±0.5 Hz, a steady-state error of 2.6±0.9%, and a steady-state variability of 2.7±0.9%. We found similar control performance in terms of responsiveness and accuracy across step sizes and between force-magnitude and position control. Increases in responsiveness correlated with reductions in other measures of control performance, such as a greater magnitude of overshooting. We modelled the observed control performance and found that a second-order model was a good predictor of external leg force control. We discuss how benchmarking force control performance in young healthy humans' aids in understanding differences in agility between humans, between humans and other animals, and between humans and engineered systems.

2.2. Introduction

Agility is an important aspect of movement performance. This is true in athletics, where success can be determined by how high a volleyball player jumps when blocking a hit or how quickly a soccer player redirects their motion when taking evasive action from an oncoming defensive player. This is also true in the wild, where to survive, animals must chase down their prey, evade predators, and negotiate variable terrain [109], [110]. And in robotic systems, agility will be necessary for legged robots to provide fundamental services to society that currently only humans can provide. For example, agile robots may assist in complex mountain rescues with rough and varied terrain, move payloads while avoiding obstacles in construction sites, and deliver mail [111].

Aspects of agility are measured in several ways. In athletics, agility has been quantified by sprint speed [112], jump height [4], and time to complete an obstacle course [113], [114]. Scientists have quantified the agility of different animals and sometimes compared agility across species, by measuring maximum sprint speed [115], maximum jump height [116], and minimum turning radius [117], [118]. To accomplish any of these agility tasks—running fast, jumping high, or changing direction rapidly—requires generating well-controlled forces against the environment (external forces). In turn, the resulting reaction force from the environment accelerates our bodies. In principle, legged animals and robots can push against the ground with any part of their body, but we most commonly do this using our legs to push our feet against the ground.

To be agile, the nervous system has to control both the magnitude of the force that the feet apply to the ground, as well as the point of application of this force. The external force beneath each foot is a vector quantity. The magnitude of three orthogonal components of force must be controlled—we refer to this as force-magnitude control. As is a convention, we represent these force components as forward and backward in the horizontal plane (or anterior and posterior), side to side which is also in the horizontal plane (or medial and lateral), and upward and downward in the vertical direction. The nervous system may use a decomposition that is different from this convention. Modulating the magnitude of each component will change the acceleration of the body along that component's direction. An accelerating sprinter selectively increases the forward component, a maximum height vertical jumper selectively increases the vertical component, and a runner changing direction may need to modulate all three components [119]. Our nervous system also needs to control the point of force application of the external force vector—we refer to the control of this point as force-position control. By selectively controlling the force-position, and components of the force-magnitude, a gymnast can change angular acceleration to initiate an aerial front flip by generating a rotational moment of force about their center of mass [120]. To control the force beneath each foot our nervous system must synergistically coordinate leg muscle activations [121], [122]. In general, the selective linear and angular acceleration of the body required for agile motion requires the rapid and accurate control of force-magnitude and force-position.

Given the importance of well-controlling external force vectors to generate agile motion, we know remarkably little about how well this is accomplished by legged biological and engineered systems. One approach to characterizing the performance of a control system

is to evaluate the system's ability to rapidly and accurately change from one commanded state to a new target state, known as the step response [123]. The response to a step-change in commanded external force has been evaluated in several engineered-legged systems. For example, the MIT Cheetah robot is able to step-change from zero vertical force beneath the feet to 1/3 of its body weight within milliseconds and does so with almost zero error [124], [125]. Similarly, a state-of-the-art foot prosthesis demonstrates millisecond-scale control of torque, allowing the prosthesis to accurately track rapidly changing commanded torques [126]. However, force control performance is not routinely measured in engineered systems, and to our knowledge, has never been quantified in humans or other legged animals.

The purpose of our study was to characterize the performance of the human leg in controlling external force-magnitude and force-position. We focused here on the control of sub-maximal forces generated by a single leg in a posture similar to how a runner actuates their motion during a run. To accomplish this purpose, we built a custom apparatus that constrained participants' bodies from moving so that their legs maintained a constant posture while allowing them to change force-magnitude and force-position. To quantify the step response, we instructed participants to best match visually displayed step changes in ground force magnitude by pushing more or less against a ground-mounted force plate (force-magnitude control), or step changes in ground force position by shifting the pressure beneath their foot forwards and backwards, or side to side (force-position control). We evaluated control performance by how quickly and accurately participants could match their force magnitude and force position to the commanded changes.

2.3. Methods

2.3.1. Participants

We recruited fourteen participants for the study (female: n = 4; male: n = 10; body mass: 72.2±6.1 kg; age: 28±2 years; foot length: 0.25±0.2m; mean±std). The Office of Research Ethics at Simon Fraser University approved the study, and the methods were performed in accordance with the relevant guidelines and regulations. All participants provided written and verbal informed consent before participating in our study.

2.3.2. Experimental Design

To characterize the performance of human leg force control, we tested the step response of participants selectively controlling leg external force. To do this, we built an apparatus that vertically and horizontally constrained participants standing over top of a ground-embedded force plate (Bertec Corporation, Ohio, USA). The apparatus was rigidly attached to the ground around the force plate, but not to the force plate itself. The force plate beneath the participant's foot sampled at a frequency of 1000 Hz and was connected to a data acquisition unit (USB-6229, National Instruments Corporation, Texas, USA), which interfaced with our computer. Although the control of all three orthogonal components of the external force vector is important, our work here focused on the characterization of the vertical component. The constraints imposed by the testing apparatus allowed participants to exert a variable but controlled vertical external force onto the ground by selectively pushing more or less against the ground with their leg (i.e. force-magnitude control) or selectively shifting the center of pressure beneath their foot anteriorly/posteriorly (forward/backward) or medially/laterally (side-to-side) (i.e. force-position control). We built the testing apparatus using 1.5"x1.5" T-Slotted aluminum bars (80/20 Inc., Indiana, USA). We mounted four adjustable scissor jacks onto the apparatus to secure and immobilize the participant to the apparatus (Figure 2.1). Two of the scissor jacks pushed down against the shoulders, and two pushed up against the forearms. An adjustable padded bar supported the leg that was not pushing on the ground. On all points where the participant came in contact with the apparatus, we secured high-density padding to reduce discomfort.

To command target step changes in force-magnitude and position, we used visual feedback to allow participants to compare their target and actual force-magnitude or position. We provided real-time visual feedback using a computer monitor mounted in front of the participants (Figure 2-1). Our custom software (MATLAB 2019a, MathWorks) displayed both real-time feedback of either the vertical force-magnitude or force-position signals that the participant's foot exerted onto the force plate and of the target step function that the participant tried to best match. We filtered the raw force signal using a zero-lag low-pass fourth-order Butterworth filter with a cut-off frequency of 10 Hz. For force-magnitude control, we then normalized the real-time signal to each participant's bodyweight and zeroed the force platform such that zero force was equivalent to one bodyweight. For the real-time force-position signal, we calculated the medial-lateral and

anterior-posterior centers of pressure and filtered the raw force signal using a zero-lag low-pass fourth-order Butterworth filter with a cut-off frequency of 5 Hz [127]. We then mathematically shifted the axes of the center of pressure on the force platform to originate beneath the participant's foot that was in contact with the force plate. To perform this shift, we had each participant stand in a comfortable position on each leg in the rig (Figure 2-1). We then recorded the values of the center of pressure while participants stood on each leg and programmed a shift of the force plate axes to originate directly below the foot the participant was standing on. We programmed all the candidate real-time signals to display at the center of the screen and constrained this signal to only vertically move up and down as the participant pushed more or less against the force plate (force-magnitude control) or as they displaced their force-position anteriorly/posteriorly or medially/laterally beneath their foot (force-position control). Finally, we programmed the target step functions to slide past the real-time signal providing participants with time to view upcoming changes in the step function before they occurred (Figure 2-1).

We provided each participant with instructions and motivation to enable them to maximize their performance in matching their real-time force-magnitude or position signal to the targets. We instructed participants to keep their foot firmly mounted to the force platform. Our instructions to them were "*your goal in this experiment is to try and match the real-time signal to the target line that you will see on your screen. For force-magnitude control, that is pushing with force against the ground. This will mean pushing down or reducing the amount you push down, as quickly and accurately as you can to match the sliding target wave moving along the screen. For force-position control, this will mean changing the pressure beneath your foot side-to-side or forward/backward to match the sliding target wave as quickly and accurately as possible. I will notify you if it will be side-to-side or forward/backward shifting*" Due to the repetitive nature of the experiment and the possibility of both physical and mental fatigue, we provided participants with 15-second intermissions between trials (trials are explained below). During this intermission, we displayed a countdown on their screen to notify them when the next trial was beginning and a scoreboard showing them the total error incurred during each trial. We calculated this error as the total root mean square error between the empirical response and the target step function to encourage both speed and accuracy when rising and falling to new target forces and positions. We informed participants that a perfect score was 0 error. We

encouraged all participants to minimize this error by best matching their real-time signal to the step targets appearing on their screen.

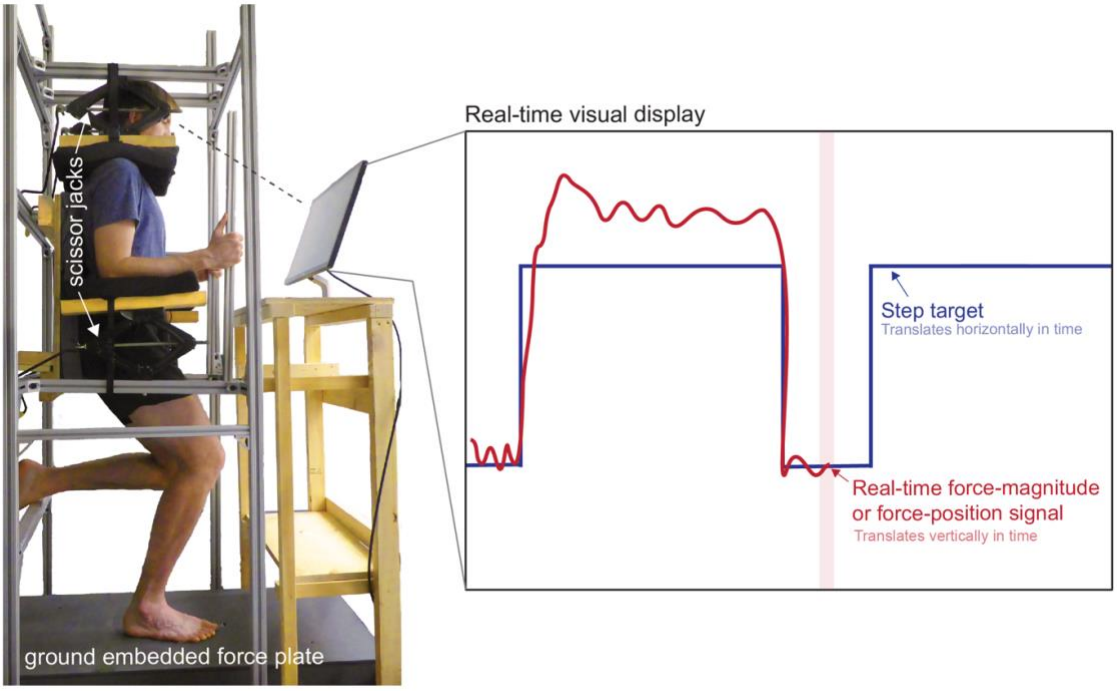

Figure 2-1 Apparatus to characterize external force control. The apparatus constrained the vertical and horizontal motion of each participant's torso using adjustable scissor jacks that pushed down on their shoulders and pushed up against their forearms, and a stiff aluminum frame securely mounted to the ground. The participants stood in a posture resembling the stance phase of a run and could selectively push more or less or shift the pressure beneath their foot against the ground-embedded force plate. The real-time feedback displayed to the participants the real-time force-magnitude or position signal that they were exerting onto the ground as well as the target step function they were to try and best match

2.3.3. Experimental Protocol

We characterized external force control over two sessions. We performed the sessions in a randomized order and on different days. In each session, we fitted participants into the experimental apparatus. When fitting participants into the apparatus, we used an analog goniometer to enforce a 15-degree knee flexion angle to approximate a posture similar to that assumed by a runner at the start of stance [128]. While maintaining this posture, we adjusted the horizontal positions of the arm and shoulder constraints such that the

participant was unable to shift horizontally within the apparatus. Next, we adjusted the vertical arm and shoulder constraints by vertically shifting the scissor jacks to apply downward pressure on the participant's shoulders. Finally, we adjusted the height of the padded bar that supported the leg that was not pushing on the ground. In the force-magnitude session, we recorded each participant's mass by having them stand on a force plate.

In one session, we characterized force-magnitude control. This session contained five conditions—one training and four testing. The training condition came first, and we designed it to familiarize participants with the experiment. It consisted of 12 trials, totalling six on each leg, with a single target step function size of 0.85 bodyweights. For reference, in these experiments, we made 0 bodyweights equivalent to the participant standing on the force plate. We choose to focus on a single target step function size in order to get many trials where a participant can practice all the aspects of the task including being comfortable in the apparatus and acquainting themselves with the visual display without the added complexity of changing the target size. In all trials, the target step function consisted of a square wave of ten matching-size target steps, each four seconds in duration, with three seconds between steps (totalling 73 seconds per trial). The four testing conditions followed the training condition. Each of these testing conditions contained a target step function size of either 0.25, 0.45, 0.85, or 1.25 body weights. Our selection of these target step sizes was based on our interest in submaximal forces that were achieved comfortably in our device. In pilot experiments, we determined that on the top range, this was 1.25 bodyweights of vertical force-magnitude and on the bottom range, this was 0.25 bodyweights. We had participants perform each of these testing conditions in random order. Testing conditions consisted of 6 trials, totalling three per leg. In all cases, participants switched the leg in contact with the ground after each trial to ameliorate the effects of fatigue.

In another session, we characterized force-position control. This session contained five conditions—one training and four testing—for anterior-posterior control and the same five conditions for medial-lateral control. In random order, we first evaluated either the conditions within anterior-posterior control or the conditions within medial-lateral control. In either case, the training condition came first, and we designed it to familiarize participants with the experiment. It consisted of 12 trials, totalling six on each leg, with a single target step function of size 2.5 centimeters anterior for anterior/posterior control

trials and a target step size of 1.0 centimeters for the medial/lateral control trials. Again, in all trials, the target step function consisted of a square wave of ten target steps, each four seconds in duration, with three seconds between steps. The four testing conditions followed the training condition. Each of these four conditions contained a single target step function size of either +2.5, +4.0, -1.0, -2.5 centimeters for the anterior (+)/posterior (-) control conditions or +1.0, +0.5, -0.5, -1.0 centimeters for the medial (+)/lateral (-) control conditions. As for force-magnitude control, we had participants perform each of these testing conditions in random order. Testing conditions consisted of 6 trials, totalling three per leg and in all cases, we asked participants to swap the leg in contact with the ground after each trial.

To determine whether visual feedback slowed the participant's ability to control external force, we eliminated visual feedback for some of the step responses in each trial. We randomly omitted the visual feedback from two of every ten steps in every trial for each condition throughout all of our experiments including the training conditions. We did this by momentarily taking away the real-time visual feedback of the force the participant is exerting onto the ground, while the target step function remains on the screen. We removed visual feedback starting from when the target steps up to when it steps back down again.

To determine how quickly force could rise when the speed of the response was prioritized over the accuracy, we had one participant perform a force-magnitude control experiment stepping up to a step target size of 0.85 bodyweights (male; body mass = 80.6 kg; foot length = 26.6 cm). Similar to the main protocol, he performed three trials with the left leg and three trials with the right leg. We instructed him that the priority was to step up as quickly to the target as they could and that it was unnecessary to match or hold the steady-state force level after stepping up to the target.

2.3.4. Data Analysis

For each step response within each trial, we evaluated the responsiveness and accuracy in controlling external force. To accomplish this, we took the results from each trial and segmented them into ten individual step responses such that each segmentation consisted of a six-second single-step response, with one second before the step-up and 1 second after the step-down (Figure 2-2). For each step response, we evaluated the rise

time (in units of milliseconds) as the time for the signal to go from 10% to 90% of the target step size value. We calculated the upper limit of bandwidth (in units of Hz) by dividing 0.35 by rise time [129] and assumed the lower limit was 0 Hz. The bandwidth measures the frequency range at which a target signal can change and still be accurately tracked by the controller. We quantified fall time (in units of milliseconds) as the time for the signal to go from 90% to 10% of the target step size value as the participant steps-down. In this chapter, we use the term responsiveness to refer to rise time, fall time, and bandwidth—a responsive system has a short rise time, a short fall time, and a high bandwidth. Next, we quantified overshoot by taking the peak value reached by the signal, subtracting the value of the target step, dividing this by the size of the step, and multiplying by 100. In this way, we expressed overshoot as the percentage that the signal exceeds the target step size value. If the signal did not surpass the target step value resulted in a negative value for the overshooting. A large overshoot can indicate under-damping in the controller—it will take longer for the system to settle and reach its target step size. We restricted our evaluation of the rise time, bandwidth, and overshoot of the response to the time interval of 0.5 seconds before the step target stepped up and up to one second after the step-up occurred. We quantified steady-state error by calculating the mean value of the signal between 2-3 seconds, subtracting the value of the target step size, and taking the absolute value. We divided this by the value of the target step size and multiplied this by 100 to express the steady-state error as a percentage of the target value. The steady-state error informs us how much error the control system has once it has reached the target size value and settled in its new state. A large error can be indicative of poor control as the system is not able to well match the target value. We quantified steady-state variability by calculating the standard deviation of the signal between 2-3 seconds, dividing this by the steady-state mean and multiplying this value by 100. The steady-state variability, expressed as a percentage of the steady-state mean, informs us how variable the system is once it has reached and settled on its new state. In this thesis, we use the term accuracy to refer to overshoot, steady-state error, and steady-state variability—an accurate system has small overshoot, small steady-state error, and small steady-state variability. We evaluated the fall time between four to six seconds (Figure 2-2). We collectively refer to the rise time, bandwidth, overshoot, steady-state error, steady-state variability, and fall time as the step response characteristics.

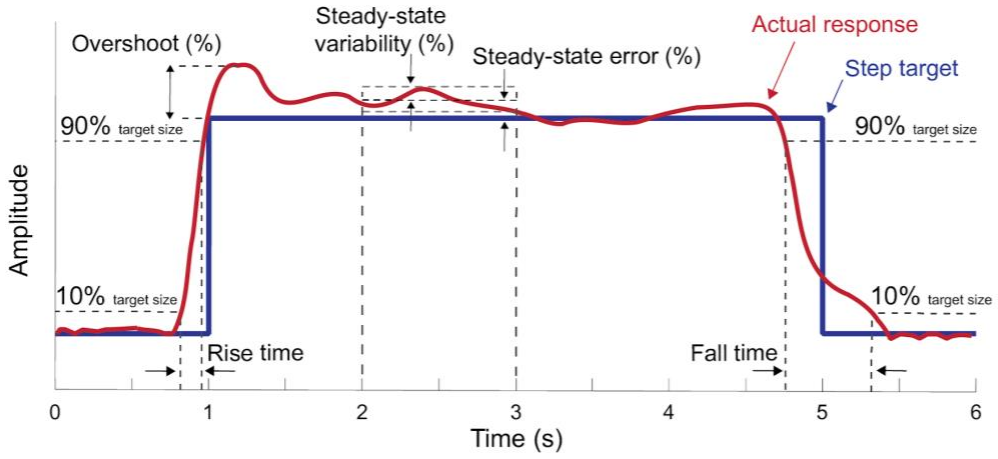

Figure 2-2 Step response characteristics. The empirical response (red line) and the step target (blue) line are shown for a single segmented target step response six seconds in length. For force-magnitude control, the step target size is in bodyweights and for force-position control, the step target size is in centimeters. The evaluated control characteristics include rise time (s), bandwidth (Hz), overshoot (%), steady-state error (%), steady-state variability (%), and fall time (s).

We used exclusion criteria to remove step responses that may poorly describe leg external force control. We used the following criteria: 1) the control response is in the opposing direction of the target step, 2) the response does not step up within 0.5 seconds after the target step function steps up, and 3) the response is already greater than 10% of the target step size value the 0.5 seconds leading up to the step-up. We removed the step responses that meet these exclusion criteria from all subsequent analyses.

2.3.5. Statistical Analysis

To estimate the fastest control performance for each participant and condition, we calculated means of step response characteristics using the five trials with the fastest rise times. We then calculated the mean and standard deviation across participants for each step response characteristic. To determine if there were differences in characteristics between different step sizes (i.e., conditions), we performed a repeated-measures analysis of variance within the force-magnitude, the medial-lateral force-position, and the anterior-posterior force-position experiments. If a difference existed, we performed pairwise comparisons between the group means to evaluate which conditions produced similar step response characteristics adjusting p-values for multiple comparisons using Bonferroni corrections [130]. We calculated the partial eta squared (η_p^2) correlation ratio

as a measure of effect size for each step response characteristic by dividing the sum of squares between conditions from the aforementioned repeated-measures analysis of variance by the total sum of squares. To understand if there were relationships between step response characteristics within each condition, we used data from every included step response, not just the five fastest responses. We used linear mixed-effects models to identify these relationships. This approach allowed for individual y-intercepts for each participant while finding a single best-fit parameter describing the slope between the two variables. We assessed the strength of a relationship using the slope magnitude, the probability that the slope is different from zero, and the R^2 value. In all cases, we used MATLAB's statistical analysis toolbox and accepted $p<0.05$ as statistically significant.

2.3.6. System modelling

To further describe the step response characteristics of leg force control, we modeled the system dynamics and used system identification to estimate the unknown parameters. As a starting point, we modelled the relationship between the commanded step response of the input, X, and the measured step response of the output, Y, as a single dynamic process comprising a time-delayed second-order linear ordinary differential equation. We modeled this system using a second-order representation as the biological response displays overshooting, which cannot be accounted for with a simpler first-order system. The mathematical representation of the proposed model takes the form:

Equation 2-1

$$\boldsymbol{Y(s) = \frac{K}{(\tau \cdot s)^2 + (2 \cdot Z \cdot \tau \cdot s) + 1} \cdot e^{-T_d \cdot s} X(s)}$$

where s denotes representation in the frequency domain. K is the gain describing the steady-state value of the output Y induced by a unit change in the input X, Z is the damping constant, τ is the time constant characterizing the rate of change of Y in response to a change in X, and T_d is the time delay (or lead time) which corresponds to the time delay (or lead time) of when the system first begins to respond. We used the five fastest step responses for each participant and each experimental condition, used only the step-up response, and fit the model to each of those step-up responses. We normalized the magnitude of each trial to unity to allow for comparisons between different step sizes. To

accomplish this normalization, we divided each step response by the size value of each step target. To fit this model to our data, we solved the unknown model parameters by using a system identification approach. This consisted of using constrained numerical optimization (fmincon, MATLAB 2019a) to minimize the squared difference between the model predicted and actual empirical response (our objective function). To estimate model step response characteristics and system parameters, we followed the same statistical procedures as with the experimental step responses. That is, we determined the step response characteristics for each model fit, averaged across step responses for each participant within each condition and then averaged again across participants within a condition. We used a repeated-measures analysis of variance within the force-magnitude, the medial-lateral force-position, and the anterior-posterior force-position models and assessed the goodness-of-fit of the estimated best-fit parameters using R^2 values.

2.4. Results

2.4.1. Step response characteristics were similar between force-magnitude and position control

When controlling the force-magnitude of the leg's external force, participants were quickest to reach the smallest target step size. At the smallest step size of 0.25 bodyweights, participants stepped up to the target at a rise time of 178$\pm$69 ms and stepped down with a fall time of 399$\pm$122 ms (Table 2-1, and Figures 2-3 & 2-4). This rise time equated to a bandwidth of 2.2$\pm$0.6 Hz. Once participants did reach the commanded target step size, they did so by overshooting it by 31.6$\pm$15.8%. Upon settling at the target, participants did so with a steady-state error of 3.9$\pm$0.4% and a steady-state variability of 4.4$\pm$1.5%. As the force-magnitude target step size increased, participants took longer to reach the target resulting in decreases in bandwidth (Table 2.1). Participants also overshot the target less and were, in general, more accurate and less variable during steady-state (Table 2-1). Fall times were always longer than rise times ($p<0.001$), and we observed no changes in fall times with increasing target step size.

The characteristics of force-position control were comparable to force-magnitude control. When participants shifted their force-position anteriorly or posteriorly, or when they shifted their force-position medially or laterally, they did so with a rise time and bandwidth that was similar to when controlling for force-magnitude. Fall times were similar to those found

for force-magnitude control and also did not change with changes in target step size for both anterior-posterior and medial-lateral control (Figures 2-3 & 2-4). As in force-magnitude control, participants overshoot the target less and were in general, more accurate and less variable during steady-state with increases in target step size in force-position control (Table 2-1)

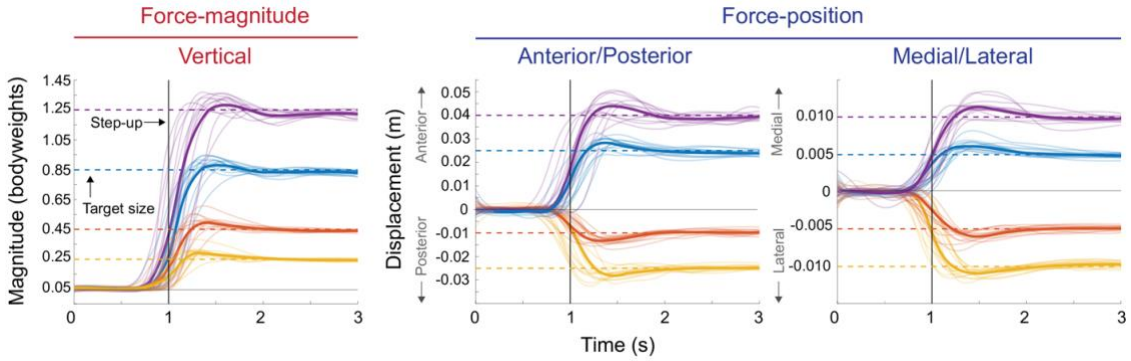

Figure 2-3 The average step-up response from each participant at each target step size (color lines) and the average of the average response (bolded color lines). The vertical line represents when the target step function steps up from its base value of 0.05 bodyweights for force-magnitude control or 0 cm for force-position control to a new target step size (dashed lines). Participants could anticipate when the step target would step up to a new target size therefore the response could precede the visual step change. Here the first second before the step-up and the two seconds after are shown. Within this time frame, we evaluated the rise time, bandwidth, overshoot, steady-state error, and steady-state variability.

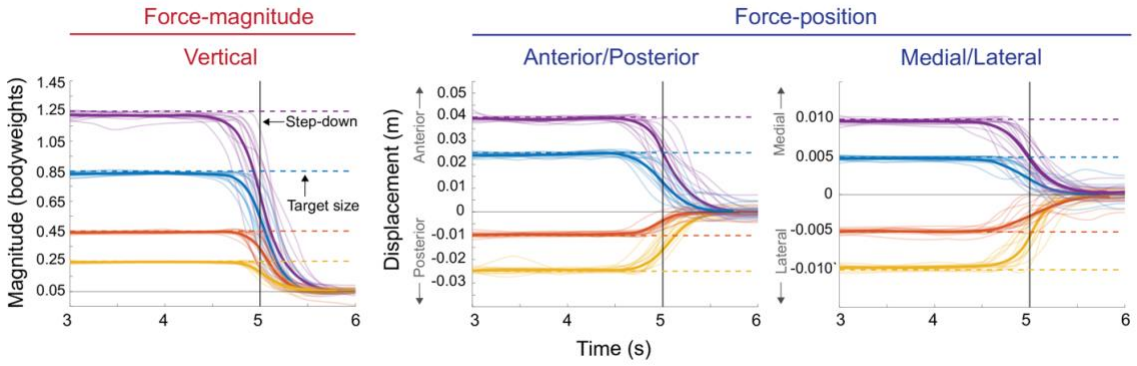

Figure 2-4 The average step-down response for each participant at each target step size (colour lines) and the average of the average response (bolded coloured lines). The vertical line represents when the step function steps down from the current step target size (dashed lines) to 0.05 bodyweights for force-magnitude control or 0 cm for force-position control (base values). Here the two seconds before the step-down are shown and the one second after the signal returns to its base value. Within this timeframe, we evaluated the fall times as participants stepped down from the step target size back down to the base value.

Table 2-1 Average control characteristics for force-magnitude and force-position control. P-values from repeated measures analysis of variance for each control metric and effect sizes (η_p^2) are presented

Vertical	**Force-magnitude control**					
Target step size (bodyweight)	Rise time (ms)	Fall time (ms)	Bandwidth (Hz)	Overshoot (%)	SSE (%)	SSV (%)
0.25	177.6 ± 69.3	399.2 ± 121.9	2.2 ± 0.6	25.3 ± 12.7	3.2 ± 1.0	3.5 ± 1.2
0.45	204.7 ± 63.5	373.8 ± 99.8	1.8 ± 0.5	17.1 ± 9.5	2.6 ± 0.9	2.7 ± 0.9
0.85	242.9 ± 92.3	389.8 ± 112.1	1.6 ± 0.5	9.8 ± 5.6	2.4 ± 1.3	2.1 ± 0.4
1.25	266.0 ± 90.5	405.5 ± 99.0	1.4 ± 0.4	7.4 ± 3.3	2.6 ± 1.3	2.5 ± 0.7
p-value	<0.001	0.8	<0.001	<0.001	0.26	<0.001
η_p^2	0.704	0.029	0.740	0.651	0.104	0.379

Anterior (+) Posterior (-)	**Force-position control**					
Target step size (cm)	Rise time (ms)	Fall time (ms)	Bandwidth (Hz)	Overshoot (%)	SSE (%)	SSV (%)
-1.0	181.1 ± 29.0	377.3 ± 155.1	2.0 ± 0.3	45.0 ± 17.8	13.9 ± 4.7	8.3 ± 2.8
-2.5	225.9 ± 47.6	417.6 ± 111.3	1.6 ± 0.3	19.4 ± 9.2	6.2 ± 2.1	3.8 ± 2.3
2.5	217.4 ± 42.6	411.8 ± 128.0	1.7 ± 0.3	20.8 ± 10.9	6.7 ± 3.3	5.0 ± 2.0
4.0	244.2 ± 46.8	423.3 ± 100.7	1.5 ± 0.3	15.8 ± 11.1	4.9 ± 2.3	4.8 ± 2.4
p-value	<0.001	0.76	<0.001	<0.001	<0.001	<0.001
η_p^2	0.5666	0.0296	0.6320	0.6186	0.6460	0.5062

Medial (+) / Lateral (-)	**Force-position control**					
Target step size (cm)	Rise time (ms)	Fall time (ms)	Bandwidth (Hz)	Overshoot (%)	SSE (%)	SSV (%)
0.5	200.4 ± 59.6	377.5 ± 103.1	1.9 ± 0.4	36.0 ± 14.1	9.1 ± 3.4	6.1 ± 2.4
-0.5	192.4 ± 39.0	312.2 ± 140.9	1.9 ± 0.3	32.1 ± 16.3	10.0 ± 4.2	5.4 ± 2.0
-1	229.4 ± 37.0	349.0 ± 115.4	1.6 ± 0.2	15.6 ± 6.2	5.5 ± 2.2	3.3 ± 1.1
1	230.6 ± 45.7	382.1 ± 114.5	1.6 ± 0.3	19.0 ± 12.8	5.9 ± 3.7	4.2 ± 2.5
p-value	<0.001	0.3	<0.001	<0.001	<0.001	0.001
η_p^2	0.2554	0.0843	0.3821	0.4440	0.3650	0.3266

2.4.2. A faster response correlated with reductions in other measures of control performance

On average, trials with higher bandwidth where faster presenting with a larger overshoot (Figure 2-5). For force-magnitude control, the relationship between the bandwidth of the response and overshooting the target was significant for all conditions ($p<0.001$). The

strongest relationship had a linear fit with an R^2 of 0.51 for target step sizes of 0.45 bodyweights, having a slope of +15.4% overshoot/Hz; the weakest relationship had a linear fit with an R^2 of 0.36 for target step sizes of 1.25 bodyweights, and a slope of +8.5% overshooting/Hz. For force-position control, this relationship was also significant for all conditions ($p<0.001$) with an average fit R^2 of 0.34 ± 0.1, and an average slope of $+17.2\pm3.6$% overshooting/Hz (representative conditions are shown in Figure 2-5). With increasing bandwidth, participants tended to be less accurate and more variable as demonstrated by increased steady-state error and variability, but these relationships were weak and not significant for most of the conditions. Finally, there were significant correlations between increases in steady-state variability and increases in steady-state error ($p<0.001$) for all the conditions for both force-magnitude and force-position control, but the fits were weak with R^2 values at best 0.34 and at worst 0.05. We found no other significant correlations between other measures of control performance.

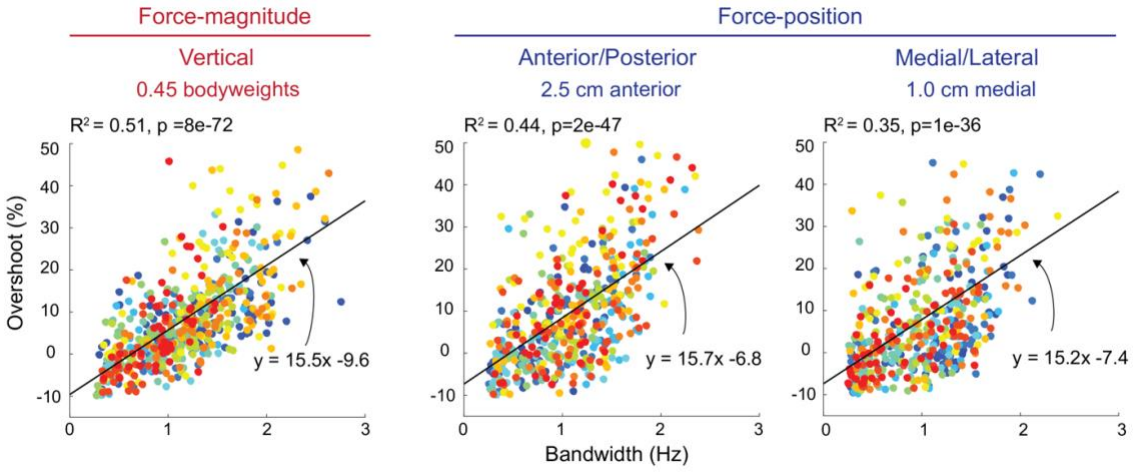

Figure 2-5 Representative findings from force-magnitude control (0.45 bodyweights), and force-position control (2.5 cm anterior and 1.0 cm medial). We fit a linear mixed-effects model to the data and plot the resultant linear fit as the black line. Each data point corresponds to the results from a single-step response while each color corresponds to a different participant. The R^2 value for the fit is shown alongside the p-value and equation of the line.

2.4.3. Leg external force control as a second-order control system

A second-order model well described the step-up control characteristics found for the control of leg external forces (Figure 2-6). Best-fit R^2 values for all step target sizes in both force-magnitude and position control were above 0.85 (Table 2-2). We chose the second-order model because the overshooting observed in the data was not a feature that could be described using a first-order model, and a third-order model was unnecessary given how well the second-order model described the observed behaviour. The second-order controller for controlling leg external force can be well approximated using the following control parameters: K (process gain) = 1, τ (time constant) = 100 ms, Z (damping constant) = 0.5, and T_d (time delay or lead time) = -100ms. A controller with these parameters has a rise time of 165 ms, a bandwidth of 2.0 Hz, overshoots by 16.3%, a settling time of 1.7s, and no steady-state error or steady-state variability.

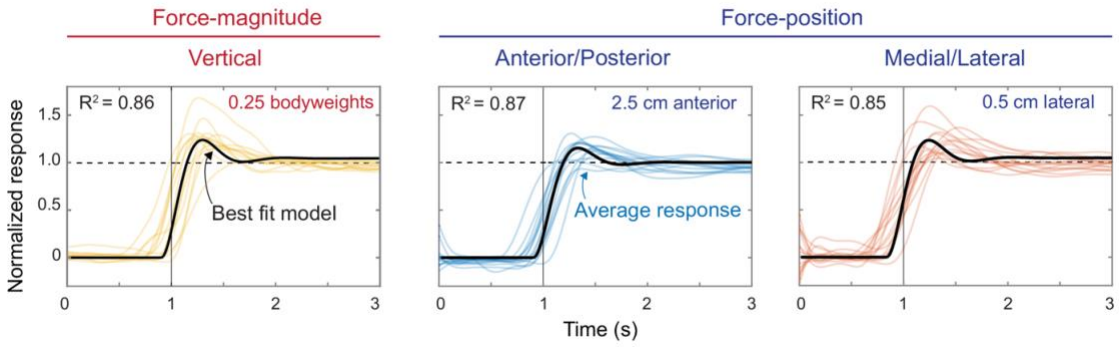

Figure 2-6 Representative modeling results for select force-magnitude and force-position target step size conditions. We plotted the second-order model using the average of the best-fitted parameters (black line) against the average of each participant's response to each step target magnitude (coloured lines). The vertical line represents when the step function steps up from zero to the normalized target value of one. The horizontal dashed line is the target step size value of 1. The R^2 value shown is the average fit of the model for that condition

Table 2-2 Average best fitting system modelling parameters describing leg force control as a second-order system. The R^2 represents the fit, K is the gain used to determine error (1 being no error in the system), τ is the time constant characterizing the rate of change of how rapidly the system changes state, Z is the damping constant where a value of < 1 indicates an underdamped system, and T_d is the time delay (or lead time) which is the time delay of when the system first begins to respond (a negative value indicates the system is predicting and responding before the step target steps up).

Force-magnitude control

Target step size (bodyweights)	R^2	K	τ (ms)	Z	T_d (ms)
x0.25	86 ± 5	1.04 ± 0.05	110.6 ± 29.5	0.5 ± 0.1	-96.4 ± 87.8
x0.45	90 ± 3	1.02 ± 0.03	103.6 ± 22.1	0.6 ± 0.1	-70.7 ± 100.5
x0.85	93 ± 2	0.99 ± 0.02	101.4 ± 17.5	0.7 ± 0.1	-56.2 ± 68.4
x1.25	93 ± 1	0.98 ± 0.03	110.7 ± 31.2	0.7 ± 0.1	-73.6 ± 104.4

Force-position control

Target step size (cm)	R^2	K	τ (ms)	Z	T_d (ms)
Anterior (+) / Posterior (-)					
-1.0	80 ± 7	1.07 ± 0.09	120.6 ± 24.4	0.4 ± 0.1	-111.1 ± 110.4
-2.5	89 ± 4	1.02 ± 0.05	116.7 ± 28.2	0.6 ± 0.2	-161.0 ± 119.0
2.5	87 ± 4	1.00 ± 0.06	116.2 ± 23.3	0.5 ± 0.1	-92.6 ± 115.4
4.0	89 ± 4	1.00 ± 0.04	119.0 ± 19.9	0.6 ± 0.1	-118.2 ± 125.7

Target step size (cm)	R^2	K	τ (ms)	Z	T_d (ms)
Medial (+) / Lateral (-)					
0.5	85 ± 5	1.07 ± 0.08	118.8 ± 20.8	0.5 ± 0.1	-124.9 ± 100.7
-0.5	85 ± 5	1.05 ± 0.09	112.6 ± 17.1	0.5 ± 0.1	-160.8 ± 94.4
-1	91 ± 1	1.02 ± 0.04	107.5 ± 13.9	0.6 ± 0.1	-135.1 ± 101.1
1	89 ± 6	1.03 ± 0.05	118.4 ± 21.9	0.6 ± 0.1	-112.1 ± 80.9

2.4.4. Practice trials were effective at training participants to perform the task

To determine whether the amount of training was sufficient for participants to reach state-state, we compared the performance of their last 15 practice steps to the 15 steps immediately prior. We found no significant improvements in the rise times when comparing these two sets of trials in either the force-magnitude task trials (average difference of 17±275 ms, p=0.40) or the force-position control in the anterior/posterior direction (average difference of 2±392 ms, p=0.93) and the medial/lateral direction (45± 377 ms, p=0.09). The allotted practice appears sufficient for participants to have reached a steady-state level of performance.

2.4.5. Removing visual feedback resulted in specific and modest increases in performance

To test whether the task's reliance on visual feedback affected force control performance, our protocol periodically eliminated the step that was displayed on the screen, removing the participant's ability to use visual feedback. For force-magnitude control, we found that participants were indeed faster without visual feedback. When comparing the rise times that participants stepped up to the step target without visual feedback to that with visual feedback participants were on average 19% faster (p=0.02) for a step target size of 0.25 bodyweights, 15% faster (p=0.04) for a step target size of 0.45 bodyweights, 13% faster (p=0.02) for a step target size of 0.85 bodyweights, and 10% faster (p=0.13) for a step target size of 1.25 bodyweights. This increase in speed with the removal of visual feedback did not carry over to force-position control—we found that participants were, if anything, slower at controlling external force-position for either the anterior/posterior and medial/lateral control at all target step sizes.

2.4.6. Prioritizing speed over accuracy increased control responsiveness but reduced accuracy

To determine how quickly force could rise when the speed of the response was prioritized over the accuracy, one participant performed a force-magnitude control experiment stepping up to a target step size as fast as possible under instructions that removed the need to hold an accurate steady-state force level. Under these conditions, this participant had a rise time of 121±28 ms, a bandwidth of 3.0±0.49Hz and overshot the target by

50.7±19.5%. This rise time was ~100% faster than when completing it under the previous instructions (rise time of 243±92 ms) where we emphasized the need for both speed and accuracy. We observed a more than five-fold increase in overshooting the target value over completing this task under previous instructions (overshot by 9.8±5.6%) indicating a reduction in the accuracy.

2.5. Discussion

Here we characterized people's ability to control leg external forces. We found that people could control the vertical magnitude of the force that they applied to the ground, and the position of that force, by responding to and closely matching commanded step changes. For both force-magnitude and position control, we observed similar control performance in terms of responsiveness and accuracy. We also observed that increases in responsiveness correlated with reductions in other measures of control performance, such as a greater magnitude of overshooting. We modeled the observed control performance and found that a second-order model was a good predictor of external leg force control. On its own, this model could be used to make predictions about step sizes that we didn't test experimentally, or the tracking of targets that are not simple step functions (e.g., a sine wave)

Our study has several limitations. One limitation is that compliance—both within our participants' bodies and within the apparatus itself—may have slowed the change in measured force-magnitude and position. To address this, we designed the apparatus using high-density padding at the contact points and adjustable scissor jacks that allow us to tightly secure each participant within the apparatus. We also reduced the possible bending of the apparatus itself by using stiff aluminum for the frame and bolting the rig securely to our laboratory floor. While it is impossible to entirely remove the effect of compliance, we aimed for our design to render the effect small.

A second limitation is that reliance on visual feedback may have slowed measured control performance. Visual feedback loops have longer loop delays when compared to spinal reflex loops, and spinal reflexes are perhaps sufficient for the neural control of leg force during tasks like running [131], [132]. Consequently, in part of our experimental design, we tested to see if control without visual feedback would be significantly faster. Indeed, we found that trials that did not rely on visual feedback were modestly faster suggesting

that our measurements are a reasonable but slightly slow approximation of control performance when controlling leg external forces with faster spinal reflexes.

A third limitation is that our experiment may not adequately capture the control approach our nervous system is using when having to rapidly control leg external forces. In support of this possibility, sprinters run with a step frequency above 4 Hz [133] whereas our experimental results suggest that force control bandwidth should not exceed about 2 Hz. One mechanism for faster control is to not rely on visual or even spinal reflex loops but instead for the nervous system to estimate the motor commands in advance and execute them in a feedforward manner. To test whether force control could indeed be performed more rapidly when the need for feedback is removed, we instructed a single participant to prioritize leg force control responsiveness over accuracy when following commanded step changes in force. We found an increase in responsiveness of ~100% but a five-fold decrease in accuracy suggesting that controlling external forces in a feedforward manner can be considerably faster than when relying on feedback control but is much less accurate. As feedback is essential for accurate performance in the face of uncertainty, this observed increase in performance is likely an overestimate of the combined feedforward and feedback approach our control system likely employs under most situations [134],[28]. Future experiments are required to better support these hypotheses.

Sensorimotor delays may limit responsiveness of leg external force control. An inherent property of biological control systems is that there are neural delays associated with sensing and transmitting neural information, and muscular delays associated with force generation. Neural delays arise from the times required to sense a stimulus, transmit neural signals along the length of nerves, and cross synapses [31], [32]. Muscular delays arise from the times required for conducting action potentials along muscle fibres, generating muscle force, and muscle shortening to stretch tendons that act in series [31], [32]. Using scaling relationships from other terrestrial mammals, we estimate the human delays to be approximately 1 ms for sensing, 20ms for sensory nerve conduction delay, 1 ms for crossing a single synapse in the spinal cord, 20 ms for motor nerve conduction delay, 1ms for crossing the neuromuscular junction, 10 ms for the electromechanical delay, and 40 ms for the force generation delay [31], [32]. This equates to an estimate of the total human sensorimotor delay of ~90 ms, which corresponds well to estimates derived from human measurements [135]–[137]. Both feedback and feedforward control of leg external force must contend with the presence of sensorimotor delays which may

set limits to responsiveness. In the feedback control approach, if the delays grow too large relative to the period of the movement, this could destabilize the system as the control signals become outdated, and the motor commands generated are no longer appropriate. To remain stable, a delayed feedback controller must use low gains resulting in low generated forces and a responsiveness that is potentially much slower than the delay itself. This may explain why a 90 ms sensorimotor delay results in controlled step changes in force that we measured here, which have a minimum period of ~500ms (2Hz bandwidth). Feedforward control of external force can generate faster responses because delays do not affect its stability. But the rate at which our muscle actuators can change between different force levels is still slow thus also limiting the bandwidth of feedforward control.

Sensorimotor noise may limit leg external force control accuracy. Like delays, there are many sources of noise in our neuromechanical system with contributions from both neural and muscular sources. Neural sources of noise arise during the processes associated with determining movement-appropriate motor commands. These include but are not limited to noise in the uncertainty of sensory feedback, and probabilistic behavior of both cellular and synaptic signal transduction [138], [139]. Muscular sources of noise arise during the transformation of motor commands to the contraction of muscles. Variability in the temporal structure of the motor commands and in the recruitment properties of motor units result in muscular noise [140]. Even when motor commands are perfectly timed, there is natural variability in the muscle forces arising from the stochastic nature of the contraction of sarcomeres within muscle tissue [138]. The net effect of this sensorimotor noise is that for a fixed command to the muscles, there is variability in force output. This sensorimotor noise is believed to limit performance in various human motor control tasks. For example, in goal-directed arm movements, variability in the endpoint position has been shown to be related to sensorimotor noise in the execution of the movement [139]. In isometric force production of the fingers, increases in external force magnitude show increases in force variability [140]. As with these other tasks, sensorimotor noise may limit the accuracy of leg external force control to the levels we measure here.

Measurements of force control performance may help in understanding differences in agility between humans and engineered systems, between humans and other animals, and between humans and other humans. The effective control of leg external forces in humans appears to be much slower and less accurate when compared to some legged-

engineered systems [111]. For example, the legs of the MIT cheetah robot have a force-magnitude bandwidth of ~100 Hz—about 50x faster than what was found in our experiment—and nearly no steady-state error or steady-state variability [124], [141]. Wearable devices such as foot prostheses and leg exoskeletons demonstrate millisecond-scale control, enabling accurate and rapid control of force [126], [142]. Yet the agility of humans continues to be greater than that of state-of-the-art legged robots suggesting that human agility is achieved not through a greater control of leg forces, but by a greater understanding of what forces to apply. This may not hold true for comparing humans to other agile animals, such as gazelles or cheetahs, which may understand what forces to apply to the ground as well or better than humans. And in some cases, better control of external forces may be responsible for the greater agility of some animals over other less agile animals. The same may hold true for more agile athletes over less agile athletes, and for the changes in agility that come with fatigue, injury, disease, and age. Our work here is a benchmark for force control performance in young healthy humans to better enable these future comparisons.

Chapter 3.

Neuromuscular fatigue reduces responsiveness when controlling leg external forces.

3.1. Abstract

In legged movement, our legs push against the ground, generating external force vectors that enable agile movements. Neuromuscular fatigue can reduce agility by causing physiological changes, such as slowing muscle reaction time, altering proprioception, and delaying neuromuscular control. Fatigue may deteriorate the nervous system's control of leg external forces, contributing to reductions in agility. In this study, we investigated the effect of fatigue on the nervous system's performance in controlling the vertical component of leg external force ground reaction forces. We hypothesized that increased leg fatigue would lead to declines in both the responsiveness and accuracy of leg force control. To test this hypothesis, we used an apparatus that allowed participants to exert controlled vertical forces with one leg against a force plate while immobilizing the rest of their bodies. Participants adjusted their leg external force to match step targets displayed on a screen. We induced fatigue by having participants maintain submaximal leg forces, and we measured leg force control performance between fatigue trials. Results showed a significant 26% reduction in mean maximum force production, leading to a substantial decline in leg force control responsiveness, as evidenced by a 23% increase in rise time and a 25% narrowing of bandwidth. However, fatigue did not significantly reduce leg force control accuracy. Understanding the effects of fatigue on leg force control can inform the development of strategies and technologies to sustain agile performance, even in the presence of fatigue.

3.2. Introduction

One-way legged animals, including humans, demonstrate agility is through effectively controlling external leg forces. We can push against the ground with any part of our bodies, but we often do this using our legs to push our feet against the ground. The resulting environmental reaction force, a vector quantity, accelerates our bodies. Here we consider the rapid and accurate control of the external force vector to be agility [15]. Examples of legged agility include accelerating from a standstill, jumping high and far over obstacles, and quickly changing movement direction, all of which require effective control of our leg's external forces.

Neuromuscular fatigue reduces agility. Fatigue leads to a decline in muscle force-generating capabilities [52] and reductions in maximum muscle shortening velocities [143], [144]. As mechanical power is the product of both force and shortening velocity, fatigue

reduces maximum muscle power [52]. The effect of fatigue on muscle power and agility is well-documented in sports performance, particularly in rapid change-of-direction sports like soccer and basketball [12], [64], [65]. For example, fatigue reduces power in jumping, leading to jumps of shorter distances and lower heights [53]–[55], [145], [146]. A second example is sprinting, in which high performance relies on fast-twitch muscle fibres. These same fibres are also the most susceptible to fatigue, leading to declines in speed in the final meters of a 100-m race [57]–[60]. Other physiological changes that may arise from fatigue include slowing of muscle reaction time [42], altering of proprioception [44], and delaying our neuromuscular control in ways that reduce the control of muscles [56]. The physiological changes described are some of the mechanisms that may explain reductions in agility and deteriorate the nervous system's control of the leg's external forces. In support of this idea, soccer players show a reduced ability to complete legged balancing tasks on unstable surfaces when fatigued [61].

Our study aimed to characterize the effect of fatigue on the nervous system's ability to rapidly and accurately control vertical external leg forces. We hypothesized that increased leg fatigue would deteriorate the leg's control of submaximal vertical external forces, characterized by reduced responsiveness and accuracy. We refer to responsiveness as to how quickly a person can control the magnitude of leg vertical external force when presented with a target force level, while we refer to accuracy as how close and variable their controlled force is to and around an intended target value. To test this hypothesis, we built a custom apparatus that constrained participants' bodies from moving, allowing their legs to maintain a static posture while controlling the external vertical force magnitude below their feet. We fatigued participants by having them hold submaximal vertical leg forces equal to 25% of their maximum voluntary external force and measured the leg’s force control performance between fatigue trials in matching commanded changes in force. We quantified fatigue as reductions in vertical force during maximal voluntary leg contractions, increases in force variability, and a shift to lower mean frequencies in leg muscle activity. To quantify force control performance, we instructed participants to best match visually-displayed target step changes in vertical force magnitude by pushing more or less against a ground-mounted force plate. We evaluated control performance based on how responsive and accurate participants were in matching their leg's external force vertical magnitude to the commanded target changes in vertical force.

3.3. Methods

3.3.1. Participants

We recruited 18 participants for the study (identifying as female: n = 11, identifying as male =7; age: 26.5±3.8y; body mass:74±16 kg; height: 171±12 cm; shoe size: 9+2 US sizing; mean±std). The Office of Research Ethics at Simon Fraser University approved the study. Participants provided us with verbal and written informed consent before participating.

3.3.2. Experimental Design

To characterize human leg force control, we tested the step response of participants as they selectively controlled external leg force. We used a custom apparatus (Figure 3-1) that we had previously built [15]. The apparatus consisted of a ground-embedded force plate (Bertec Corporation, Ohio, USA) that participants stood on, constrained in both the vertical and horizontal directions. The force plate was connected to a computer through a data acquisition unit (USB-6229, National Instruments Corporation, Texas, USA), which sampled data at 1000 Hz. Participants could exert a variable but controlled external force vector onto the ground by selectively pushing down with their leg. Our device has rigid supports that constrain participants at the shoulders and forearms, preventing vertical and horizontal movement of their upper body. Although control of force-position in the medial-lateral and anterior-posterior directions (i.e., center of pressure control) and control of all three orthogonal force magnitude components of the external force vector is important, our work here focused only on controlling vertical force magnitude. In our prior work, we characterized the control of different step sizes of medial-lateral and anterior-posterior force positions and the control of a range of sub-maximal vertical force magnitudes. We found negligible differences in control characteristics for these different components of the external force vector [15]. By focusing on only the vertical component of force, we believe our findings will represent the range of control characteristics for all aspects of controlling the external force vector at submaximal forces and any control changes resulting from fatigue.

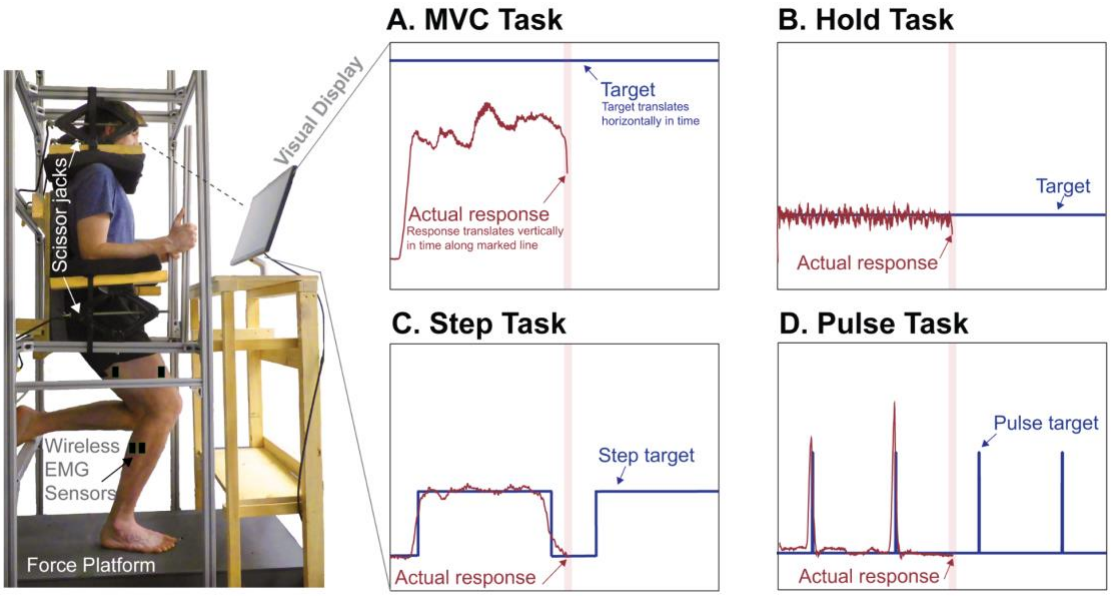

Figure 3-1 Apparatus used to characterize external force control and fatigue participants. The setup consisted of adjustable scissor jacks that constrained the vertical and horizontal motion of the participants' torso, pressing down on their shoulders and against their forearms, and a stiff 80/20 aluminum frame securely mounted to the ground. Each participant stood on their right leg in a posture resembling the mid-stance phase of a run and applied a vertical force to the ground by pushing down with their foot onto a force platform. The real-time feedback displayed to the participants showed the vertical force they were applying to the ground, as well as the target they were trying to match. There were four different tasks with four distinct visual targets: A. the MVC Task, which involved pushing down maximally for 10 seconds while trying to reach a motivating but unattainable target (5.0 BW); B. the Hold Task, which required participants to match a target equivalent to 1.4 times their body weight (1.4 BW) for 73 seconds; C. the Step Task, which involved rapidly and accurately controlling vertical force to match 10 upcoming step targets in 73 seconds; and D. the Pulse Task, which required participants to rapidly match 10 upcoming step targets in 73 seconds by changing their vertical force to match a target force that approximated a pulse.

To objectively quantify fatigue, we recorded electromyography (EMG) from the leg muscles of each participant. We placed wireless EMG sensors (Delsys, Natick, USA) on the middle of the muscle belly on the vastus medialis, vastus lateralis, rectus femoris, bicep femoris, gastrocnemius medialis, and gastrocnemius lateralis of the right leg muscles of each participant. Before placing the sensors, we prepared the location by removing any excess hair using a razor and rubbing it down with an alcohol swab. We synchronized our EMG system with our force plate using a custom code, which triggered

the collection of both force plate and EMG data. We used an EMG sampling rate of 2000 Hz.

After placing the EMG sensors, we fitted participants into the experimental apparatus. When fitting participants, we adjusted the apparatus such that participants maintained an approximately 15-degree knee flexion angle in their right leg, a posture similar to that assumed by a runner at the start of the stance phase [15], [128]. In this fitting process, we moved components of the apparatus to push down on the participant's shoulders and up on their arms by manually rotating four scissor jacks (Figure 3.1). Our goal was to ensure that we fixed participants tightly within the apparatus and were unable to move side-to-side or vertically.

To assess the effects of leg fatigue on the control of leg external force, we commanded four types of force control tasks. Participants stood on their right leg in all tasks unless otherwise instructed. We used visual feedback to allow participants to compare their actual vertical force magnitude to a target that we instructed them to match. We provided real-time visual feedback using a monitor, where our custom-developed software displayed both the real-time feedback of the vertical force magnitude signal that the participant's foot exerted onto the force plate and the target that the participant tried to rapidly and accurately match. For visual display, we normalized the real-time signal to each participant's body weight and filtered the raw force signal using a low-pass fourth-order Butterworth filter with a cut-off frequency of 10 Hz. We programmed the real-time signal to display at the center of the screen and constrained it to only move up and down as the participant pushed more or less against the force plate. We programmed the target to slide past the real-time signal, giving participants time to view any upcoming changes in the target before they occurred.

In the first force control task, the Maximum Voluntary Contraction Task (MVC Task), we evaluated the maximum effort of voluntary force that the leg could exert on the ground. To collect the MVC Task, we asked participants to push down against the ground as hard as possible and try to reach an unattainable target of 5 times their body weight (5.0 BW) displayed on the screen. From pilot experiments, we found that providing participants with a target to reach, even if it was not attainable, motivated them to push harder to try and reach it. Each MVC Task lasted 10 seconds as participants pushed down with their foot against the ground as hard as they could.

We designed the second force control task, the Hold Task, to fatigue each participant's right leg. In the Hold Task, we asked participants to match and hold a target equal to their body weight plus 25% of their pre-fatigue maximum voluntary contraction, as determined in the MVC Task before the onset of any leg fatigue [147]. This type of sustained voluntary contraction progressively recruits more motor units and leads to muscle fatigue in the active muscles [147], [148]. For each Hold Task, we asked participants to hold their force level to the best of their ability to match the target for 73 seconds, the same duration as the third leg force control task.

In the Step Task, the third leg force control task, we probed force control characteristics by commanding target step changes in leg vertical force magnitude. Because both initial speed to the new target and steady-state accuracy around the new target are objectives, we anticipate that the nervous system will depend on feedback control to accomplish this task. In a single Step Task, the target step function consisted of a square wave of ten matching size target steps, each 4 seconds long, with 3 seconds between steps (totalling 73 seconds per task). The lower value of the step target was 1.0 BW (i.e. standing upright on one leg), and the upper value (i.e., the size of the target) was 1.4 BW. We selected the target step size based on a previous experiment where we studied step responses by commanding a range of target step sizes, both smaller and larger than the magnitude chosen here [15]. We observed minor changes in control characteristics between targets of varying step sizes, so we chose an intermediate step size for this experiment.

In the fourth force control task, which we called the Pulse Task, we aimed to probe rapid force control by asking participants to respond as rapidly as possible to changes in the target. Because this task emphasizes the initial speed of response over steady-state accuracy, we anticipate that the nervous system will emphasize feedforward control over feedback control when accomplishing this task [149]. The target in this task resembled a pulse, changing momentarily for 0.05s from 1.0 BW to the target step size of 1.4 BW (the same step size as in the Step Task). In a single Pulse Task, we programmed the target pulse to go from body weight to the target step size ten times over 73 seconds.

3.3.3. Experimental Protocol

We conducted the experiment in a single session. The session included five conditions: Training, Pre-Fatigue, Fatigue-1, Fatigue-2, and Fatigue-3 (Figure 3-2). We started the

study with the Training condition to familiarize participants with the experiment. In this condition, we explained and demonstrated how the visual feedback and force plate pushing worked. Then, we asked each participant to perform two repetitions of the MVC Task followed by three repetitions of the Step Task. From our previous work, we believe this is enough training in the apparatus to eliminate any learning effects. After the Training condition, we gave participants a 1-minute break to stand freely on both feet in the apparatus. Next, in the Pre-Fatigue condition, we had participants perform two repetitions of the MVC Task followed by a 1-minute break, then three Step Tasks followed by a 1-minute break, and then two Pulse Tasks. We then gave participants a 1-minute break to rest before the next condition. Next, we started the sequence of three fatigue conditions. Each Fatigue condition consisted of a Hold Task followed by an MVC Task, which was repeated three times within each Fatigue condition. After the third and final MVC Task in each Fatigue condition, we immediately had each participant perform three repetitions of the Step Task to probe force control. For each Fatigue condition, we repeated this same sequence of tasks. On the third Fatigue condition and after the final Step Task, participants performed two Pulse Tasks. We gave participants a 1-minute break between Fatigue conditions.

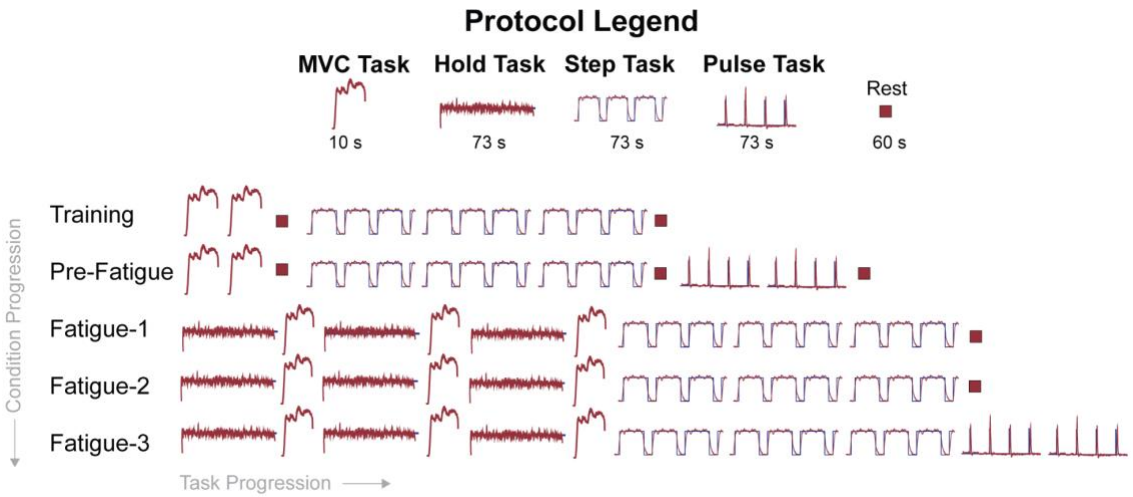

Figure 3-2 A schematic of the experimental protocol, which consisted of 5 conditions: Training, Pre-Fatigue, First Fatigue, Middle Fatigue, and Final Fatigue. Each condition was composed of a combination of our force control tasks: Maximum Voluntary Contraction MVC Task, Hold Task, Step Task, and Pulse Task. The progression within each condition is shown as going from left to right, and the progression of conditions goes from top to bottom, starting from Training and finishing with Final Fatigue.

3.3.4. Data Analysis

For each MVC Task, we evaluated the mean vertical force output as one objective measure of fatigue (Figure 3-3-A). We quantified the mean vertical force output by taking the average of the signal during the midway point of the MVC Task between the 4-8 second time interval.

For each Hold Task, we evaluated the force variability of the response (Figure 3-3-B). We segmented each Hold Task data into one-second segments to quantity changes over time. We omitted any further analysis from the first 5 seconds of this signal as participants adjusted their vertical force to match the target during this time frame. For each 1-second segment, we then quantified force variability by calculating the standard deviation of the signal during each 1-second segment, dividing this by the mean of the signal during that time frame and multiplying this value by 100. This expresses variability as a percentage of the force magnitude.

For each step response, within each Step Task, we evaluated the responsiveness in controlling leg external force (Figure 3-3-C). To accomplish this, we took step data from

each Step Task and segmented it into ten individual step responses such that each segmentation consisted of a six-second single-step response, with one second before the step-up and one second after the step-down. For each step response, we evaluated the rise time (in units of milliseconds) as the time for the signal to go from 10% to 90% of the target step size value [15]. We calculated bandwidth (in units of Hz) by dividing 0.35 by the rise time [129]. The bandwidth measures the maximum frequency at which a target signal can change and still be accurately tracked by the controller. We remind readers that as we calculate bandwidth using rise time, bandwidth is not an independent measure of responsiveness but depends on any changes in rise time. We restricted our evaluation of the rise time and bandwidth of the response to the time interval of 0.5 seconds before the step target stepped up to its high value and up to one second after the step-up occurred. Finally, we quantified fall time (in units of milliseconds) as the time for the signal to go from 90% to 10% of the target step size value. We evaluated the fall time between four to six seconds when the step signal stepped down from the target step size to 1 BW. In this chapter, we use the term responsiveness to refer to rise time, bandwidth, and fall time. In robotic systems, and how we think of responsiveness in this thesis, a responsive system that is capable of high-fidelity tracking of a target possesses a short rise time, a wide bandwidth, and a short fall time [150].

For each step response, within each Step Task, we evaluated the accuracy of controlling leg external force (Figure 3-3-C). We quantified overshoot by taking the peak value reached by the signal, subtracting the value of the target step, dividing this by the size of the step, and multiplying by 100. We expressed overshoot as the percentage that the signal exceeds the target step size value. A large overshoot can indicate under-damping in the controller—it can take longer for the system to settle into a steady state, but it may be faster to reach its target step size [15]. We restricted our evaluation of the overshoot of the response to the time interval of 0.5 seconds before the step target stepped up and to one second after the step-up occurred. Next, we quantified steady-state error by calculating the mean value of the signal between 2-4 seconds, subtracting the value of the target step size, and taking the absolute value. We divided this by the value of the target step size and multiplied it by 100 to express the steady-state error as a percentage of the target value. The steady-state error informs us how much error the control system has once it has reached the target size value and settled in its new state. A large error can be indicative of poor control as the system is not able to well match the target value. We

quantified steady-state variability by calculating the standard deviation of the signal between 2-4 seconds, dividing this by the steady-state mean and multiplying this value by 100. The steady-state variability, expressed as a percentage of the steady-state mean, informs us how variable the system is once it has reached and settled on its new state. From pilot studies, we found that using the 2-4 second interval to measure steady-state error and steady-state variability was a sound assumption as participants had at this point reached a steady state. In this chapter, we use the term accuracy to refer to overshoot, steady-state error, and steady-state variability—an accurate system has small overshoot, small steady-state error, and small steady-state variability. We collectively refer to the rise time, bandwidth, overshoot, steady-state error, steady-state variability, and fall time as the step response characteristics.

For each Pulse Task, we evaluated the responsiveness of the response (Figure 3-3-D). To accomplish this, we took the data from each Pulse Task and segmented it into ten individual step responses such that each segmentation consisted of a 3-second single-step response, with 1.5 seconds before the step-up and 1.5 seconds after the step-down. Following the same definitions of responsiveness as for the Step Task, we quantified the rise time, bandwidth, and fall time for each step in every Pulse Task.

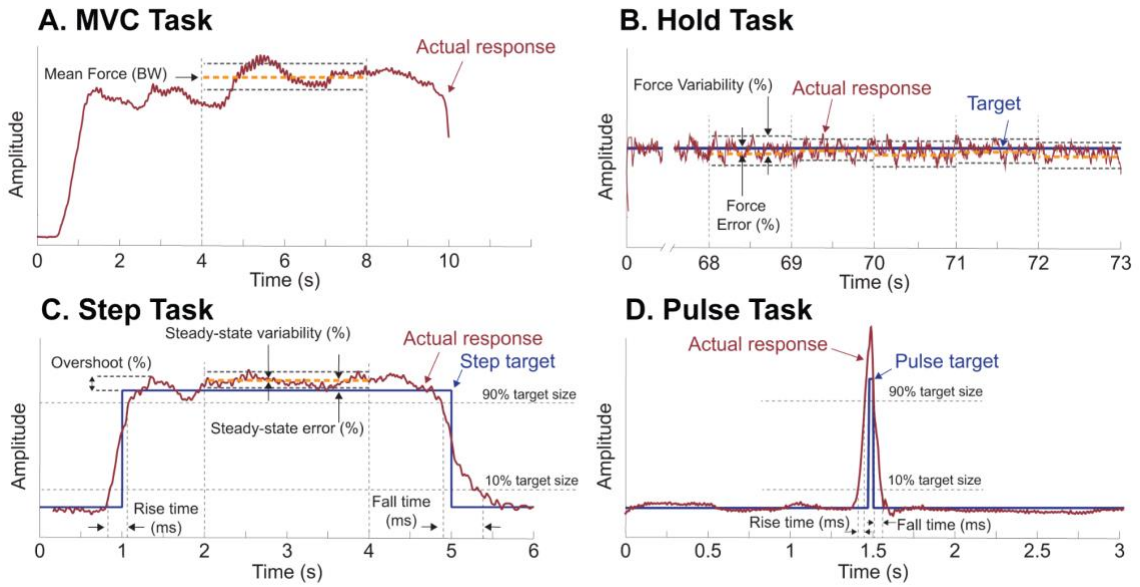

Figure 3-3 A visual analysis of the four leg force control tasks evaluated during the experiment. A. In the MVC Task, we evaluated the mean force of the signal between 4-8 seconds. B. In the Hold Task, we omitted any analysis during the first 5 seconds but calculated force variability for each 1-second interval for the duration of the task. C. We evaluated the responsiveness (rise time, fall time, bandwidth) and accuracy (overshoot, steady-state error, steady-state variability) for each step response in the Step Task. D. For each Pulse target in the Pulse Task, we evaluated the responsiveness.

We analyzed the EMG data to quantify changes in muscle frequency, one objective measure of fatigue. We used a fourth-order zero-lag Butterworth filter for bandpass filtering between 30 and 400 Hz, effectively reducing non-muscular noise and motion artifacts [29]. Next, we used a bandstop filter between 57–63 Hz to eliminate any lingering 60 Hz powerline interference. Following the filtering process, we transitioned to frequency analysis by calculating the EMG median frequencies, an acknowledged metric of local muscle fatigue [151]. To enable this calculation, we transformed the time-domain signal into the frequency domain using fast-Fourier analysis, which permitted us to compute the power spectrum. Subsequently, we calculated out the median frequency [152], [153]. A trend of decreasing median frequencies over time is typically regarded as a sign of local muscle fatigue, although it may also signify other changes, such as changes in motor unit recruitment [152], [154].

We used exclusion criteria for the Step Tasks and Pulse Task to remove responses that may poorly describe the measured response. For the Step Task, we used the following

criteria: (1) the response steps up 0.5s before the target step function steps up, (2) the response does not step up within 0.5s after the target step function steps up, (3) the response is already greater than 10% of the target step size value during the 0.5s leading up to the step-up (4) the response steps down 1s or more before the target step function steps down. For the Pulse Task, we used the following criteria: (1) the response rises up 0.25s before the pulse target steps up, and (2) the response does not fall down until greater than 0.25s after the pulse target steps down. We removed the step responses that meet these exclusion criteria from all subsequent analyses.

3.3.5. Statistical Analysis

To determine the effects of our protocol on fatigue, we evaluated several objective measures. The first measure we evaluated was changes in mean force magnitude during the maximum voluntary contraction (MVC) task. A decrease in maximum vertical force is one indicator of fatigue [148]. To calculate this measure, we compared the mean force values from the final MVC tasks completed in each condition for each participant. Our second measure was force variability during each of the consecutive Hold Tasks in each fatigue condition. Increased force variability as fatigue progressed is an indicator of local muscle fatigue [155], [156]. To calculate this measure, we compared the mean force variability for the final ten seconds of each Hold Task repeated in each fatigue condition for each participant. To estimate force variability before the onset of fatigue (referred to as "Pre-Fatigue"), we also calculated the mean force variability for the first ten seconds of the Hold Task in the first Fatigue-1 condition. Our third measure was reductions in median EMG frequency. As with force variability, we compared the mean of the median EMG frequencies determined for the first ten seconds before the onset of fatigue and the final ten seconds of each fatigue condition. To evaluate the effects of our protocol on leg external force control, we next determined step response characteristics. For all conditions, we took the mean value of each step response characteristic for the first five Step Task responses for each participant immediately following the final MVC task. We used the same approach to characterize step response characteristics for the Step Task and the Pulse Task. To determine if there were differences in mean values between conditions, we performed a repeated-measures analysis of variance. If a significant difference was found, we conducted post hoc pairwise comparisons between the group means to identify which conditions produced similar mean values. We adjusted p-values

for multiple comparisons using Bonferroni corrections. In all cases, we used MATLAB's statistical analysis toolbox and accepted $p<0.05$ as statistically significant. Unless otherwise stated, we present all data in the text as mean± standard deviation

3.4. Results

3.4.1. Participants fatigued during the protocol

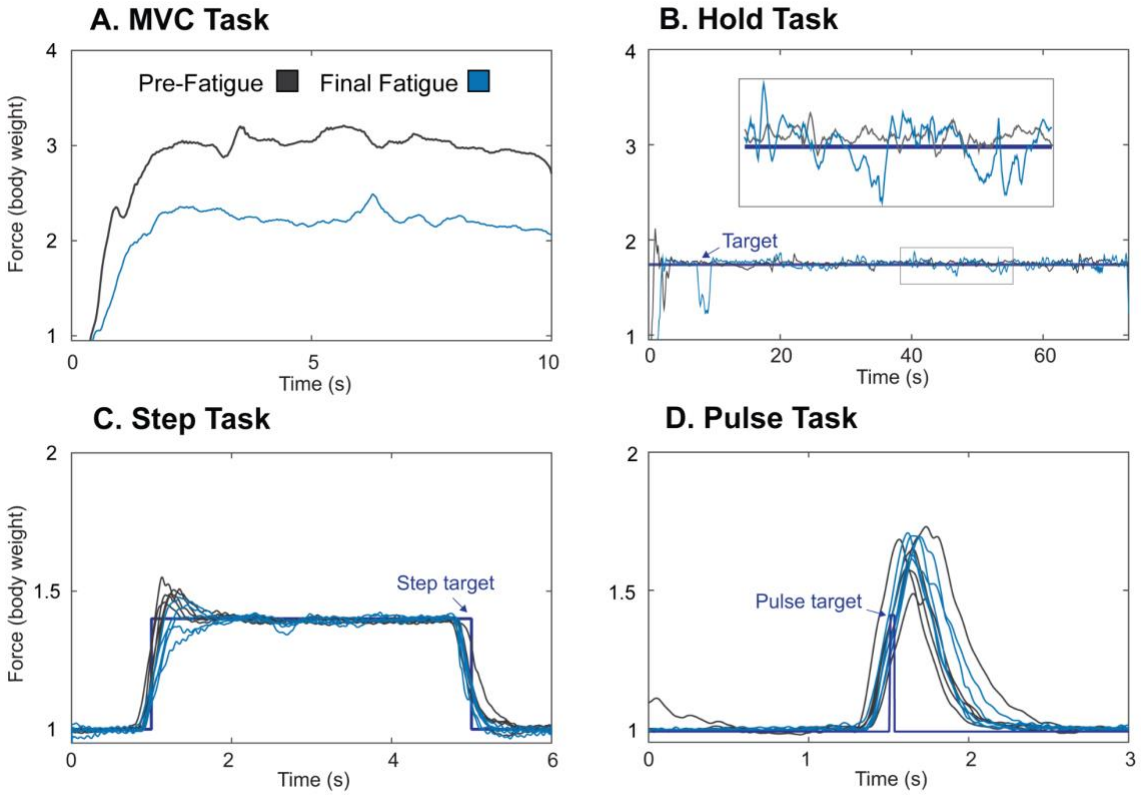

Figure 3-4 Representative data for one participant comparing the Pre-Fatigue (grey) and Final Fatigue (blue) conditions for the A. MVC Task, B. Hold Task, C. Step Task, and D. Pulse Task. For C. and D., the first five responses immediately following the final MVC Task in each condition are shown. As the participant progressed through the protocol, they exhibited fatigue, as indicated by a reduction in force for the MVC task and increased force variability during the Hold Task.

Objective measures of fatigue demonstrated that participants were fatigued during the protocol. Task data for a representative participant are shown in Figure 3-4. Fatigue was demonstrated by a reduction in the mean maximum MVC force (Figure 3-4A). As participants progressed through the protocol conditions, they exhibited significant

reductions (p=1.3e-12) in the mean force magnitude during the MVC Tasks (Figure 3-5-A). During Pre-Fatigue, participants on average exerted a vertical mean leg force of 2.95±0.58 BW and by the final fatigue condition, participants exerted a mean force of 2.20±0.47 BW, a significant (p=4.7e-6) reduction of 26% in mean maximum force production. Next, we found significant increases in force variability (p=0.002) as participants progressed through Fatigue conditions executing the Hold Tasks (Figure 3-5-B). During Pre-Fatigue, participants had a mean force variability of 0.61± 0.31% and by the final condition, participants had a mean force variability of 2.83±2.93%, a significant (p=0.027) increase of 368%. Finally, we found significant reductions in the mean, median frequency for several muscles, specifically the gastrocnemius lateralis (p=0.002), gastrocnemius medialis (p=0.0019), and the bicep femoris (p=0.003) (Figure 3-5-C). Comparing the Pre-Fatigue to the final fatigue condition, the gastrocnemius lateralis medialis exhibited a significant (p=0.016) reduction of 10% in frequency reducing from 126±24 Hz to 113±27 Hz; the gastrocnemius medialis exhibited a significant (p= 0.048) reduction of 10% reducing in frequency from 133±28Hz to 119±34Hz; and the bicep femoris exhibited a reduction of 11% reducing in frequency from 90±12Hz to 79±13Hz, but this only approached but did not reach significance between these two conditions (p=0.074). The other three muscles (vastus lateralis, vastus medialis, and rectus) showed no significant changes in EMG median frequency.

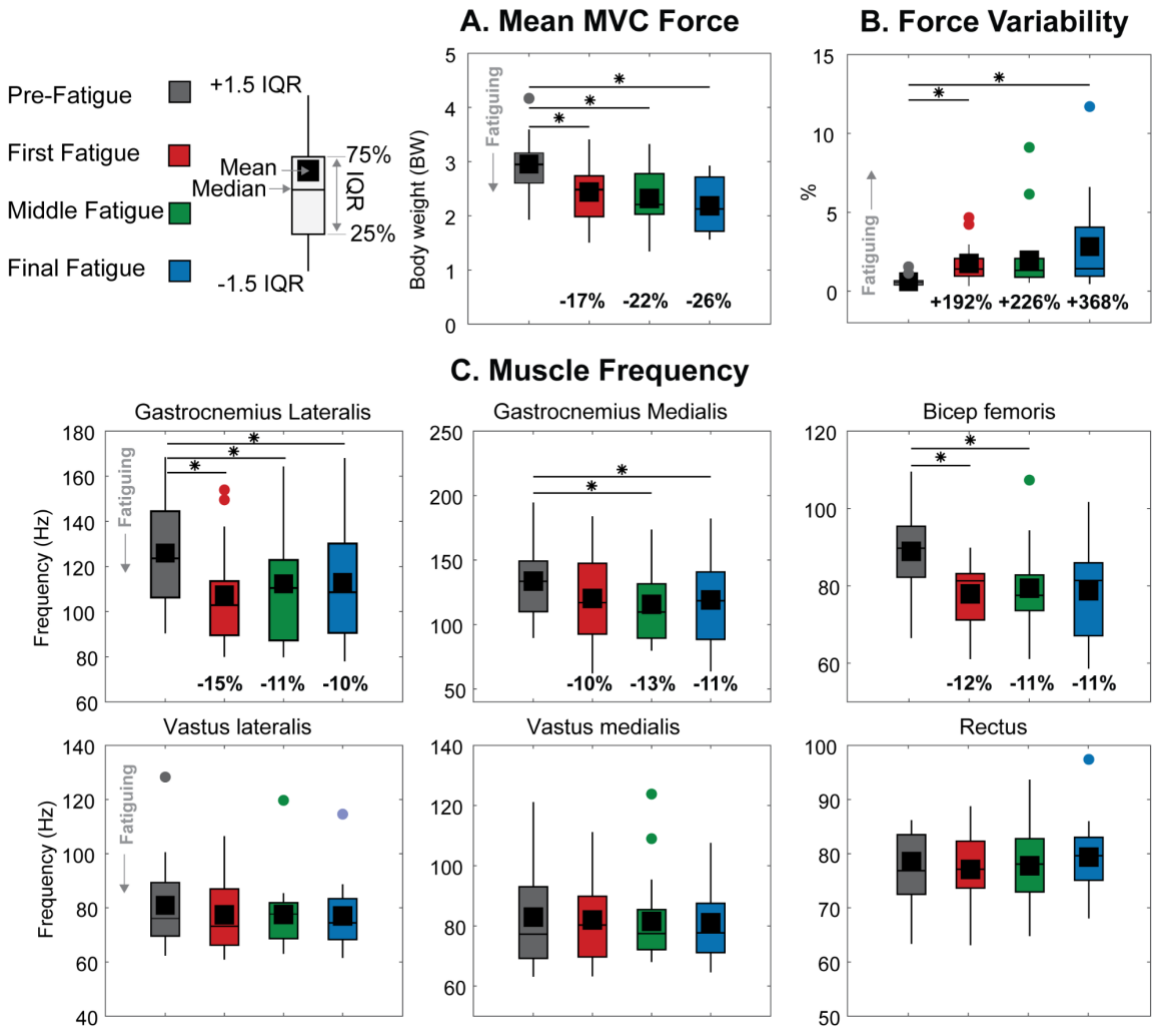

Figure 3-5 Objective measures of fatigue. As participants progressed through the protocol (Fatigue 1-3), they demonstrated A. A decline in Mean MVC vertical force, B. An increase in force variability, and C. A reduction in the median EMG frequency of several of the measured leg muscles. If we found the repeated measure ANOVA to be significant, we show any significant pairwise comparisons indicated with an asterisk. The legend on the top left explains the values shown in the box and whiskers plots

3.4.2. Fatigue led to reductions in leg force control responsiveness

As participants grew fatigued, their responsiveness decreased, demonstrated by a significant increase in rise time ($p = 0.0011$) and a decline in bandwidth ($p = 0.0014$). However, this decrease in responsiveness wasn't reflected in changes in fall time ($p = 0.109$) (Figure 3-6-A). Comparing the rise time of 303 ± 100 ms in the Pre-Fatigue

condition to 373 ± 94 ms in the final fatigue condition, we observed a significant (p = 0.0006) increase of 23%. Simultaneously, bandwidth decreased significantly (p = 0.04831) from 1.33 ± 0.6 Hz to 1.00 ± 0.25 Hz, a reduction of 25%. Despite these changes, we did not observe any alteration in force control accuracy between these two conditions (Figure 3-6-B).

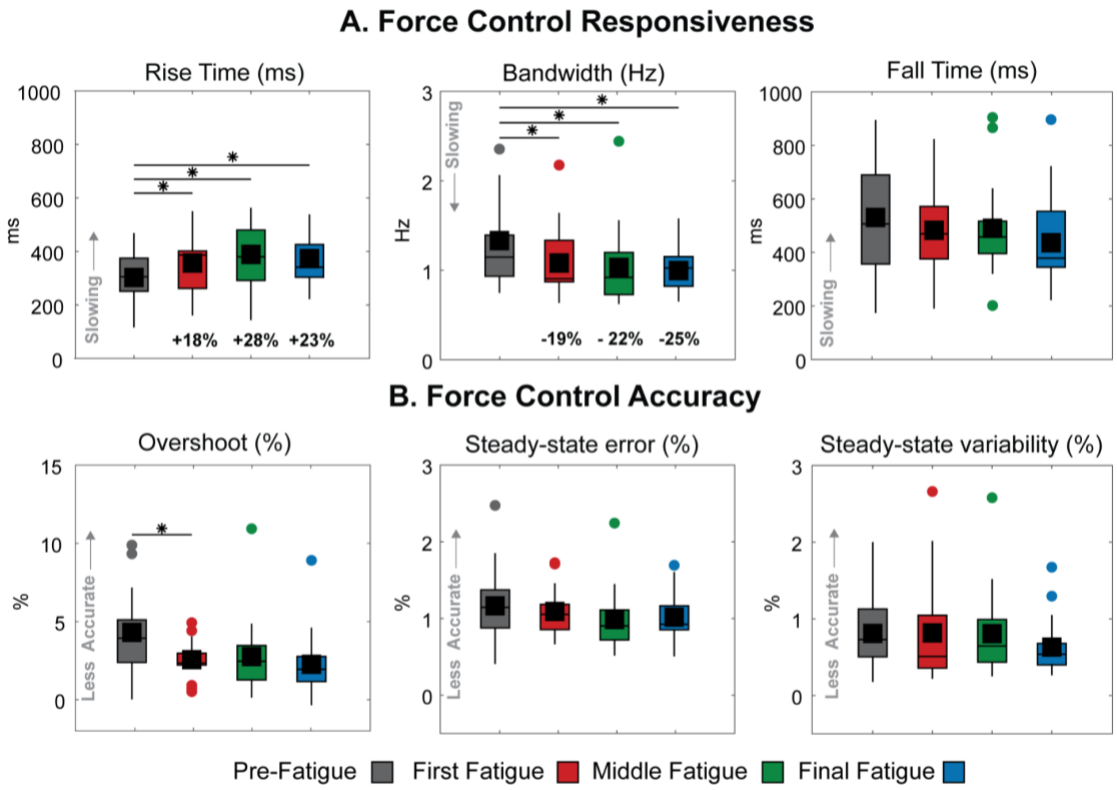

Figure 3-6 We assessed force control responsiveness by examining rise time, bandwidth, and fall time changes. B. We evaluated force control accuracy through alterations in overshoot, steady-state error, and variability. In cases where we found the repeated measure rANOVA significant, we displayed significant pairwise comparisons, denoted by an asterisk *.

3.4.3. The Pulse Task was resilient to the effects of fatigue

As participants grew fatigued, they did not exhibit changes in responsiveness during the Pulse Task (Figure 3-7), evidenced by the absence of significant changes in rise time (p=0.9722), bandwidth (p=0.9147), or fall time (p=0.7830). Since the primary objective of the Pulse Task was responsiveness, we did not evaluate accuracy.

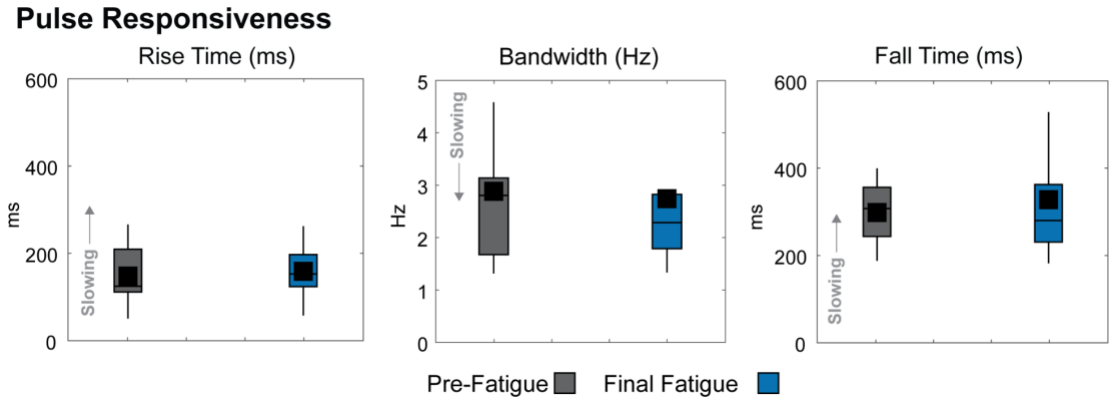

Figure 3-7 Pulse Task responsiveness, assessed by rise time, bandwidth, and fall time, comparing the Pre-Fatigue condition to the final fatigue condition, Fatigue-3. We did not evaluate the accuracy of the Pulse Task, as its primary objective was responsiveness. When the need for accuracy was removed from the objective, participants exhibited greater responsiveness compared to the Step Task, which required both responsiveness and accuracy.

3.4.4. Participants exhibited higher responsiveness in the Pulse Task compared to the Step Task

We observed that participants demonstrated greater responsiveness in the Pulse Task than in the Step Task across all measures. In comparing the Pre-fatigue responsiveness of the two tasks, participants in the Pulse Task had a rise time of 148 ± 64 ms, a bandwidth of 2.88 ± 1.47 Hz, and a fall time of 299 ± 68 ms. In contrast, participants in the Step Task had a rise time of 303 ± 100 ms, a bandwidth of 1.33 ± 0.60 Hz, and a fall time of 531 ± 199 ms. During Pre-Fatigue, the Pulse Task exhibited a 51% faster rise time (p = 6.8e-6), a 116% wider bandwidth (p = 4.0e-4), and a 42% faster fall time (p = 6.0e-4) than the Step Task.

3.5. Discussion

In this study, we investigated the impact of fatigue on the ability to control the vertical component of leg external ground forces, finding that fatigue led to a decrease in force control responsiveness (speed). Our protocol successfully fatigued participants, as shown by several objective measures, including a decrease in mean maximum voluntary contraction force during the MVC Task, increased force variability during the Hold Tasks, and reductions in median EMG frequency in multiple lower leg muscles. Consistent with our hypothesis, we observed that fatigued participants demonstrated a significant decline in responsiveness, marked by a 23% increase in rise time and a corresponding 25% reduction in bandwidth. However, contrary to our hypothesis, we found that fatigued participants did not exhibit significant changes in leg force control accuracy. Furthermore, we found that in the Pulse Task—a task in which participants displayed overall greater responsiveness when compared to the Step Task—control was resilient to the effects of fatigue.

There are several limitations to our study. One limitation is that mechanical compliance, both within the participants' bodies and within the testing apparatus, may have influenced the measured force. To minimize this potential issue, we used stiff materials and securely fixed the participants in the apparatus, as described in [15]. Another limitation is that we only evaluated force control at a single sub-maximal vertical force level. In real-life situations, leg external forces vary widely depending on the task. However, previous research suggests that aspects of force control might not differ significantly at different sub-maximal force levels of up to 60% of MVC when fatigued [15], [157]. A third limitation is that our study results may not generalize to other populations, such as older adults or individuals with chronic conditions. These groups could exhibit different control characteristics even before the onset of fatigue [158]. [159], [160]. Lastly, our study used a standardized fatigue protocol that might not accurately reflect real-world conditions in which fatigue occurs. For example, real-world conditions can involve not only physical but also cognitive demands, both of which may affect motor control and be subject to fatigue [161]. Our study targeted fatigue at the neuromuscular level and did not actively investigate the separate effects of physical and cognitive fatigue [162].

There are several mechanisms through which fatigue can affect responsiveness. One way is through the inhibition of feedforward connections from the brain to the muscles or neural

drive. Neural drive refers to the intensity or strength of the feedforward signals sent from the central nervous system to the muscles [48]. This reduction in neural drive may be due to a decrease in the release of neurotransmitters, an alteration in the firing patterns of motor neurons, or a reduction in the sensitivity of muscle fibres to neurotransmitters [48]. When an individual is fatigued, the intensity of these feedforward signals may be reduced, leading to a decrease in muscle force-generating capabilities [163], [164]. It may also be the case that fatigue leads to a reduction in the sensory feedback gains involved in the control of muscle force. In a feedback control system, responsiveness is determined, in part, by the ratio between output (e.g., muscle force) and sensory input (e.g., muscle length or velocity), known as feedback gains. Sensory feedback gains can be adjusted dynamically to achieve task success [165]. As feedback gains decrease, the control system becomes less responsive [166]. A comparison of the responsiveness results from the Step Task—which relied on feedback control and was affected by fatigue—and the Pulse Task—which relies more on feedforward control and is not affected by fatigue—suggests that in our experiment, fatigue primarily affected sensory feedback pathways and not neural drive.

The distinction between the effects of fatigue on feedback and feedforward control is important for understanding how the nervous system adapts to fatigue and could inform the development of interventions to maintain or improve motor performance under fatigued conditions [167]. For example, targeted interventions could focus on enhancing feedforward control through training programs [168] or provide external sensory feedback to optimize performance in the presence of fatigue [167]. The ability of individuals to maintain optimal performance in fatigued conditions is critical, particularly for athletes. Therefore, identifying and developing effective interventions can significantly impact their ability to perform at their best, even when fatigued.

Our observed reductions in leg force control responsiveness are large enough that they could negatively impact agile performance. Agile performance relies on quickly and accurately responding to environmental changes. A decrease in responsiveness can increase the time needed for the system to respond accurately to these changes, leading to a decline in performance. This has been illustrated in simulation experiments using robotic legs, where reductions in responsiveness, as indicated by increases in rise time and narrowing of bandwidth, were observed when the controller time delay was increased [169]. And in hardware experiments with legged robots— narrowing bandwidth and

increasing controller time delay resulted in the robot failing to land properly during a drop landing task [169]. However, as observed in our study, the consequences of a 25% reduction in responsiveness on a system's or individual's agility may depend on their specific abilities and the task. For instance, the MIT Cheetah, a highly agile-legged robot, has a leg force responsiveness that is 100 times faster than that measured in humans—a 25% reduction in responsiveness may not significantly affect its performance [124], [170]. On the other hand, humans already exhibit comparatively slow rise times and narrow bandwidths, suggesting that a 25% decrease in responsiveness is more likely to impair agile performance. Indeed, fatigue-induced temporal changes in humans affect agile performance—fatigued athletes exhibit prolonged drop landing contact times [61] and decreased running speed [171].

Fatigue reduces leg force control responsiveness, potentially raising the risk of injury during physical activities. Individuals may compensate for these decreases by altering their body mechanics to preserve performance. For example, fatigued athletes land from jumps with more flexed knees or shift their load from plantar flexors to knee extensors [64]. Such fatigue-induced changes in body mechanics can compromise stability and heighten injury risk by placing extra stress on specific joints or muscles not typically engaged or active during certain movements [172], [173]. In men's collegiate soccer matches, for example, players sustained approximately 50% more injuries in the second half compared to the first half [174].

In our experiment, we developed a method for fatiguing participants and benchmarking the impact of fatigue on leg force control performance, laying the groundwork for studying interventions that address fatigue and enhance agility. Potential interventions, such as strength training or exoskeletons, could be explored in diverse populations, including athletes, military personnel, and older adults. By understanding the effects of fatigue on leg force control responsiveness and accuracy, it may be possible to develop targeted strategies that mitigate the consequences of fatigue and optimize agility across various tasks and populations. This research will help with future work focused on identifying, assessing, and implementing effective interventions that cater to the unique needs of individuals relying on leg force control for optimal performance.

Chapter 4.

Studying the limits of vertical jumping using a physics-based model that predicts external ground reaction forces

4.1. Abstract

To understand better the fundamental principles governing vertical jumps, we developed a physics-based model that accurately predicts vertical external forces during jumps from various initial depths using a single set of optimally determined actuator properties. The model achieved a mean R^2 of 0.89±0.10 and a RMSE of 0.45±13 body weights across all depths. Our findings highlight the importance of force-velocity properties and maximal force (F_{max}) in determining jump height. When we eliminated the force-velocity relationship or when we increased F_{max} by 1000%, we observed substantial increases in jump height, averaging 300% and 416%, respectively. Furthermore, our model accurately predicted preferred jumping depths, aligning with empirical data. We found that participants optimized their jumping performance by balancing the goals of maximizing jump height and minimizing jump duration, achieving large speed improvements with minimal losses in jump height. Our simplified model provides a clear understanding of the fundamental principles governing vertical jumps. The insights from this study have potential applications in athletic training, rehabilitation, and developing technologies to augment jump height.

4.2. Introduction

Vertical jumping is a fundamental form of movement in legged bipeds, such as humans. It involves the rapid application of a downward force against the ground, generating external ground reaction forces. These forces propel the jumper's body upward until the legs fully extend and lose contact with the ground, enabling the jumper to become airborne. The magnitude of the upward acceleration produced by the external ground reaction forces during this process plays a crucial role in determining the vertical take-off velocity of the jumper and, ultimately, the height that can be achieved in a jump.

Two primary physical factors play a crucial role in maximizing the vertical take-off velocity (v_{to}) and, consequently, the height of a jump. The first factor is the length of the leg's extension on the ground [175]. Human legs have inherent limitations in extension, but longer extensions can generally facilitate the generation of more force, thereby enabling higher jumps [68]. The extent of leg extension influences the distance over which force

can be applied to generate acceleration. The second factor influencing jump height is the average magnitude of the vertical ground reaction force (F_{vGRF}) that exceeds the force of gravity (mg) exerted by the jumper against the ground throughout the jump's duration [175]. By generating larger magnitude forces, the jumper can produce more energy to accelerate their body's center of mass, increasing vertical take-off velocity and higher jump heights. Therefore, to maximize jump height within the constraints of a specific allowable leg extension, it becomes essential to maximize the magnitude of the vertical external force (F_{vGRF}) throughout the jump's duration.

Maximizing the magnitude of external force generated during a jump while the legs are in contact with the ground is fundamentally a product of the mechanics of biological muscle contractions. During a jump, muscles serve as actuators, generating force that is transmitted through our skeletal system to push against the ground. In response, the ground exerts an equal and opposite force (as per Newton's third law), propelling us upwards. Thus, our muscles play a crucial role in enabling us to jump. However, muscles are not perfect actuators; they cannot produce force infinitely and instantly [176] The properties of muscle actuators impose limitations on force production as the muscle's state changes. One such muscle actuator property is the relationship between muscle force and its kinematic state, i.e. its velocity and length. As the velocity of a shortening muscle increases, the force it can generate decreases. At a certain maximum velocity, the muscle ceases to produce any force [37]. Additionally, muscles exhibit a roughly parabolic relationship with their length. They generate maximum force at an optimal length, and the force decreases when the length deviates from this optimal range [37], [38]. Furthermore, muscles operate in conjunction with elastic tendons, which can store and release energy through moment arms, determining the resultant joint torques. These inherent properties of muscle actuators, along with their mechanical implications, are critical in determining the external forces generated during a vertical jump and, ultimately, the height of the jump [177]. Understanding the relationships between muscle force, velocity, and length is essential for maximizing the resultant magnitude of external forces and enhancing jump performance.

Mathematical models can be invaluable for studying the intricate relationship between muscles and resultant movement. Mathematical models can be built to integrate morphological, physiological, and neuromuscular variables, providing a platform for studying the mechanics of biological systems [10], [66], [80], [81], [83], [178]. Simple

models, focusing on essential variables and relationships, have been instrumental in gaining insights into movement and, specifically, walking mechanics [179]–[181]. Vertical external forces result from the complex interplay between the body's muscular, skeletal, and nervous systems. Therefore, a model that can accurately predict these forces can offer insights into these systems' functioning during a jump. Humans, with a generally fixed set of muscle properties, can jump from various initial depths and positions, highlighting our muscular system's versatility and intricate control mechanisms. However, no existing jumping model has accurately estimated leg external forces across a range of jumps with varying initial starting depths [10], [66], [68], [83], [182]. Developing a simple model capable of generating external forces from any depth that aligns well with those observed during human jumps will enable a detailed study of how model actuator properties can limit or augment vertical jump height.

Our objective is to characterize how muscle actuator properties augment vertical jump height. To achieve this, we first sought to develop a simple physics-based model capable of jumping from different initial starting depths while accurately predicting vertical external forces. Given that humans do not alter their muscle actuator properties to accommodate jumps of varying depths, we sought to design our model to also jump from various depths using a single set of optimal actuator properties. We recruited ten participants who performed vertical squat jumps from five different initial starting depths to develop such a model. During these jumps, we collected their external leg forces using a ground-mounted force platform. We then developed and assessed vertical jumping models of increasing complexity. By leveraging simulation and optimization techniques, we aligned the model's predicted vertical external forces with the empirical data for each jump. Eventually, we arrived at a model that could jump from various depths and generate vertical external forces that closely matched empirical data, all while using a single set of optimal actuator properties. We then used this model to probe how incremental changes in actuator properties affect the generated vertical external forces and how this impacts vertical jump height. Finally, we used this model to determine what factors contribute to preferred jump depth when participants jumped maximally.

4.3. Methods and Models

4.3.1. Participants

We recruited ten participants for our study (one female, nine males; body mass: 67.6±9.3 kg; age: 26.5 ±3.5 years; leg length: 94.6±3.3 cm; mean±standard deviation). The Office of Research Ethics at Simon Fraser University approved the study, and all experiments complied with relevant guidelines and regulations. Participants provided written informed consent before participating.

4.3.2. Experimental Protocol

We conducted two experiments to collect a wide range of external forces generated during jumping. In these experiments, participants performed squat jumps from various initial starting depths. A squat jump involves initiating a jump from a static position and accelerating the center of mass upward. We used a force plate from Bertec Corporation (Ohio, USA) to record participants' vertical ground reaction forces. In the first experiment, we focused on maximum-height vertical squat jumps. Participants performed jumps from five different initial squat depths, as shown in Figure 4-1. To ensure consistency in starting depths, we designed and used a simple device consisting of a flexible horizontal pole attached to a vertical stand. This device served as a visual reference and assisted participants in achieving the desired squat depth. We marked three additional depths on the simple device, creating a total of five starting depths. The shallowest and deepest starting depths were determined based on participants' ability to perform jumps without countermovement. After trial and error, we adjusted the pole to the desired starting positions between a shallow and deep jump. Each participant completed four maximum-height jumps at each of the five initial depths, resulting in 20 jumps per participant. We randomized the order of depths to minimize potential bias or order effects.

In the second experiment, we removed the guidance device and instructed participants to perform maximum-height vertical squat jumps from their chosen starting depths. In this experiment, we aimed to collect data on each participant's preferred starting depth, allowing us to investigate the factors influencing the choice of jump depth when aiming for maximum height. We gave each participant the following instructions: "*We have now removed the guidance device. From your chosen initial position, please jump as high as*

you can. The goal is to jump as high as possible without using a countermovement." We asked participants to perform 10 jumps like this, providing a one-minute rest between each jump to prevent fatigue. In both experiments, we instructed participants to tuck their arms into their chest during jumps to minimize the impact of arm swing on the jump [183].

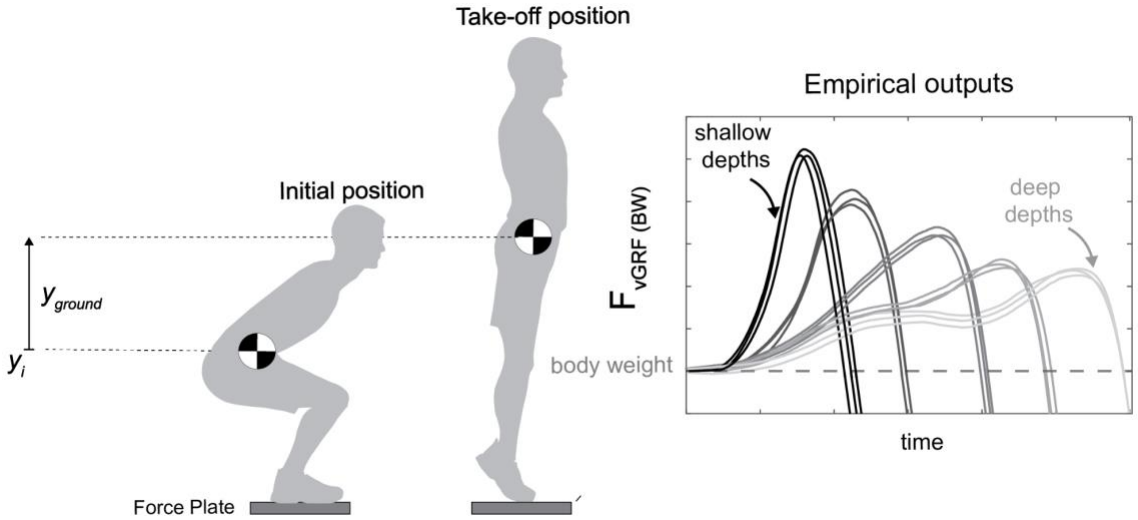

Figure 4-1 Participants (n=10) performed vertical squat jumps from a range of five predetermined initial depths (experiment 1) as well as from their own self-selected depths (experiment 2), with their arms tucked into their chests. Vertical ground reaction force $\boldsymbol{F_{vGRF}}$ profile for a range of initial depths for the range of shallow to deep depth jumps is shown for one representative participant.

4.3.3. Data Preparation

We curated the empirical data to support our model development. First, we trimmed the time-series data of the collected vertical ground reaction forces to begin when the participant started to vertically accelerate their center of mass and end at the instant they left the ground. Since participants were instructed to remain stationary at the start of the vertical jump, their ground reaction force was approximately equal to their body weight. We used a 3% change in vertical acceleration as a threshold to determine when the participant began to vertically accelerate, marking the beginning of their jump. From experimenting with different thresholds, we found that 3% was the minimum that worked for over 95% of our jumps. To confirm, we visualized all the marked predictions of the start of all the jumps. We adjusted any visually incorrect predictions by manually shifting where the jump-started. In these cases, the participants displayed movement fluctuations in their

center of mass positions that the algorithm incorrectly marked as the start of the jump. We then trimmed the data to end at the instant the participant took off from the ground when the vertical force reached zero ($F_{vGRF} = 0$). We excluded any jumps exhibiting a countermovement motion (i.e., the acceleration profile showed a downward acceleration followed by an upward acceleration as the jump began) from subsequent analyses. For all remaining jumps, we calculated the center of mass velocity by integrating the acceleration, assuming an initial velocity of zero. To determine the position of the center of mass, we integrated the velocity, assuming an initial position of zero.

To ensure direct comparison across different individuals, we transformed our variables into dimensionless quantities. This normalization process involved several steps. Firstly, we normalized forces by dividing by the participant's body weight. Secondly, we normalized lengths by dividing by the participant's leg length (L). Thirdly, we normalized time by dividing it by the time it takes to fall to the ground from the height of the leg length under the influence of gravity sqrt (L/g) where (g = 9.81 m/s^2). Lastly, to represent the position change of the center of mass as a percentage of the leg length, we subtracted the resultant value from 1. This adjustment established a reference point where the initial position corresponds to a certain percentage of the leg length, with take-off occurring at a position equivalent to 1 leg length. By transforming our variables into dimensionless quantities through these normalization procedures, we achieved a consistent and standardized framework for comparing our model's predictions across different individuals, allowing for more meaningful and reliable comparisons.

4.3.4. Model Development

Our goal is to create a simple physics-based model capable of performing jumps from varied initial starting depths while accurately predicting vertical external forces. As we aim for our model to accommodate jumps from different depths using a single set of optimal actuator properties, this section provides an overview of our modelling approaches, optimization techniques, and outlines the steps undertaken to reach this goal. Our models will be available on Zenodo through GitHub repository:

https://zenodo.org/badge/latestdoi/697932895

Our approach to optimizing and evaluating the performance of all of our models involved a two-step process: initialization and optimization. As will be further described in the fourth coming paragraphs, each of our models has unknown parameters that needed to be optimized. To optimize unknown parameters in our models we initially generated 3000 random initial guesses for each actuator property required in the model. The goal was to thoroughly explore the parameter space and increase the likelihood of finding the optimal actuator properties. Each of our models had different actuator properties, and the number of these properties varied with the models. The 3000 initial guesses for each combination of actuator properties were generated through uniformly distributed random number generation within reasonable bounds for each actuator property. After the initialization step, we optimized every model's actuator properties, starting with each of these initial guesses. We used MATLAB's (2022) constrained optimization function fmincon to do this. We set our optimization objective to minimize the differences between the model-predicted external forces and the depth-matched external ground reaction forces for five different depths ranging from the shallowest (i=1) to the deepest (i=5) simultaneously.

Equation 4-1 $$\text{ObjFunction} = \sum_{i=1}^{5} \frac{\left(F^{i}{}_{vGRF\ Empirical} - F^{i}{}_{vGRF\ model}\right)^{2}}{length\left(F^{i}{}_{vGRF\ Empirical}\right)}$$

We use an objective function that optimizes a single set of actuator properties for multiple depths simultaneously, to enable the model to simulate jumps from a wide range of depths successfully. For each of the 3000 initial guesses, we optimize the actuator properties, refining and fine-tuning the model's predictions to achieve the closest alignment with the observed ground reaction forces. This approach enhances our confidence in the accuracy and reliability of the model's predictions. We ranked the 3000 solutions based on their objective function values after optimization. We observe that solutions with objective function values close to the smallest value also have similar parameter values. Consequently, we select the solution with the smallest objective function value as optimal, acknowledging that many near-optimal solutions with similar parameter values exist.

However, no optimization process can guarantee a globally optimal solution, especially in complex, multi-dimensional spaces. There is always a possibility that a more optimal solution exists but was not found due to the inherent limitations of optimization algorithms or our lack of knowledge. While this may be true, we believe that our methodology, which involves generating a large number of initial guesses and then refining these through optimization, provides a good balance between searching the entire parameter space and

converging on promising solutions. Following this approach increases the likelihood of finding a broad range of high-quality solutions.

4.3.5. Model A: A single-segment linear actuator

In Model A, we simplify the musculoskeletal system and jumping to its most fundamental concepts. The model represents the body as a point mass (m) and includes a massless telescoping leg actuator attached to the ground (Figure 4-2). The actuator generates a force based on its kinematic states, such as velocity and length. For example, the force decreases as velocity increases and varies with deviations from the optimal length (y_{opt}) (see Figure 4-2 for details). Additionally, the actuator exhibits laggy activation dynamics $a(t)$, requiring time for the force to reach its full output (again, see Figure 4-2). These resultant force characteristics are captured by Equation 4-2, which governs the actuator force in this model:

Equation 4-2

$$F = F_{max}\,[\,a(t) * F_v(v) * F_L(L)]$$
$$a(t) = Ce^{(-t/tau)} + 1$$

Where v is the velocity of the actuator and L is the length. We solve for the unknown parameter C by considering the initial conditions for each jumper. This includes an initial velocity (v_i) of 0 and an initial position (y_i) of 0, and a known initial vertical force, which is approximately equal to the body weight. In this model, then, there are five unknown actuator properties: maximal force (F_{max}), optimal length (y_{opt}), maximal velocity (V_{max}), parabolic force-length width (w), and tau the rate constant for the activation dynamics. Our goal is to optimize these actuator properties to ensure that the model's external force data best align with empirical data.

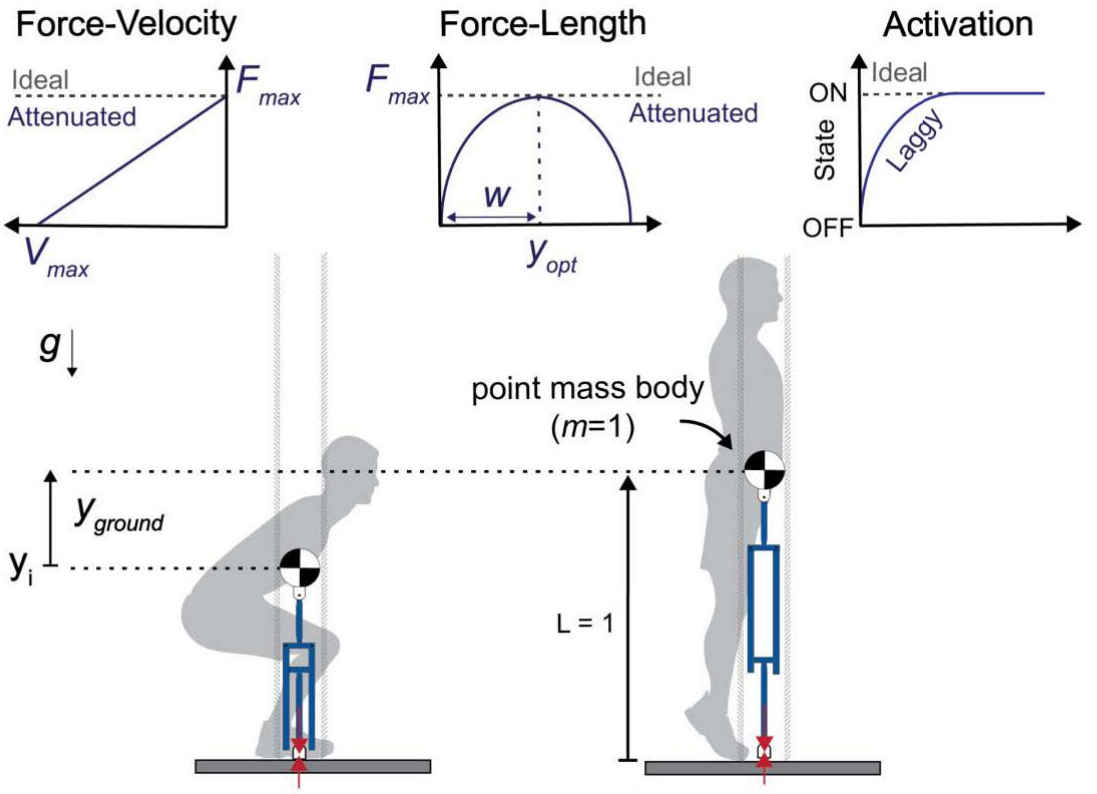

Figure 4-2 Our simplified jumping model (Model A), in which the body is represented as a point mass actuated by a massless actuator. The actuator force can be subject to properties that limit its ability to generate force, similar to a biological muscle. These actuator properties include length-dependent force limitations (F-L), velocity-dependent force limitations (F-V), and activation dynamics. An ideal force actuator, depicted as a gray line, would not face any force attenuation at any length or velocity, nor would it have any activation dynamics that delay its force generation. Conversely, an attenuated actuator, represented as a dark line, has properties that limit its force generation capabilities with changes in length and/or velocity. For instance, as the actuator's velocity increases, its force generation capability decreases, reaching a maximal velocity ($\boldsymbol{V_{max}}$) beyond which it can't generate any force. At an optimal length ($\boldsymbol{y_{opt}}$), the actuator develops its maximal force ($\boldsymbol{F_{max}}$), and the force declines outside this optimal length. Lastly, the actuator's activation dynamics result in a lag in force generation, necessitating a time delay to reach full activation and full actuator force.

4.3.6. Model B: A 2-link-segment model actuated by a torque generator

In Model B, we introduce two segments and a rotary actuator at the joint where the segments intersect to increase the complexity of our model (Figure 4-3). By incorporating multiple segments, we can better mimic the musculoskeletal system and joints in the human body. The rotary actuator is a massless torque generator that produces joint torque, aiming to emulate the behaviour of muscles that cross a given joint [184]. Although the rotary actuator does not fully replicate biological muscles, similar to in Model A, we incorporate actuator properties that mimic muscle behaviour, including angle-dependent and velocity-dependent torque limitations and laggy activation dynamics (Figure 5-3).

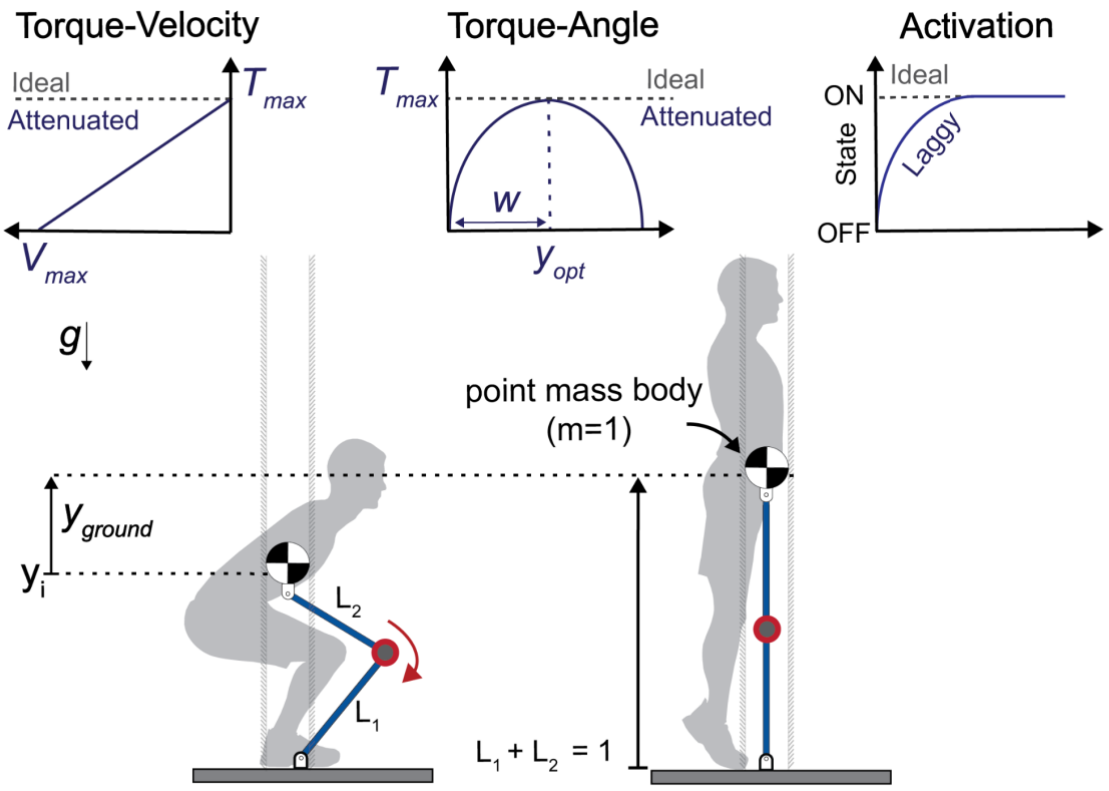

Figure 4-3 Our two-segment point mass model (Model B) features a rotary actuator at the joint where the segments intersect. This actuator torque can mimic the properties of a biological muscle, including limitations that affect its ability to generate torque. These limiting properties can encompass angle-dependent torque limitations, velocity-dependent torque limitations, and activation dynamics. An ideal torque actuator, illustrated by a gray line, would not experience any torque attenuation at any length or velocity, nor would it have any activation dynamics that would limit its ability to generate torques. Conversely, an attenuated actuator, depicted by a red line, has properties that restrict its torque generation capabilities with changes in length and/or velocity. For example, at an optimal length ($\boldsymbol{y_{opt}}$), the actuator produces its maximum torque ($\boldsymbol{T_{max}}$), and the torque decreases outside this optimal length. As the actuator's velocity increases, its torque generation capability also increases, reaching a maximum velocity ($\boldsymbol{V_{max}}$) beyond which it cannot generate any torque. Lastly, the actuator's activation dynamics result in a delay in torque generation, requiring time to reach full activation.

In this model, there then are five unknown actuator properties: maximal torque (T_{max}) , optimal angle (y_{opt}), maximal velocity (V_{max}), a parabolic torque-angle width (w), and τ the rate constant for the activation dynamics. Our goal is to optimize these unknown

actuator properties to maximize the alignments between the model's external ground reaction force data with the empirical data over all jumping depths.

4.3.7. Model C: 2-link-segment model actuated with a hill-type muscle-tendon actuator

In Model C, we enhance the previous model by incorporating a linear Hill-type muscle actuator, moment arms (Figure 4-4). Including the Hill-type muscle model allows for a more accurate representation of muscle contraction and force generation, considering factors such as stiffness, and elasticity in addition to force-velocity and force-length relationships, thus more closely resembling the behaviour of biological muscle-tendon unit [39]. In addition, we capture the mechanical advantage observed in the musculoskeletal system by incorporating moment arms, which represent the lever arms between the attachment points of the hill-type muscle actuator and the joint center. Importantly the actual force exerted by a muscle on the skeleton depends not only on the force generated by the muscle actuator but also on the geometry of its attachment providing a more realistic depiction of the functioning of the human body during jumping movements.

This two-link-segment model is actuated by a linear actuator with a unique origin (U_o) and insertion point (U_i). As the actuator shortens, it generates a joint torque about the two link segments, simulating the muscle's contribution to the movement. This model incorporates nine free actuator properties elaborated upon in Figure 4-4. These properties include the origin (U_o) and insertion points (U_i) of the tendon-like actuator, the force-length (F-L) and force-velocity (F-V) properties and accompanying properties F_{max}, V_{max}, Y_{opt} , w. Additionally, the model incorporates a series elastic element with a slack length L_{slack}, a stiffness force-strain stiffness (K_s), and a rate constant for the activation dynamics, τ.

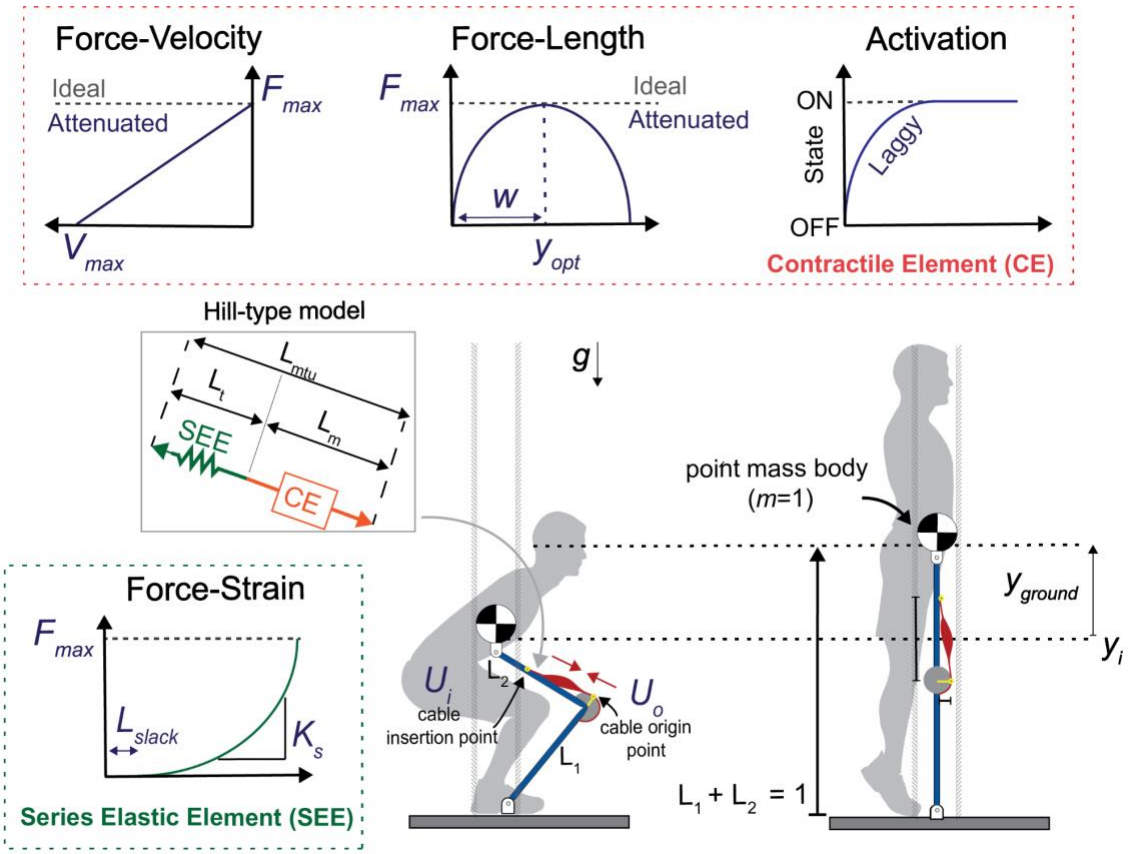

Figure 4-4 Our two-segment jumping model is actuated by a Hill-type muscle actuator (Model C). There are nine free properties in this jumping model that need to be optimized. The two-link-segment model is actuated by a muscle-like actuator mimicking muscle behaviour, with a unique origin (U_o) and insertion point (U_i), which generates a moment arm at the knee joint. An example Hill-type muscle model illustrating the series elastic element ($\boldsymbol{SEE}$), contractile element ($\boldsymbol{CE}$), muscle-tendon unit length ($\boldsymbol{L_{MTU}}$), and total muscle length ($\boldsymbol{L_T}$) is shown in the figure. This model represents the mechanical behaviour of skeletal muscles and provides insights into muscle force generation. $\boldsymbol{F_{max}}$ represents the maximal force of the contractile element ($\boldsymbol{CE}$). The series elastic element ($\boldsymbol{SEE}$) represents the elasticity of tendons and other compliant structures that store and release energy during muscle contraction. The SEE exhibits properties where the tension increases as length extends beyond a predefined slack length ($\boldsymbol{L_{slack}}$) and has a stiffness $\boldsymbol{K_s}$. The contractile element ($\boldsymbol{CE}$) is responsible for generating force and has force-length and force-velocity properties. Force declines when muscle length deviates from an optimal length ($\boldsymbol{y_{opt}}$), and force decreases with increasing shortening velocities up to a maximal velocity ($\boldsymbol{V_{max}}$). By capturing these characteristics of muscle behaviour, including force production, energy storage, and mechanical properties, the Hill-type muscle model enables simulations and analysis of muscle function.

4.3.8. How does each model parameter limit jump height?

To evaluate how changes to the optimal parameters influence the model's ability to generate external forces and consequently affect the predicted jump height, we performed a sensitivity analysis. We parametrized each participant's model using their individually optimized parameters and then sequentially increased each parameter that directly affected the contractile element's ability to generate force. This included changing F_{max}, V_{max}, and w by +2.5%, +5%, and +25%, respectively. We documented how these modifications influenced external force generation and the corresponding changes in jump height. This approach helped us understand the implications of alterations in the modelled muscle parameters on performance. Additionally, to understand the contributions of these parameters further, we selectively removed the actuator limitations, transforming the model into an ideal actuator. We examined how eliminating muscle force dependencies influenced the generation of external force and, consequently, how this affected the model's jump height. To avoid introducing singularities into the simulation when doing this, we assigned high numeric values to the muscle parameters of interest, effectively nullifying their influence [11]. Specifically, we set $V_{max}$to a high value to negate the force-velocity relationship, assigned a large value to w to negate the force-length relationship and increased F_{max} by up to 1000%.

4.3.9. Optimal jump depth

To compare the preferred depth of our model with the self-selected optimal jumping depths of the participants from Experiment 2, we configured another optimization task. We again used each participant-specific model. Each model was able to jump from various starting positions with the goal of maximizing jump height. As the nervous system's objective in maximizing jump height could also involve minimizing the movement duration on the ground [185], we introduced an extra term in our objective function to decrease jump duration and explore this idea. As we do not know the weight the nervous system may place on prioritizing movement time, we managed the objective of maximizing jump height and minimizing jump time using a weight parameter (W). We carried out optimizations across a W range from 0 to 1 in increments of 0.1, resulting in 10 distinct optimizations for each value of W. When we set W to 0, the model solely aimed to jump as high as possible. Conversely, when we set W to 1, the model optimized only for jump duration, thereby

reducing the time each jump took. For any value between 0-1, the model balanced the priority of jump height and jump time, as seen in Equation 4-3. We tested each optimization from 100 different initial positions and again used fmincon to find the lowest value of the objective function.

Equation 4-3 $$min[(1 - W) * \frac{1}{H_{model}} + (W * t_{push-off})]$$

Where H_{model} is the jump height achieved by the model and and $t_{push-off}$ is the total time spend on the ground generating external force.

4.3.10. Statistics

To assess the performance of our models, we used the coefficient of determination R^2 and root mean square error (RMSE) as our primary statistical metrics. We chose R^2 to provide an indication of the proportion of the variance that our model could explain and RMSE to offer an estimate of prediction error, indicating how closely our model's predictions in external force aligned with the observed empirical values of external force. The R^2 used in our analysis differs from the conventional R^2 used in regression analyses. Commonly, R^2 quantifies the proportion of the variability in the dependent variable that can be explained by the independent variables. However, in our approach, we calculated R^2 using the squared differences between each data point of the model and zero instead of the mean. This method, sometimes referred to as "uncentered" or "raw" R^2, is suitable for our analysis as it allows us to measure the total variability in the dependent variable (model predict external force) without factoring in the mean [186]. It's particularly beneficial when there is no meaningful or interpretable zero value, and the mean does not necessarily represent a typical or average value [186]. This is frequently the case in physiological and biomechanical studies, where relative differences or proportions are more informative than absolute differences from the mean. Despite the difference in the calculation, the interpretation of R^2 remains the same, where a higher R^2 value indicates a greater variance explained by our model and a better fit of our model to the data. We also used RMSE to calculate the average difference between the predicted and actual values, estimating prediction error. A model exhibiting a smaller RMSE demonstrates predictions closer to the observed values.

We performed a separate analysis using the jumping data from all participants and depths to investigate the relationship between model-predicted jump heights and empirical data across all jumping depths. We leveraged two metrics to gauge the quality of the linear regression models: the correlation coefficient (r-value) and the standard error of the estimate (SEE). The r-value, ranging between -1 and 1, indicates the strength and direction of the relationship between the two variables. A higher absolute r value in our analysis suggests that the independent variable accurately predicts the dependent variable. We used the SEE to assess the precision of our model predictions. The SEE estimates the standard deviation of the residuals, i.e., the differences between the observed and predicted values. A lower SEE in our research implies that our model is more precise, as the observed values closely align with the model's predictions. Finally, to compare point metrics such as peak vertical force, and jump height, we used a one-tailed paired t-test. In all instances, we used Matlab's statistical analysis toolbox and set $p<0.05$ as statistically significant.

4.4. Results

4.4.1. Evaluation of models

After optimizing for actuator properties in Model A (F_{max}, y_{opt},V_{max}, w, and τ) , we converge on a separate model for each participant that can successfully perform jumps from a range of depths using a single set of optimal actuator properties. However, when comparing the model's predicted external forces (F_{vGRF}) to the empirical data, we observe a large variance (Table 4-1). The model's predictions do not align well with the observed forces during vertical jumping, especially for jumps from deeper depths. At the shallowest jumps, the model demonstrates a good fit with an R^2 value of 0.93 ± 0.04 and an RMSE of 0.51 ± 0.16 body weights. However, as the jumper progresses to deeper depths, the model's performance deteriorates. At the deepest depth, the R^2 value decreases to 0.26 ± 0.36, while the RMSE increases to 1.60 ± 0.73 body weights, indicating a large discrepancy between the predicted and empirical forces. This model fails to accurately capture the dynamics and variations in force generation during jumps from increasingly deeper depths.

The model's simplicity may limit its ability to predict empirical forces during vertical jumping accurately. To understand why this is, we re-optimized the model using a modified

objective function that minimizes the difference between the model's external force and the measured data for only specific depths at a time. This approach enabled us to achieve good fits for each depth using depth-specific optimal parameters. While evaluating this re-optimized model, we observe that to jump from deeper depths, the optimal parameters widen the force-length actuator properties. For instance, in the analysis of a representative participant, as the initial depth of the jumper increases, the optimal width of the force-length relationship expands by 116%, 142%, 205%, and 262%, respectively. This expansion enables the model to generate force over the full duration of each jump, better aligning with the force production requirements for deeper jumps that necessitate a more extended leg extension. Furthermore, we conducted simulations using a model specifically optimized for the deepest jumps to evaluate its performance in shallower jumps. Although this optimized model can jump from shallower jumps, it falls short in accurately replicating the external force observed in the empirical data for shallower jumps. This discrepancy suggests that the model's capabilities are more suited for deeper jumps, where it demonstrates greater accuracy. In contrast, when simulating a model optimized solely for shallow jumps, it failed to generate sufficient force for the extended duration required in deeper jumps and was poorly aligned with the empirical data. These findings emphasize the limitations of Model A in capturing depth-dependent force generation.

In the subsequent model (Model B), we will actively incorporate an additional segment into the leg to evaluate its impact on the model's behaviour. By decoupling the muscle actuator from the direct line of action with the external force and enabling the generation of torque around a joint, we aim to capture the intricate relationship between joint angles, muscle actuator force, and force generation during vertical jumps across various depths more accurately. This two-segment representation offers the potential to accommodate a wider range of leg extensions using a single set of optimal parameters, ultimately resulting in improved alignment between the model's predictions and the external force observed in empirical data. Indeed we find that model B can jump using one set of optimal actuator properties for the range of different depths (Table 4-1). We find that the model performs reasonably well across all of the depths, with performance again deteriorating for the deepest jumps. Shallow jumps showed an R^2 value ranging from 0.90± 0.008 and RMSE 0.57± 0.17 body weights, while deep jumps 0.65± 0.23 and RMSE 0.81± 0.32 body weights (Table 4-1).

Despite Model B's improved performance over Model A and effectively accounting for a greater portion of the observed variance, it continues underperforming during deeper jumps. To probe this further, we employed a similar strategy as in Model A, re-optimizing our model with a revised objective function designed to minimize the discrepancy between the model's external ground reaction force and the recorded data for particular depths. Evaluating this re-optimized model revealed a trend toward the broadening of torque-angle actuator properties for increasing jump depths. For instance, in the analysis of a representative participant, we noted an expansion in the width of the torque-angle relationship by 270%, 870%, 3142%, and 3513% corresponding to each incremental increase in initial depth. This observation suggests that as the initial depth of the jumper increases, a wider torque-angle relationship becomes necessary, reflective of the greater joint angle changes required for deeper jumps and longer-duration external forces.

Interestingly, we find that this re-optimized model, when optimized for deeper jumps, can still execute shallower jumps, though with compromised alignment between the model's external force and empirical data. In contrast, a model re-optimized specifically for shallow jumps fails to generate the necessary torque for deeper jumps. These observations hint that while a single set of parameters might not provide an exact fit for all jump depths, it nonetheless offers a useful approximation across a spectrum of depths. Thus, our model strikes a practical balance between depth-specific accuracy and broad applicability. To enhance its performance further, particularly for deeper jumps where previous models demonstrated deteriorating performance, we next plan to augment our model by introducing moment arms. This is important because the actual force exerted by a muscle on the skeleton depends not only on the force generated by the muscle actuator but also on the geometry of its attachment, particularly the muscle's moment arm. For a given muscle force, a larger moment arm will result in a larger joint torque and vice versa. Furthermore, moment arms change with joint angles, altering the force a muscle can exert at different points in a movement.

Finally, after optimization of the Model C actuator properties, we observe that the model produces excellent fits between the predicted external force and the measured data (Table 4-1). This level of agreement is evident when comparing the model outcomes to the measured data across a wide range of jumping depths (Figure 4-5 in the Results). Although there may exist even more optimal solutions within the framework, the remaining variance between the measured data and the model predictions is reasonable and does

not require further explanation. In comparison to Model A and Model B, this model explains a greater portion of the variance in the data and does not deteriorate across different jumping depths. Considering the balance between the fit and complexity of this model, we have decided to use it for further analysis in subsequent steps.

Table 4-1 The group average R^2 and root mean square error (RMSE, units: bw) values for three models (A, B, C) based on all the evaluated jumps for 10 participants (4 jumps per depth, 5 depths). The table provides an overview of the model performance, showing the effectiveness and accuracy of each model in predicting vertical external forces across various depths using one set of optimized actuator properties per participant.

	Model A			Model B			Model C		
y_{ground}	R^2		sd	R^2		sd	R^2		sd
Shallowest	0.93	±	0.04	0.90	±	0.08	0.90	±	0.08
	0.50	±	0.30	0.70	±	0.27	0.89	±	0.08
	0.24	±	0.30	0.64	±	0.24	0.86	±	0.12
	0.19	±	0.31	0.65	±	0.16	0.87	±	0.10
Deepest	0.26	±	0.36	0.65	±	0.23	0.90	±	0.11
Mean	**0.43**	**±**	**0.26**	**0.71**	**±**	**0.20**	**0.89**	**±**	**0.10**
	RMSE (bw)		sd	RMSE (bw)		sd	RMSE (bw)		sd
Shallowest	0.51	±	0.16	0.57	±	0.17	0.54	±	0.12
	1.34	±	0.56	0.92	±	0.49	0.50	±	0.11
	1.68	±	0.56	0.97	±	0.35	0.42	±	0.11
	1.74	±	0.62	0.91	±	0.25	0.47	±	0.15
Deepest	1.60	±	0.73	0.81	±	0.32	0.33	±	0.15
Mean	**1.37**	**±**	**0.53**	**0.84**	**±**	**0.32**	**0.45**	**±**	**0.13**

Our approach here has led to the development of a model that incorporates a two-link-segment system and a Hill-type muscle actuator to simulate the mechanics of vertical jumping from various depths (Model C). This model enables us to capture essential aspects of the musculoskeletal system and muscle behaviour during jumping. The

simplicity of this model allows us to analyze and comprehend the key factors influencing jump height and performance more effectively. With the simplest model in hand, we can now conduct controlled and systematic investigations into various aspects of vertical jumping. We can study the interplay between muscle actuator properties and external forces. In the continued methods sections, we provide further details of our approach before presenting the results.

4.4.2. Predicting external forces and jump height

Our physics-based jumping model is capable of predicting vertical external forces across a range of initial starting depths using one set of optimal model parameters. Among the models evaluated, Model C, which incorporates two link segments actuated by a hill-type muscle actuator, emerged as the most accurate. By optimizing the model actuator parameters, we achieved a high level of accuracy in replicating the empirical external ground reaction forces observed in the data. This is evident from the good correlations between the predicted vertical ground reaction forces (F_{vGRF}) of Model C and the actual measured forces, as demonstrated by the high R^2 values (Table 4-1). Additionally, a visual comparison of the model-predicted forces with the empirical data (Figure 4-5) confirms the close alignment. The shallowest jumps had the highest RMSE error 0.54±0.12 BW while the deepest jumps had the lowest RMSE error 0.33±0.15 BW.

When we examined the relationship between the model-predicted jump heights and the actual jump heights, we observed a strong linear fit with a correlation coefficient r of 0.92 (0.89-0.94 95% CI) (Figure 4-6). While the r-value indicates a strong linear relationship, it is important to note that the alignment of the data points with the line of identity provides more meaningful insight. The closeness of the data points to the line of identity demonstrates how closely the predicted jump heights match the actual jump heights. Our analysis revealed that the model systematically but only slightly underestimated the vertical jump heights.

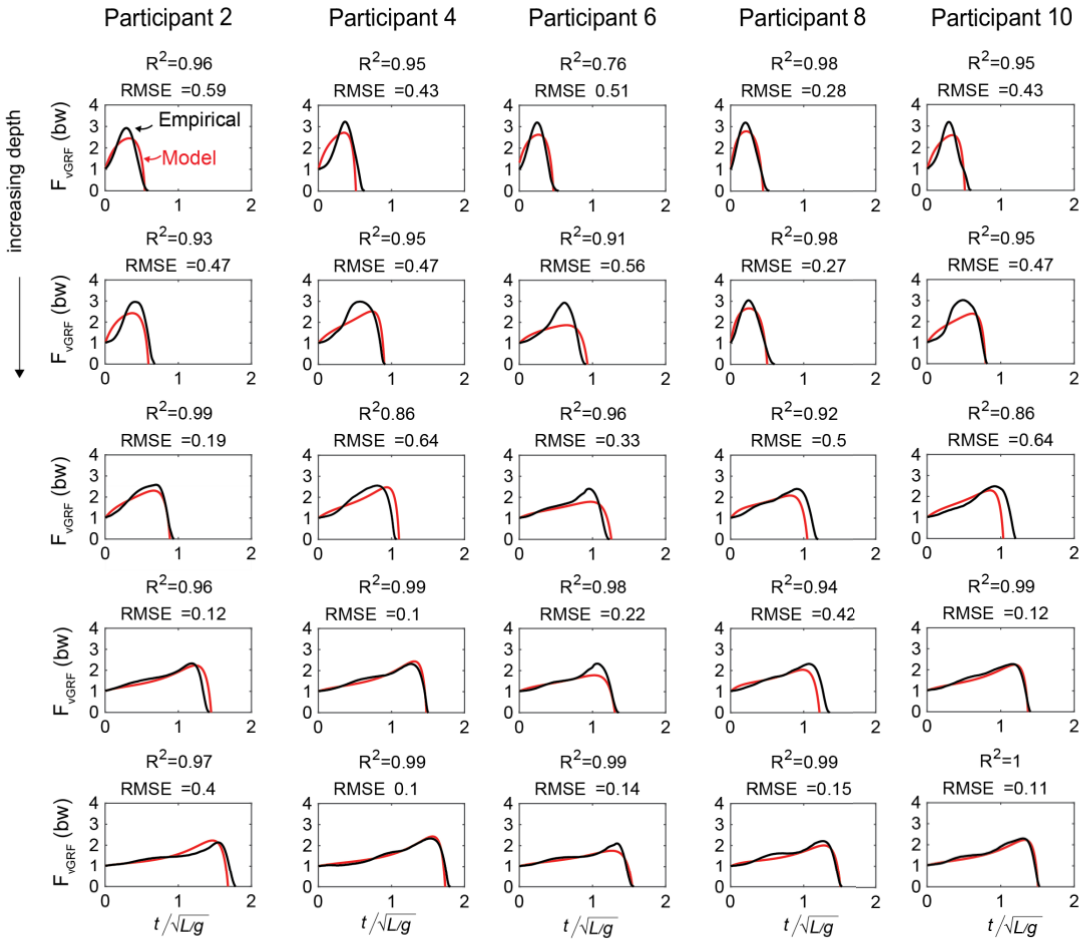

Figure 4-5 The results from Model C displaying a variety of jump depths. The empirical vertical ground reaction forces, $\boldsymbol{F_{vGRF}}$ (in black), and the model-predicted $\boldsymbol{F_{vGRF}}$ (in red) are displayed for five representative participants from left to right with the initial jumping depth increasing from the top to the bottom of the figure. The R2 and root mean square error (RMSE, expressed in body weight, BW) values for each jump are provided, offering a comparative evaluation of the empirical and model-predicted jumps. This figure highlights the model's predictive performance across diverse jump depths and different individuals.

Our model converged on strong predictions of vertical external forces compared to the empirical data, but discrepancies exist. In our optimization, our objective function was for the model to best match the external force during the entire duration of each jump. Although we found good fits, variations were most noticeable for jumps initiated from the shallowest starting positions, as outlined in Table 4-2 and Figure 4-5. Notably, on average, the model's predictions for the peak vertical force for the shallow jumps were 21% lower than empirical measurements (p=0.001). The model predicted a peak force of 2.47±0.36

body weights (BW) for these jumps, compared to depth-matched peak forces of 3.14±0.35 BW documented in the empirical data. For the deepest jumps, the model's predicted peak force was about 5% lower than the depth-matched empirical measurements (p=0.344). Nonetheless, these differences in peak vertical force did not result in significant differences in jump heights. The jump heights produced by the model for the shallowest jumps did not significantly differ from those recorded in the empirical data (p=0.99). This was also the case for jumps initiated from depths between the shallowest and deepest points (p=0.199) and the deepest depths (p=0.709).

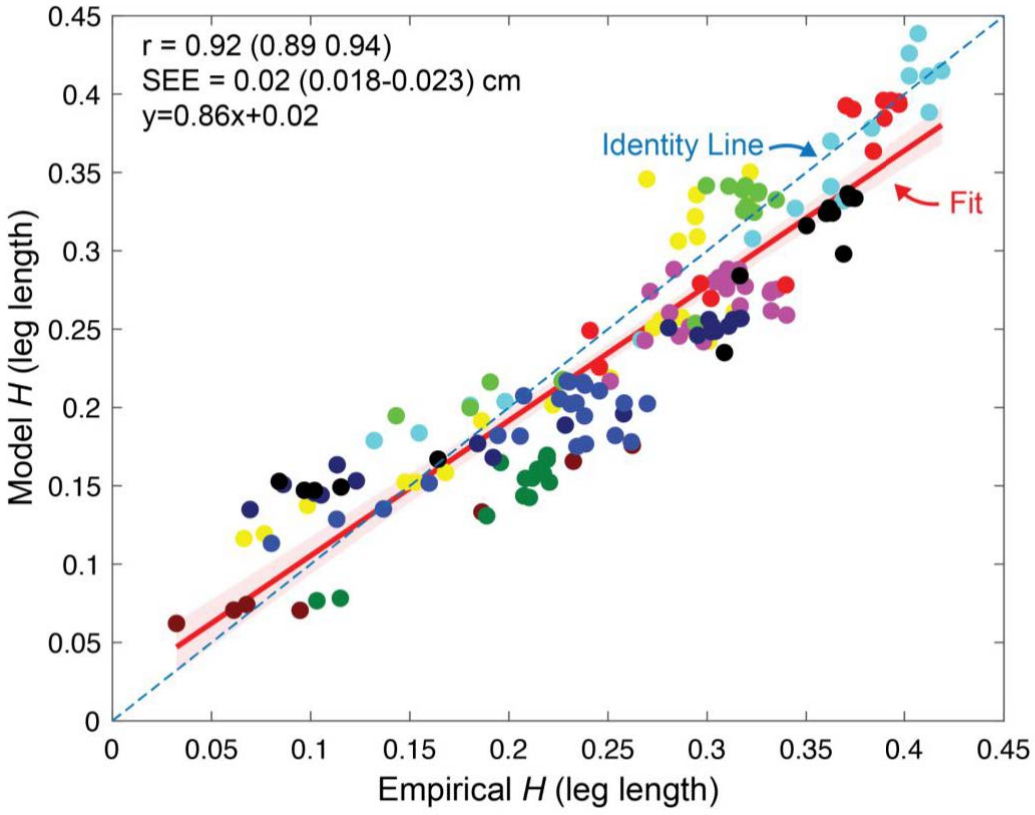

Figure 4-6 Comparison between the vertical jump heights H of the empirical data and the model-predicted jump heights for all participants. Each participant is represented by a different colour dot. The figure includes the line of identity (dotted line) to demonstrate the ideal scenario where the predicted jump heights perfectly match the empirical data. The line of best fit (solid red line) is also shown, indicating the trend between the predicted and empirical jump heights. The shading on the best-fit line indicates the 95% confidence interval. The corresponding r-value and standard error of the estimate (SEE) statistically measure the goodness of fit between the predicted and empirical data

Table 4-2 Comparing empirical and model peak vertical ground reaction forces, $\boldsymbol{F_{vGRF}}$ (bw), and the jump heights, $\boldsymbol{H}$ (leg length), across jump depths from shallow to deep jumps. Corresponding p-values from the t-test are shown. sd = standard deviation.

y_{ground}	**Empirical**			**Model**			***p*-value**
	Peak F_{vGRF} (bw)		sd	Peak F_{vGRF} (bw)		sd	
Shallow	3.14	±	0.35	2.47	±	0.36	0.001
	2.91	±	0.29	2.34	±	0.34	0.002
	2.47	±	0.20	2.16	±	0.30	0.069
	2.27	±	0.15	2.11	±	0.27	0.134
Deep	2.18	±	0.19	2.08	±	0.29	0.344
	H		sd	H		sd	
Shallow	0.15	±	0.08	0.15	±	0.06	0.999
	0.26	±	0.08	0.20	±	0.08	0.179
	0.29	±	0.07	0.26	±	0.09	0.199
	0.31	±	0.07	0.28	±	0.10	0.653
Deep	0.31	±	0.07	0.30	±	0.09	0.709

4.4.3. Force-velocity and maximal force $\boldsymbol{F_{max}}$ limit jump height through the attenuation of external force

Now that we have a model capable of accurately predicting jump height from various depths using a single set of parameters, we can analyze it to determine the factors that limit jump height (Table 4-3). By completely removing the force-velocity (F-V) relationship from our actuator in the model, we eliminated the dependence of the actuator's force on its velocity. This removal freed the actuator from the constraints imposed by its force-velocity characteristics, allowing it to generate higher forces irrespective of its velocity. Consequently, jump heights increased, with average increments of 283±91% for shallow depths and 304±91% for the deepest depth (Table 4-3). On the other hand, increasing the maximal force (F_{max}) involved enhancing the actuator's force-generating capacity. By increasing F_{max}, the actuator could exert greater forces during the jumping motion. A 25%

increase in F_{max} resulted in an average jump height increase of 20.1±5.1% for shallow jumps and 26.7±6.1% for deep jumps. Whereas a 1000% increase in F_{max} led to large jump height improvements, with increases of 336±129% for shallow jumps and 416±201% for deep jumps. Conversely, removing the force-length (F-L) relationship had a minimal overall impact, yielding average increases of 4±3% for shallow jumps and 17±10% for deep jumps.

Eliminating the F-L and F-V relationships led to the largest increase in jump heights across all starting depths. However, these improvements were only modestly higher than those achieved by solely removing the F-V relationship, as illustrated in Figure 4-7. This outcome highlights the limitations imposed by the F-V relationship and F_{max} attenuating jump height.

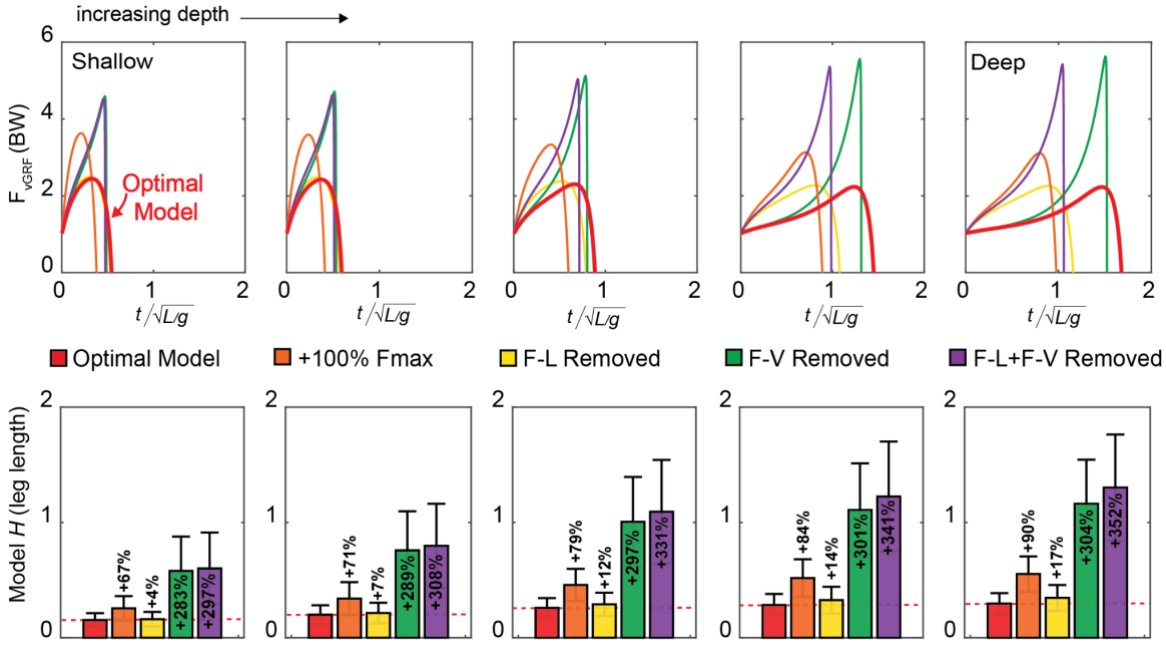

Figure 4-7 A. Vertical external forces predicted for our optimal model (red), our model with +100Fmax (orange), F-L removed (yellow), F-V removed (green), and with both F-L and F-V removed. The force traces here are of one participant's optimal parameter set. B. Group mean and standard deviation (error bars) of the resultant jump heights of the optimal model and for each corresponding parameter change.

Table 4-3 Sensitivity analysis of our optimal jumping model. Each participant's model was parameterized using their individually optimized parameters. We then sequentially increased each parameter ($\boldsymbol{F_{max}}$, $\boldsymbol{V_{max}}$,and $\boldsymbol{w}$) by +2.5%, +5%, and +25%. An increase in $\boldsymbol{V_{max}}$ reduces the effects of the force-velocity (F-V) relationship, while an increase in $\boldsymbol{w}$ reduces the effects of the force-length (F-L) relationship. To study the individual effects of these constraints, we also removed the F-L and F-V properties and increased the value of $\boldsymbol{F_{max}}$ up to 1000%. The table shows the resultant simulated changes in jump height with changes to model parameters. Jump height is shown in mean±std % change

Force-Length (F-L)												
y_{ground}	+ 2.5% w			+ 5.0% w			+ 25% w			w removed		
Shallow	0.2	±	0.2	0.4	±	0.3	1.6	±	1.2	4.4	±	3.3
	0.3	±	0.2	0.6	±	0.5	2.3	±	1.8	6.5	±	4.8
	0.6	±	0.4	1.1	±	0.8	4.2	±	3.0	11.7	±	8.2
	0.7	±	0.4	1.3	±	0.8	5.2	±	3.2	14.3	±	8.5
Deep	0.8	±	0.5	1.6	±	1.0	6.0	±	3.8	16.6	±	10.2
Force-Velocity (F-V)												
	+ 2.5% V_{max}			+ 5.0% V_{max}			+ 25% V_{max}			V_{max} removed		
Shallow	2.7	±	0.5	5.3	±	1.0	25.1	±	4.8	282.8	±	91.1
	2.7	±	0.5	5.4	±	0.9	25.2	±	4.6	288.9	±	89.6
	2.7	±	0.5	5.4	±	0.9	25.4	±	4.6	297.4	±	91.1
	2.8	±	0.5	5.4	±	0.9	25.5	±	4.6	300.8	±	89.5
Deep	2.7	±	0.5	5.4	±	0.9	25.6	±	4.5	303.7	±	90.6
F-V + FL												
	+ 2.5% V_{max} , w			+ 5.0% V_{max} , w			+ 25% V_{max} , w			V_{max} , w removed		
Shallow	2.9	±	0.5	5.8	±	1.1	27.0	±	5.2	296.6	±	97.1
	3.0	±	0.6	6.0	±	1.1	27.9	±	5.5	307.6	±	98.4
	3.3	±	0.7	6.5	±	1.4	30.3	±	6.8	330.7	±	107.9
	3.4	±	0.7	6.8	±	1.4	31.5	±	6.6	341.6	±	107.6
Deep	3.6	±	0.8	7.1	±	1.5	32.7	±	7.3	351.8	±	111.8
Increased F_{max}												
	+ 2.5% F_{max}			+ 5.0% F_{max}			+ 25% F_{max}			+1000% F_{max}		
Shallow	2.2	±	0.6	4.3	±	1.1	20.1	±	5.4	336.8	±	129
	2.3	±	0.6	4.5	±	1.1	21.3	±	5.6	348.9	±	130
	2.5	±	0.6	5.0	±	1.1	23.8	±	5.5	379.7	±	154
	2.7	±	0.5	5.4	±	1.1	25.2	±	5.5	402.8	±	191
Deep	2.9	±	0.6	5.7	±	1.2	26.7	±	6.1	416.4	±	201

4.4.4. Participants preferred to jump at depths that balance maximizing jump height and minimize jump time.

In Experiment 2, participants executed jumps from their preferred positions to maximize their jump heights. We then examined if each participant's optimized model could predict their preferred jumping depth without prior training on the data collected in Experiment 2. To achieve this, we adjusted the weight parameter (W) between 0 and 1 in our objective function to balance the goals of maximizing jump height and minimizing movement time. When solely focused on maximizing jump height (W=0), the models' predictions favored deeper starting positions (Figure 4-8). However, these predictions did not align with the observed vertical external forces from our experimental data (Figure 4-8). We further explored a range of W values to adjust the priorities in the objective function and identified model outputs that accurately matched the observed vertical external forces for each participant, even without prior training on the data collected in Experiment 2 (Figure 4-8).

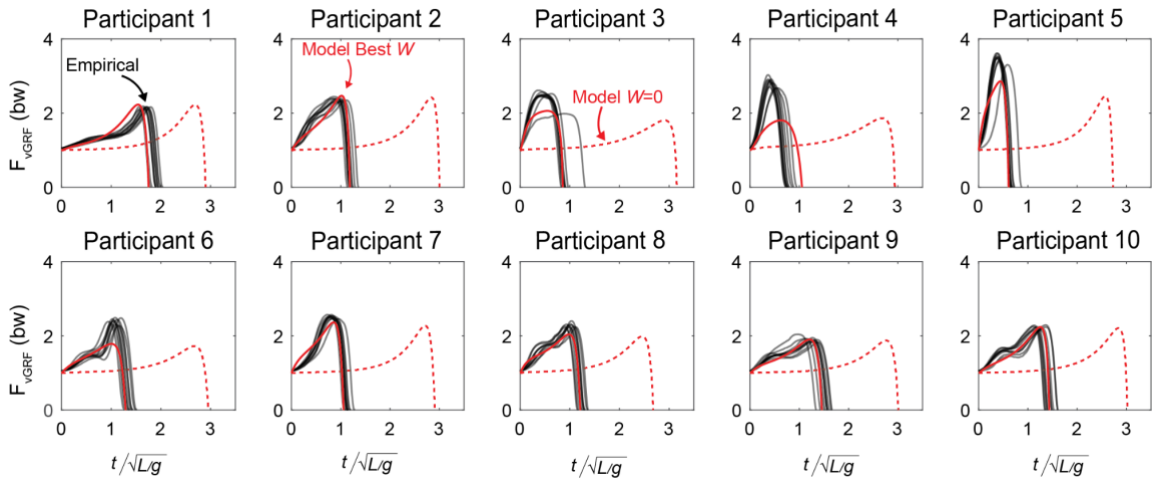

Figure 4-8 Comparison between the preferred maximum vertical jump external forces for each participant (black) and the model-predicted optimal jumping depths external forces (red). Participants performed ten jumps from their preferred starting positions, and we optimized the starting depth of individual-specific models to simultaneously maximize jump height and minimize jump time. The objective function incorporated weights to prioritize jump height, jump time, or a balance of both. When the objective function focused solely on jump height (red dashed line), participants tended to select longer jump durations from deeper starting positions, but this did not align closely with the empirical data. In contrast, when the objective function balanced jump height and jump time with varying weights (W), the optimized models accurately predicted the empirically optimal starting positions for each participant, even without prior exposure to this data. This demonstrates the importance of considering both jump height and jump time in determining the ideal starting position for vertical jumping

Participants in our study demonstrated a preference for jumping in a manner that optimized both jump height and movement time. To examine this further, we plotted the relationship between the preferred jump height and a range of objective weight parameter values, representing the trade-off between prioritizing jump time (W=0) and jump height (W=1). The model that best fits the empirical data was placed on this line. From the analysis, we observed that when the model objective solely prioritized jump height, it achieved higher jumps. However, the model best fitting the empirical data showed a balance between jump height and time. We quantified the loss in jump height for this preferred model and calculated the ratio of speed improvements. The results revealed that most participants achieved speed improvements with minimal losses in jump height (Table 4-4). This indicates that participants could optimize their jumping performance by increasing speed while maintaining satisfactory jump heights.

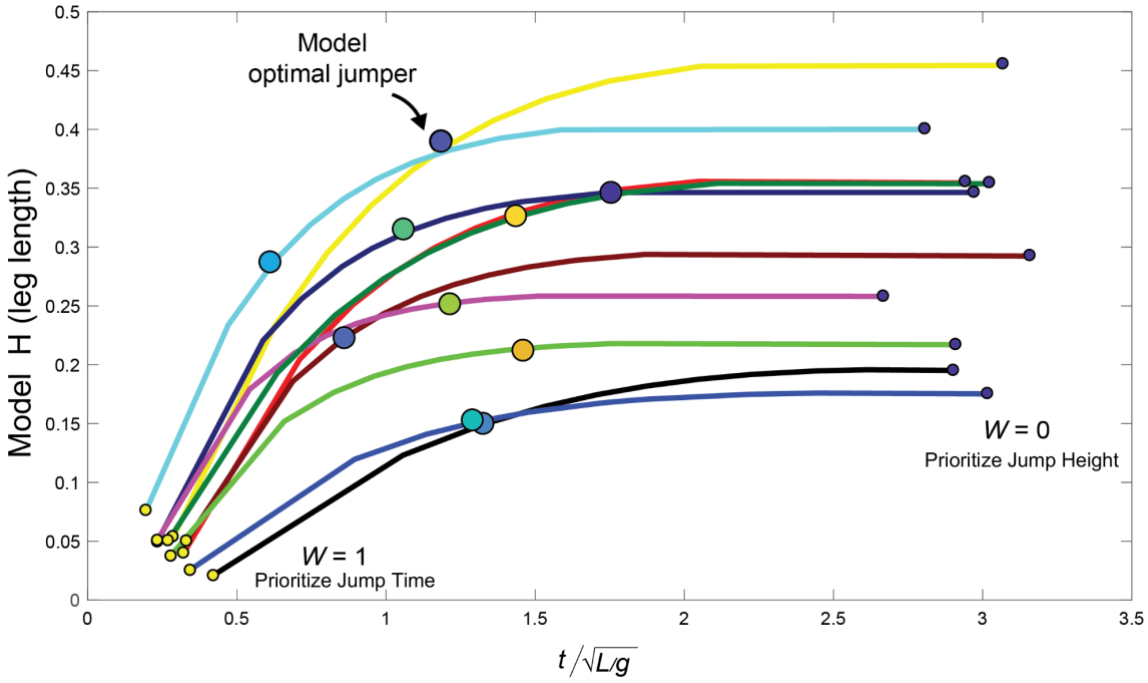

Figure 4-9 Model jump height predictions for the full range of W values from 0 to 1. When the objective function prioritizes jump time (W=1), jumpers have the shortest duration of jumps and achieve the lowest height. Conversely, jumpers achieve the highest jumps when the model prioritizes jump height (W=0). The optimal model that fits the empirical data (represented by large circles) for each participant strikes a balance between maximizing jump height and reducing jump duration

Table 4-4 Comparison of jump height reductions and speed improvements for each participant's optimal depth model

Participant	Jump Height Reduction (%)	Speed Improvement (x)
P9	2.4	2.0
P8	2.7	2.2
P1	2.7	1.7
P10	8.0	2.1
P7	9.1	2.8
P6	13.0	2.3
P2	14.5	2.6
P4	23.7	2.2
P3	23.9	3.7
P5	28.3	4.6

4.5. Discussion

Our study presents a physics-based model that accurately predicts the vertical external forces generated during vertical jumps from a range of initial depths using a single set of optimally determined actuator properties. Across all depths, our model could predict the vertical external forces with a mean R^2 of 0.89±0.10 and an RMSE of 0.45±13 body weights. Our findings highlight the importance of the force-velocity relationship and the maximal force (F_{max}) in determining jump height. Reducing the impact of the force-velocity relationship by increasing V_{max} resulted in proportional increases in jump height relative to each participant's optimal parameters. A 5% increase in V_{max} increased jump height by 5% across all depths; removing V_{max} all together had the largest increase of ~300%. We found a similar finding for increases in F_{max}, where the actuator showed a higher F_{max} the model would jump higher. Reducing the effects of the force-length relationship by widening the parabola had only a small effect on improving jump height. Our study also showed that when instructed to jump high from their own self-selected initial starting depths, participants demonstrated a preference for jumping in a manner that traded off between both jumping high and minimizing jump duration. By jumping quicker and not solely maximizing jump height, our model showed alignment with the experimental data with only

minimal reductions in jump height. For example, some participants demonstrated only ~3% jump height reductions but gained ~2x speed improvements.

Our study has several limitations, simultaneously serving as avenues for future research. First, we intentionally simplified the biomechanical processes. While this approach effectively captures the jump movement and aligns well with empirical data on resultant vertical external forces, it does not consider muscle coordination, which may be significant for maximizing jump height [187], [188]. However, our model's simplicity facilitates a focused analysis of the fundamental principles governing vertical jumps, a strategy proven effective for understanding bipedal locomotion using simplified walking models [179], [180]. Second, our model employs a single muscle actuator to signify the collective behaviour of all involved muscles, thereby not accounting for the role of bi-articular muscles, which span two joints and enhance jumping performance [187], [189], [190]. This simplification, while reducing some detail, effectively captures the overall resultant forces of the jump. The strength of starting with this simplified model lies in its clarity. The simplicity allows for a precise and focused understanding of vertical jumps' core principles. We could introduce more complexity to the model as we progress, such as incorporating bi-articular muscles or additional link segments. With each added layer of complexity, we can discern the specific value it brings, the insights it uncovers, and the degree to which it refines our understanding of vertical jumping mechanics. This iterative process allows us to appreciate the specific contributions of more intricate components like bi-articular muscles while maintaining a grounded understanding of the foundational principles. Lastly, while our model currently focuses on vertical jumping, our framework enables us to extend our study to other jumping movements, such as high and long jumps. This further demonstrates the utility of beginning with a simpler model and progressively adding complexity based on the specific goals of the research.

Our findings align with those from a more sophisticated musculoskeletal model. Our model and the intricate model encompassing four-link segments actuated by eight Hill-type muscle actuators identify force-velocity properties as the primary constraint on jump height [81]. When we eliminated the force-velocity relationship in our model, jump height increased by 300%, echoing the 271% increase observed in the complex model. Both studies highlight the role of the maximum isometric force (F_{max}) in maximizing jump height. Doubling $F_{max,}$ in the complex model resulted in a 143% jump height increase, while in our model, the same action results in an 80% average increase across various starting depths.

Both models also agree on the relatively minor influence of the force-length relationship on jump height, with our model showing up to a 17% increase and the complex model a 29% increase when the force-length relationship width was doubled. Despite the complexity differences between the two models, they are not mutually exclusive but complementary. Each offers unique insights: the more intricate model provides data on coordination and 8 muscle actuators, while our simplified model facilitates a more direct, foundational examination.

Optimizing for jump height while minimizing jump duration is a strategy that the nervous system may employ, with only minor losses in performance. Our findings suggest a slight decrease in performance when jumping faster, which is offset by a noticeable increase in speed. Other simulations have also shown minimal performance loss within a range of jump durations, provided that adjustments are made to the initial position and overall muscle activations [185]. Humans may make near-optimal adjustments with minimal practice by leveraging proprioceptive information from their initial posture [191]. This may contribute to why similar vertical jump heights can be achieved from a range of initial starting positions [80]. The ability to generate force over longer periods potentially facilitates increased external force production and acceleration of the center of mass. Nonetheless, our research suggests that force-velocity properties may limit the possibility of substantial enhancements in jump height, even with prolonged jump durations. This necessitates maintaining a careful balance between maximizing limb forces and extending the time these forces apply to the ground [192]. The constraints imposed by force-velocity properties could result in diminishing returns in force generation. Bearing that the nervous system may prioritize energy optimization, a trade-off may exist between jump height and duration aimed at conserving energy [193]. This notion is supported by another jumping model that, using reinforcement learning to prioritize energy efficiency, achieved a slightly lower jump height but was 18% more energy-efficient than the model that solely prioritized jump height [194]. While further study is needed with human participants, it's plausible that the nervous system might concurrently optimize jump height, duration, and energy efficiency.

Understanding how biology circumvents force-velocity constraints could offer valuable insights for developing technology to enhance human jumping performance. For example, humans can attain greater vertical jumps through countermovement jumping, a feat partly credited to the increased stiffness of tendinous tissues. This stiffness is believed to reduce

the contraction velocity of muscle fibers, thereby increasing the resultant force [189], [195], [196]. Specialized jumping animals have evolved unique adaptations to overcome the constraints of the force-velocity relationship. Kangaroos, for example, have elongated limbs that allow for a larger acceleration distance, reducing the need for rapid muscle contractions and enabling higher force generation [68]. Insects have developed a different strategy, generating significant force through slow muscle contraction and storing this energy in elastic structures within their bodies [197], [198]. This approach capitalizes on the force-velocity relationship, allowing high force production at low velocities. Insects gradually contract their muscles, storing the generated force as potential energy in elastic structures. Upon release, this stored energy propels them into action. Fleas use it to leap impressive distances, mantis shrimps employ it for exceptionally fast punches, and click beetles rely on it to catapult themselves into the air.

Looking ahead, our model has the potential to offer person-specific insights valuable for both training and rehabilitation. By optimizing a model's actuator properties to correspond with a specific athlete's external forces, coaches could monitor changes in muscle actuator properties and resultant external forces. For instance, a coach could modify parameters such as the maximum isometric force (F_{max}) and force-velocity relationship in the model to anticipate an athlete's potential improvement in jump height during strength training. This would enable them to prescribe and assess the effectiveness of training and plyometric exercises, which are known to boost the force and velocity of movements [199]. Similarly, following ACL surgery or other musculoskeletal injuries, the model could be a valuable tool for monitoring recovery progress during rehabilitation. On a practical level, the model could help shape training program design and potentially guide equipment development to enhance jump performance. Nevertheless, these applications would necessitate further research to verify the model's predictive accuracy and efficacy in these contexts. The model's utility could even extend to the field of robotics, potentially influencing the mechanics of jumping robots, although such a broad application would require additional study.

Chapter 5. Estimating ground reaction forces and vertical jump height from video using pose estimation and machine learning

5.1. Abstract

Video data presents an opportunity that is widely accessible for taking biomechanical measurements out of the lab and into the field. In this study, we introduce a new method for predicting external ground reaction forces during vertical jumps using video data. We recruited 30 participants, capturing their movements on video from front and side views as they performed a series of vertical jumps. Simultaneously, we recorded each leg's ground reaction force using force plates. We processed the video data using OpenPose to extract kinematic landmarks of each participant's body during the jump. We then inputted these landmarks into a transformer-based neural network, which we trained to predict external ground reaction forces. The network achieved high accuracy, with an average R2 of 0.94 ± 0.05 and an RMSE of 0.12 ± 0.05 bw when using front-view video. We found that video perspective significantly impacts prediction accuracy, with front-view videos consistently outperforming side view. When using our measured external forces to predict jump height, we observed small group mean differences ranging from -0.63 to 0.14 cm when using front-view videos and -1.63 to 1.1 cm when using side-view videos. The front view videos showed a standard error of the estimate of 1.8 cm (range: 1.69 - 1.95 cm), with a correlation coefficient (r) of 0.68 (95% CI: 0.62-0.70). Implementing our approach could improve the accessibility of detailed biomechanical analysis, allowing for more available and convenient tracking of an individual's movements outside the traditional lab settings.

5.2. Introduction

Our ability to move is rooted in how we manipulate the forces when our feet contact the ground. Well controlling external ground reaction forces enables is one reason we can move in many different ways and environments [15], [200]. Accurate measurement of external forces is critical for assessing performance and is a key tool in preventing, diagnosing, and treating injuries related to movement [201]. External force measurements require specialized equipment, such as force platforms, designed to quantify the forces exerted by the body precisely [127]. However, the reliance on this type of sophisticated and sensitive equipment poses a challenge, as it restricts accurate force estimation to lab environments, limiting the scope of practical applications and real-world context.

Efforts to estimate ground reaction forces outside of the laboratory have led to various innovative solutions, one of which includes the use of wearable sensors. These portable devices can deduce biomechanical movement parameters using physiological data and

gravitational accelerations. Researchers have achieved reliable external force estimation by integrating this sensor data with machine learning algorithms. For instance, placing accelerometers on the hip and shoe is effective in accurately estimating continuous vertical ground reaction forces during varied speeds and gradients of running [99], [202]–[204] Other wearable technologies like pressure sensors embedded in shoe insoles and inertial measurement units for tracking whole-body movement have also demonstrated efficacy in predicting external forces across different activities [101], [205], [206]. However, wearable sensors are not without challenges; correct sensor placement is crucial, and users must be willing to acquire, remember to use, and regularly charge these devices [207], [208].

The ubiquitous integration of video cameras into smartphones enables easy video capture, creating opportunities to leverage video for performance monitoring and healthcare applications. Researchers can predict detailed movement biomechanics without needing a laboratory by merging video data with computer vision and machine learning techniques [92], [209]. Using computer vision techniques like markerless motion capture, in-depth human movement tracking is possible without physical markers or specialized equipment [210], [211]. These advancements can simplify biomechanical analyses and broaden data accessibility to a broader population equipped with cameras [85], [86]. With continued advances in computer vision, portable systems incorporating smartphone video capture capabilities enable large-scale biomechanical analysis beyond the limitations of traditional lab environments [93]. Using video presents exciting opportunities for laboratory-level biomechanical analysis with minimal patient interaction and time commitment [92]. Although initial efforts in estimating external forces from videos show promise [212], [213], this area remains an emerging topic.

Our work aims to address this gap by developing a machine-learning approach capable of accurately estimating external ground reaction forces from RGB video. To do this, we recruited 30 participants to perform vertical jump tasks. Here we focus on a single task, vertical jumping, where we use RGB video to predict the leg's external ground reaction forces during the duration of the ground phase of the jump and then use this to estimate vertical jump performance and peak vertical forces. We first simultaneously recorded each participant's ground reaction forces using a ground-mounted force plate and front and side plane videos using hardware-triggered cameras. We then applied a pose estimator, OpenPose, to each video to extract 25 kinematic landmarks of each participant's body

performing the jump. We then input these predicted kinematics into a transformer-based neural network, testing different combinations of training inputs for model performance. Finally, we evaluated the model's performance against the gold standard lab-collected ground reaction forces.

5.3. Methods

5.3.1. Participants

We recruited 30 participants for our study (n=18 identifying as female, n=11 identifying as male, and n=1 identifying as non-binary). The participants' demographic data is as follows: age, 33.0±9.5 years; body mass, 68±12 kg; height, 171±11 cm (mean±std). Simon Fraser University's Office of Research Ethics approved the study, ensuring all experiments complied with relevant guidelines and regulations. Before participating, all participants provided informed written consent. We requested participants to wear form-fitting t-shirts, shorts, and their preferred running shoes for the study.

5.3.2. Experimental Setup

We instrumented our lab to collect gold-standard ground reaction force data with time-synchronized RGB videos. We incorporated two force plates (Bertec Corporation, Ohio, USA) connected through a USB DAQ board (National Instruments USB-2289), sampling at 800Hz. We then installed two hardware-triggered video cameras (Blackfly-S, FLIR) to collect video data from the sagittal and frontal perspectives. We positioned the cameras 2.5 meters from the force plates, ensuring they adequately captured the desired volume of interest. We established a hardware trigger to synchronize the force plates with our cameras and the cameras with each other. This trigger responded to a +5V square wave, activating each camera at a frequency of 80Hz. We configured the hardware trigger using a GIPO connection to the camera, adhering to the manufacturer's recommended protocol.

5.3.3. Data Collection

We asked participants to execute vertical squat jumps. We recorded external ground reaction forces from both legs during these tasks and simultaneously captured the

associated videos (Figure 5-1). We randomized the task sequence. However, this paper focuses solely on the jumping task as a proof of concept for our system.

For the jump task, we instructed participants to perform squat jumps, which begin from a stationary position at a predetermined depth from the ground, followed by rapid upward acceleration. We used a flexible horizontal pole on a vertical stand for the initial fifteen jumps to guide participants to start from specific depths. This approach allowed us to collect data for five different jumping depths three times each. After that, we removed the pole device, allowing participants to select their preferred squat depth for the next five jumps. We asked participants to maximize jump height while keeping their hands firmly on their hips throughout all jumps.

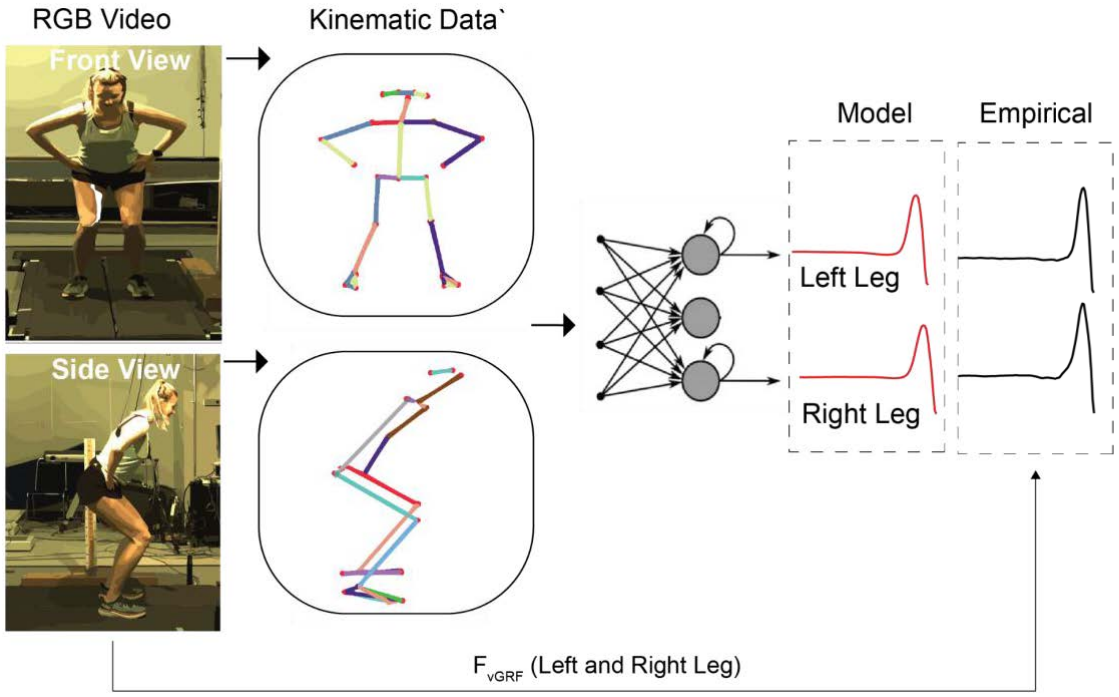

Figure 5-1 Experimental setup. We recorded RGB video from the front and side views as participants performed jumps in the laboratory. We used an instrumented force platform to capture each leg's external ground reaction force vectors for each leg. We achieved synchronization between the force platform and cameras through a hardware trigger. Following video capture, we employed OpenPose, a computer vision module, to predict the 2D positions of 25 body landmarks for each frame in the video. We used subsets of these landmarks as inputs to train a neural network model to predict the vertical external forces based on the kinematic inputs.

5.3.4. Data Preparation

We began by extracting kinematic features from each video frame by frame using a computer vision approach called pose estimation. We processed all videos using OpenPose, a commonly used neural network-based software for predicting human poses in video frames [90]. For every participant in each video frame, OpenPose identifies the 2D position of 25 body landmarks: the nose, neck, midpoint of the hips, bilateral shoulders, elbows, wrists, hips, knees, ankles, eyes, ears, first metatarsals, fifth metatarsals, and heels. We applied OpenPose to each video frame, maintaining the original frame rate of 80 Hz at which we collected the videos. This methodology proved effective as we did not have to drop video frames from any of our participant's jumping data. One major reason for this success is the static nature of our cameras and the excellent views of each participant in each camera's view.

Next, we prepared this kinematic data to train our machine-learning model. The preparation involved gap-filling, filtering, and normalization. First, we implemented a gap-filling method to fill any gaps in the pose data [92]. We then converted any missing observations not gap-filled as NaN in our input data. We then filtered the data using a 4th-order Butterworth filter that handled missing data [92]. Finally, we reformatted the kinematic data by centering and normalizing each landmark. We did this by subtracting the coordinates of the right hip and then scaling all values by dividing by the Euclidean distance (measured in pixels) between the right hip and the right shoulder. We did this to help with generalization across participants of heights and sizes [92]. We later addressed gaps in our data marked as NaN within our machine learning architecture by implementing a mask in the neural network that would ignore this data as missing and not use it for training [214].

Next, we prepared our kinetic data collected from the force plates. This included the vertical left and right leg ground reaction forces. First, we down sampled the data to 80Hz to match the kinematic data by resampling every tenth frame. We then used a dual-filtering approach involving a notch filter and a Butterworth low-pass filter. Here we used a Nyquist frequency of 400 Hz and a cutoff frequency of 30 Hz for the Butterworth filter. We designed the notch filter to eliminate specific noise at 60 Hz. The initial step involved the removal of the 60 Hz noise from the raw data using the notch filter. Subsequently, we applied the Butterworth filter to the notch-filtered data to suppress frequencies above 30 Hz.

Finally, we trimmed the kinetic data to end at the period when the participants' feet left the ground and the left and right external force readings on the force plates were approximately zero. Due to equipment noise, this value typically hovered around zero but was never zero. We implemented a simple threshold algorithm to trim the data, which was detected when the ground reaction force dropped below 0.001 body weights. Once we detected this threshold, we set the subsequent value for the force to zero, marking the completion of the ground phase of the jump. We then trimmed the kinematic data to also stop at this point.

5.3.5. Machine learning model

We trained a neural network architecture tailored for time series tasks. Initially, we constructed a bidirectional Long Short-Term Memory (LSTM) architecture. We began with a framework that had previously succeeded in a similar task [99], and from there, we optimized the hyperparameters, such as the number of LSTM layers, the number of LSTM units per layer, and the learning rate, using Keras-Tuner [215]. We employed the Adam gradient descent optimization algorithm, set the mean squared error as the loss function, and selected hyperparameters that minimized the root mean squared error (RMSE) on the validation set. We then incorporated a TransformerBlock with multi-head attention mechanisms, which, as per our pilot testing, improved the neural network predictions.

Our model used a Transformer-based architecture central to a custom class called TransformerBlock. This class integrates several elements of Transformer functionality, including a multi-head attention mechanism, a feed-forward neural network, two-layer normalization processes, and two dropout layers. After the attention calculation, we implemented a dropout layer to mitigate overfitting [216]. The outputs of the attention mechanism were then subjected to LayerNormalization and added back to the original inputs through a residual connection [217]. This technique addresses the vanishing gradient problem, which can hinder learning in the earlier layers of deep neural networks compared to the later ones [19]. We applied the same approach—residual connections and normalization—to the outputs of the feed-forward network, ensuring that the entire network benefits from these techniques. We set the TransformerBlock parameters—an embedding size of 64, two attention heads, and a hidden layer size of 32 for the feed-forward network—based on the requirements of our data and from pilot testing with different combinations of parameters. We then passed the processed inputs through the

TransformerBlock, and the outputs through additional dropout and dense layers, with Relu activation functions applied. The final layer of the model is a Dense layer with two neurons, one for each leg, using a linear activation function to generate continuous output predictions. We optimized this Transformer model to learn effectively from the provided data through optimization and trial and error pilot testing.

We used the kinematic data from OpenPose as inputs to our models and the kinetic data (external force) from the force plate as the output. Our approach involved data reduction to determine the optimal set of kinematic data inputs to predict the output kinetics. We began with a comprehensive set of body landmarks predicted by OpenPose, which we call Major. This set comprises the landmarks for the bilateral shoulders, elbows, wrists, hips, knees, ankles, and heels. In the next iteration, Core, we reduced the data to include only bilateral shoulders, hips, knees, and ankles. Finally, in Reduced, we further streamlined the data to include bilateral shoulders and hips. In all cases, each of these landmarks provided two dimensions of data - the 'X' and 'Y' coordinate values, representing horizontal and vertical positions, respectively. Therefore, for each participant and each jump, we acquired a time series of vectors, each with a dimensionality of #landmarks*2 (for example, eight landmarks, each having 'X' and 'Y' coordinates, resulting in a 16-dimensional vector). The length of the time series varied with the duration of the jump. This high-dimensional, time-series data served as the input to our neural networks. Through training, we optimized the networks to learn and predict the dynamic motion characteristics intrinsic to human jumping, as described by the coordinated movement of these key anatomical landmarks.

5.3.6. Data Analysis

To test our networks' accuracy and generalizability, we employed the leave-one-participant-out (LOPO) cross-validation method. As a variation of K-fold cross-validation, LOPO divides the dataset by participant [218]. In each iteration, we reserved one participant's data for testing and used the remaining data to train the network. We repeated this process until we tested the network with each participant's data, creating an ensemble of networks and their accuracy metrics. There is an inherent computational demand for LOPO cross-validation necessitating as many rounds of network training and testing as there are participants (n = 30). Still, this approach enables us to produce the best set of

accuracy metrics. We avoid artificially inflated accuracy reports by not including the same participant's data in training and testing subsets [219].

Next, we assessed our model's accuracy in predicting jump heights by comparing the model's predicted outcomes to the empirical data. We calculated the jump height based on the impulse-momentum principle using the vertical ground reaction force (GRF) data gathered from force plates and the model predictions. This GRF data consisted of the normalized left ($\underline{F}_{left}$) and right ($\underline{F}_{right}$) ground reaction force values in body weight units. We converted these normalized forces back to kilograms by multiplying by each participant's mass m and gravitational force g =9.81 m/s², allowing us to output jump height in meters. We then determined each jump's time variable for integration, allowing us to integrate the force numerically. By doing this, we obtained the impulse for each leg from the beginning of the jump t_i to the moment of take-off from the ground t_f:

Equation 5-1 $$\int_{t_i}^{t_f} \underline{F}_{left_{vertical}}\, mg\, dt + \int_{t_i}^{t_f} \underline{F}_{right_{vertical}}\, mg\, dt - \int_{t_i}^{t_f} mg dt = mv_{to}$$

We rearranged Equation 5-1 to find the vertical take-off velocity v_{to}. We can understand the relationship between jump height and take-off velocity v_{to} by applying the law of conservation of mechanical energy to both the ground and flight phase of the jump. Assuming negligible air resistance and considering the changes in kinetic energy and gravitational potential energy of the center of mass between the instant of takeoff from the ground and the instant the jumper's center of mass reaches the peak of the jump (at which point velocity is 0), we can use the following equation:

Equation 5-2 $$1/2mv_{to}{}^2 + mgy_{to} = 1/2mv_{peak} + mgH$$

If we define the final position at the take-off of the center of mass to be y_{to} = 0 and the velocity at the peak of the jump to being v_{peak}= 0, we can solve for jump height:

Equation 5-3 $$H = v_{to}{}^2/2g$$

Jump height (H) is directly proportional to the square of the take-off velocity (v_{to}), and inversely proportional to twice the gravitational acceleration (g). Finally, we assessed our model's accuracy in predicting peak vertical force magnitude. Here we took the peak value of the vertical external force for each empirical force data and the model predicted force data.

5.3.7. Statistics

We used R^2 (coefficient of determination) and RMSE (root mean square error) to evaluate the accuracy of the predictions made by the deep learning model in comparison to the empirical data for the left, right, and total (left+right) external ground reaction force magnitudes. We used the jumping data from all participants and depths to investigate the relationship between model-predicted jump heights and empirical data across all jumping depths. To do this we used linear mixed-effects models. We leveraged two critical metrics to gauge the quality of the linear regression models developed: the correlation coefficient (r-value) and the standard error of the estimate (SEE). The r-value, ranging between -1 and 1, indicates the strength and direction of the relationship between the two variables. A higher absolute r value in our analysis suggests that the independent variable accurately predicts the dependent variable. Alongside the R-value, we used the SEE to assess the precision of our model predictions. The SEE estimates the standard deviation of the residuals, i.e., the differences between the observed and predicted values. A lower SEE in our research implies that my model is more precise, as the observed values closely align with the model's predictions. Additionally, we calculated descriptive statistics, including the mean, standard deviation, and the percentage difference between the means, to summarize the differences in jump heights.

5.4. Results

5.4.1. Accurate estimates of vertical ground reaction forces during vertical jumping

In our leave-one-participant-out (LOPO) cross-validation, the predictions from our model for the time series of the combined (left+right combined) vertical ground reaction force waveforms of each participant were robust. Using the front view video and the Core landmarks for training, we found an average R^2 of 0.94 ± 0.05 and an RMSE of 0.12 ± 0.05 (Table 5-1). We found promising results for the side view videos trained on the Core landmarks set, with an average R^2 of 0.83 ± 0.12 and an RMSE of 0.20 ± 0.07 (Table 5-1). The front view camera was consistently better than the side view camera, resulting in higher R^2 values and lower RMSE for all landmark sets used in training, including Major, Core, and Reduced landmarks. We did not observe notable differences across the models in predicting external forces when trained on different data sets for the front-view video.

The side view videos, on the other hand, showed the best overall performance when using the reduced marker set for training with an average R^2 of 0.91 ± 0.08 and an RMSE of 0.14 ± 0.06 (Table 5-1).

Table 5-1 The R^2 and RMSE values for the model predictions obtained from the front and side view videos. The estimates include vertical force for the leg, right leg, and combined force. The values are mean ± standard deviation (sd).

Front View Video									
Training Data	Right Leg Force			Left Leg Force			Combined Force		
	R^2		sd	R^2		sd	R^2		sd
Major	0.91	±	0.07	0.91	±	0.07	0.93	±	0.05
Core	0.92	±	0.06	0.91	±	0.07	0.94	±	0.05
Reduced	0.89	±	0.08	0.88	±	0.10	0.92	±	0.06
	RMSE (bw)		sd	RMSE (bw)		sd	RMSE (bw)		sd
Major	0.07	±	0.03	0.07	±	0.03	0.12	±	0.05
Core	0.07	±	0.03	0.07	±	0.03	0.12	±	0.05
Reduced	0.08	±	0.03	0.08	±	0.03	0.13	±	0.06
Side View Video									
	Right Leg Force			Left Leg Force			Combined Force		
	R^2		sd	R^2		sd	R^2		sd
Major	0.83	±	0.10	0.82	±	0.12	0.86	±	0.10
Core	0.80	±	0.13	0.80	±	0.15	0.83	±	0.12
Reduced	0.87	±	0.12	0.87	±	0.10	0.91	±	0.08
	RMSE (bw)		sd	RMSE (bw)		sd	RMSE (bw)		sd
Major	0.10	±	0.04	0.10	±	0.04	0.18	±	0.07
Core	0.11	±	0.04	0.11	±	0.04	0.20	±	0.07
Reduced	0.08	±	0.04	0.08	±	0.03	0.14	±	0.06

5.4.2. Our model captured trends across distinct jumps and participants.

The predictions of vertical ground reaction forces, closely mirroring the characteristics of the observed empirical data, further substantiate this capability (Figure 5-2 and Table 5-1). Although our models, on average, accurately predicted the overall vertical forces, the prediction distribution had some degree of variability (Figures 5-3 and 5-4). The model exhibited a strong performance across all three training sets for the front-view videos, with most of the R^2 values exceeding 0.9 (Figure 5-3). Conversely, the distribution for side-view videos was somewhat more dispersed, with most R^2 values falling within the 0.8 to 0.9 range. The side-view videos exhibited a higher error rate than the front-view videos (Table 5-1, Figure 5-4).

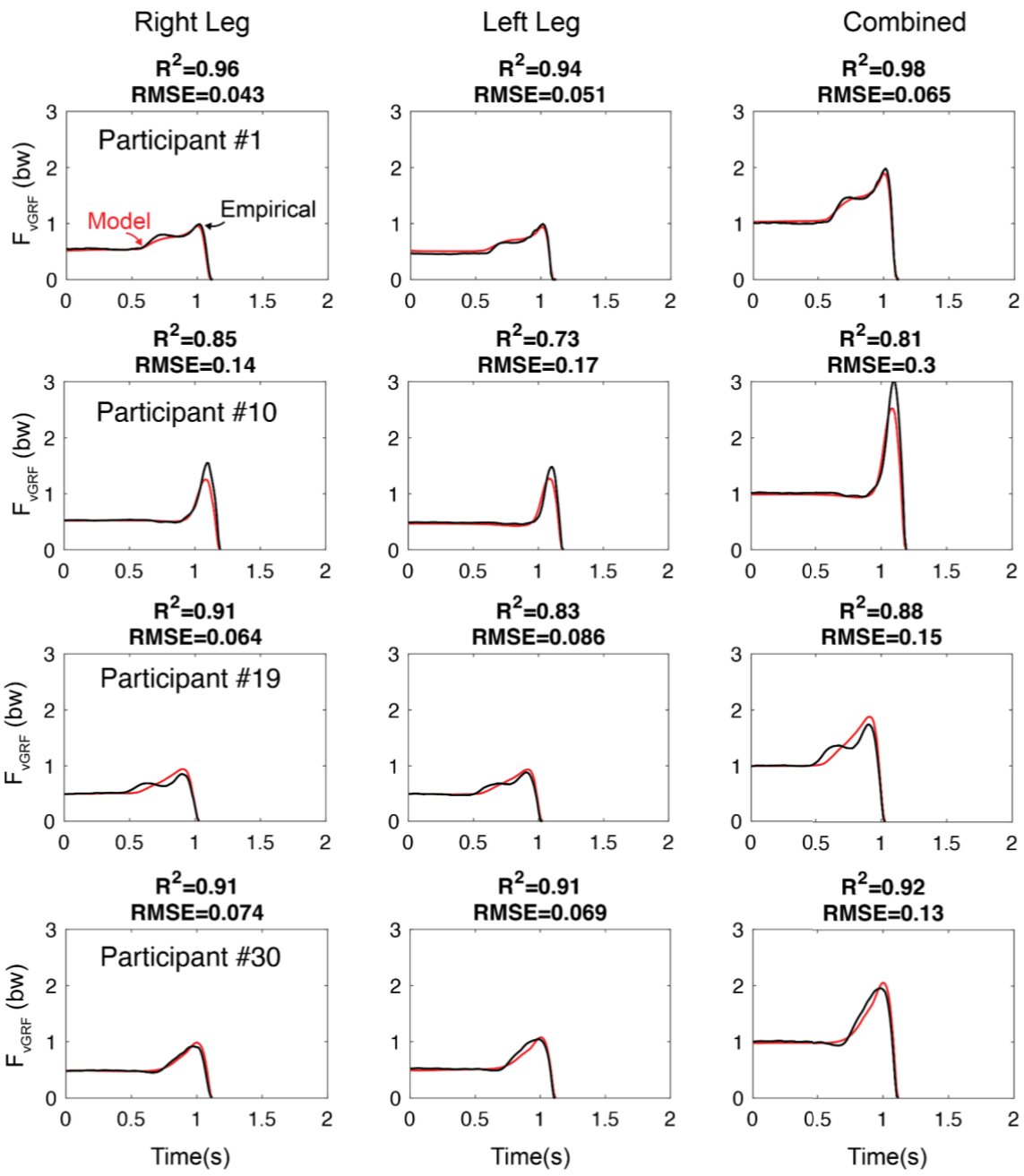

Figure 5-2 Representative data for five participants, comparing predicted and empirical vertical ground reaction forces. The figure demonstrates the alignment between the model predictions and the observed empirical data. Each jump includes the corresponding R^2 and RMSE values, quantitatively measuring the model's predictive accuracy.

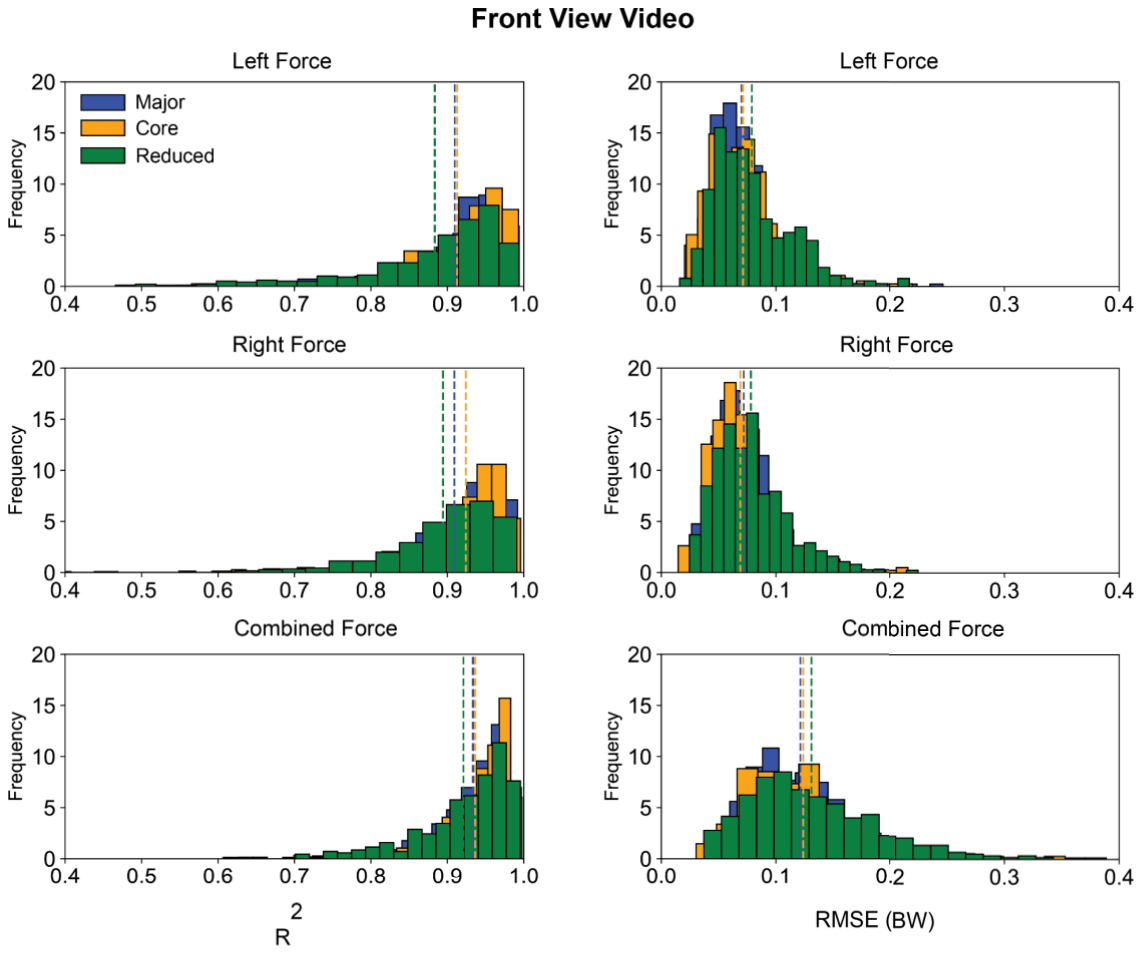

Figure 5-3 Histogram distributions of R2 (left) and RMSE Values (right) for model predictions using the front view videos. Three different model training datasets were evaluated: Major (blue), Core (yellow), and Reduced (green), representing datasets with decreasing numbers of kinematic landmarks. Vertical dotted lines indicate the mean value for each distribution.

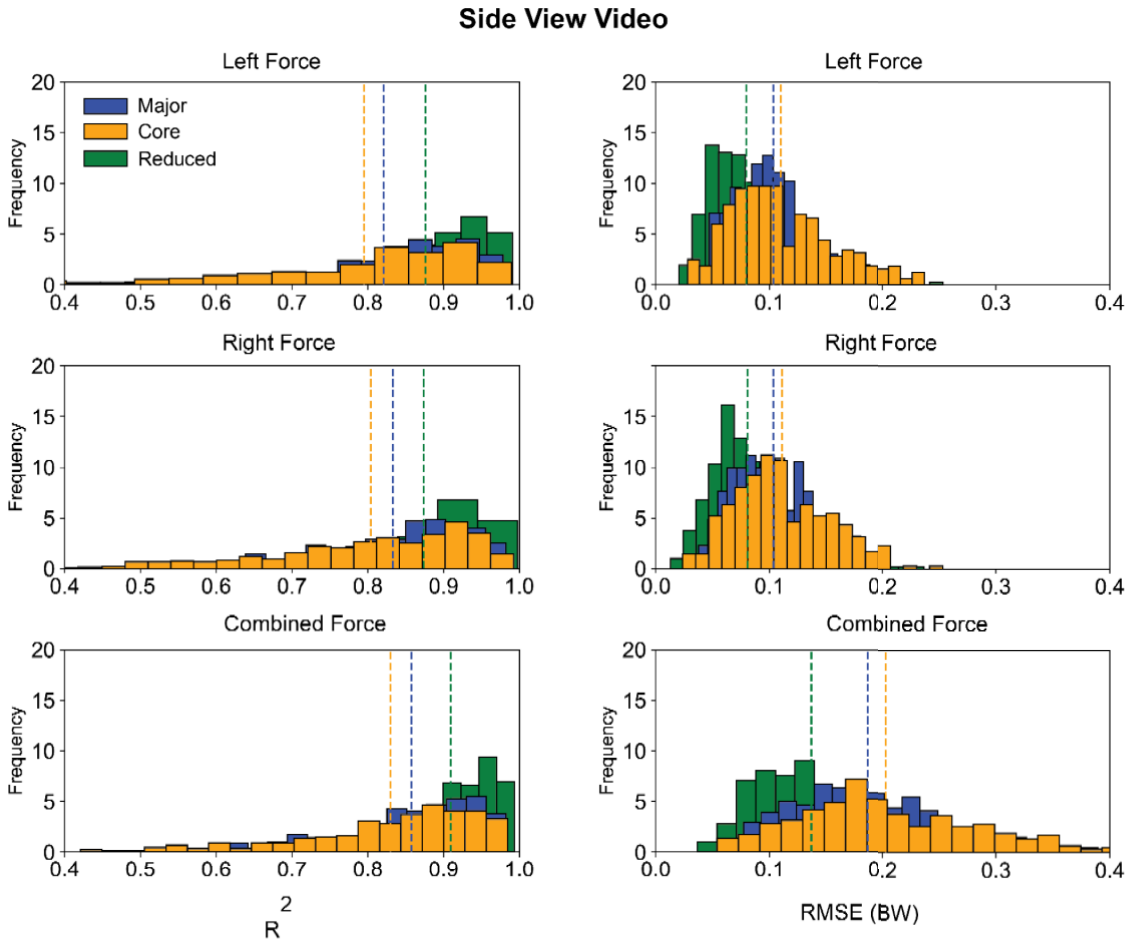

Figure 5-4 Histogram distributions of R2 (left) and RMSE Values (right) for Model Predictions Using the side view videos. Three different model training datasets were evaluated: Major (blue), Core (yellow), and Reduced (green), representing datasets with decreasing numbers of kinematic landmarks. Vertical dotted lines indicate the mean value for each distribution.

We compared jump heights predicted by our model against empirical data, finding only negligible discrepancies (Figure 5-5). We used video data and machine learning to estimate leg external ground reaction forces and predict jump height. In contrast, we obtained the empirical data by directly measuring these forces with force plates. According to empirical data, the participants' average jump height was 17.51± 4.8cm. When we used the front view video trained on different subsets of training data (Major, Core, Reduced), the predicted jump heights deviated from the empirical data by 0.8%, 3.6%, and 0.1%, respectively. Even when we used side view videos trained on various data subsets (Major, Core, Reduced), the predicted jump heights differed from the empirical data only by -9.3%,

-0.3%, and +6.1%, respectively. These differences, though present, were slight, ranging from 0.05-1.63 cm (Figure 5-5).

We observed negligible differences in the peak vertical forces our model predicted compared to the empirical data (Figure 5-5). The empirical data showed an average peak force of 2.07±0.3 body weight (bw) across the group. Using front-view video data and different training data subsets (Major, Core, Reduced), our model deviated from the empirical data by 0.6%, 0.12%, and 0.5%, respectively. Conversely, using side view video data with different training subsets (Major, Core, Reduced), our model's predicted peak forces differed from the empirical data by 2.3%, 3.8%, and 0.1%, respectively.

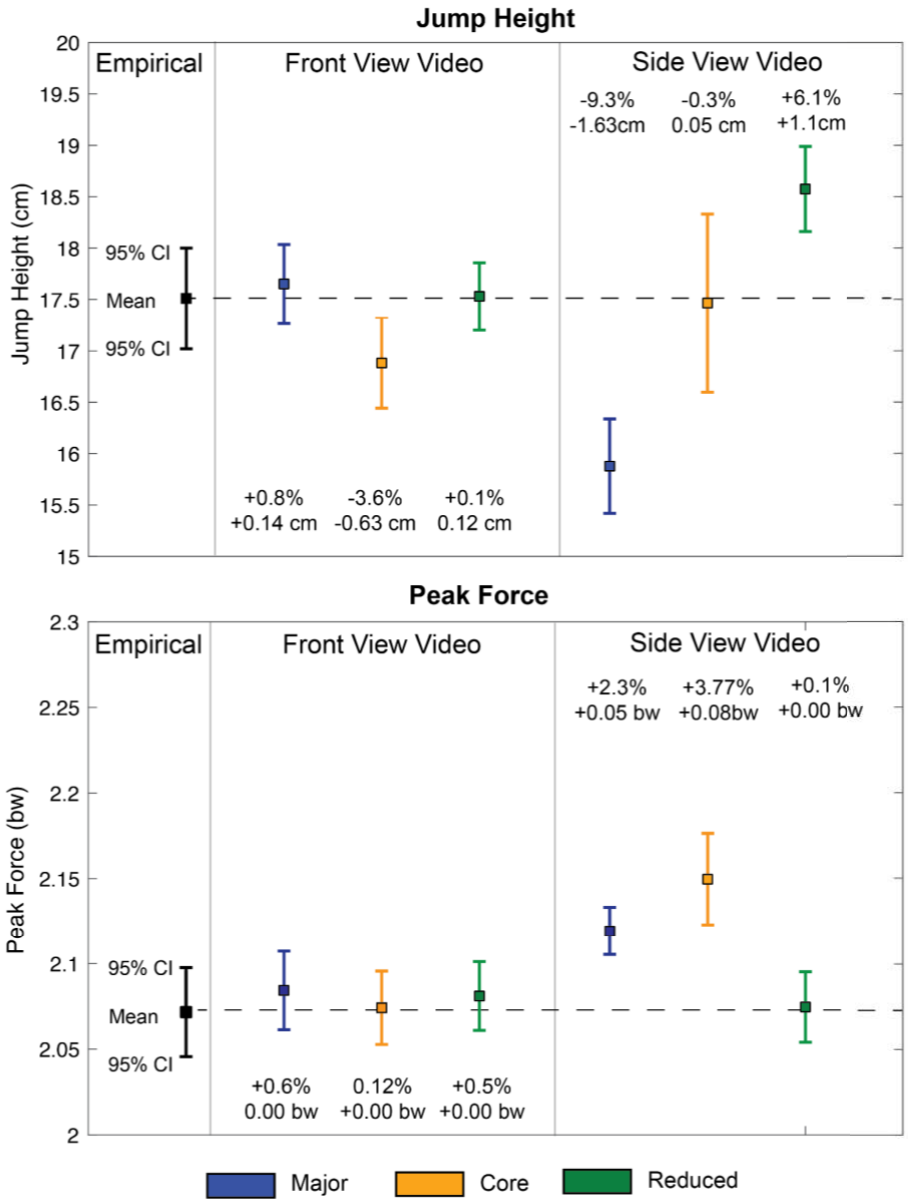

Figure 5-5: Comparison of jump height and peak vertical force differences between our empirical estimates and the predictions made by our model. We evaluated these predictions using either front-view or side-view videos. We tested three different model training datasets: Major (blue), Core (yellow), and Reduced (green). These datasets decreased the number of kinematic landmarks used for each subsequent set. The error bars represent 95% confidence intervals.

Our examination of the linear relationship between the model-predicted jump heights and actual jump heights revealed a modest linear fit, evidenced by a correlation coefficient (r) of 0.68 (0.62-0.7, 95% CI) (Figure 5-6). Although the r-value suggests a moderate linear

relationship, it is the alignment of data points with the line of identity that yields more profound insights. The proximity of data points to this line reflects the extent to which predicted jump heights correspond to actual jump heights. Our analysis indicated a standard error of estimate (SEE) of 1.8 cm, which indicates the typical difference between model-predicted jump heights and actual measurements. Thus, the actual jump height is typically about 1.8 (1.69-1.95) cm away from the model's prediction. Lastly, the line of best fit suggests that for every unit increase in predicted jump height, the actual jump height increases by 0.63 cm.

The same analysis between the model-estimated peak vertical forces and actual peak vertical forces revealed a strong linear fit, denoted by a correlation coefficient (r) of 0.84 (0.8-0.86, 95% CI). Our analysis found a standard error of estimate (SEE) of 0.003 (0.003-0.004) bw, signifying a negligible typical difference between the model's estimated peak vertical forces and actual measurements. Finally, the line of best fit suggests a perfect one-to-one relationship, meaning for every unit increase in estimated peak vertical force, the actual peak vertical force also increases by one unit.

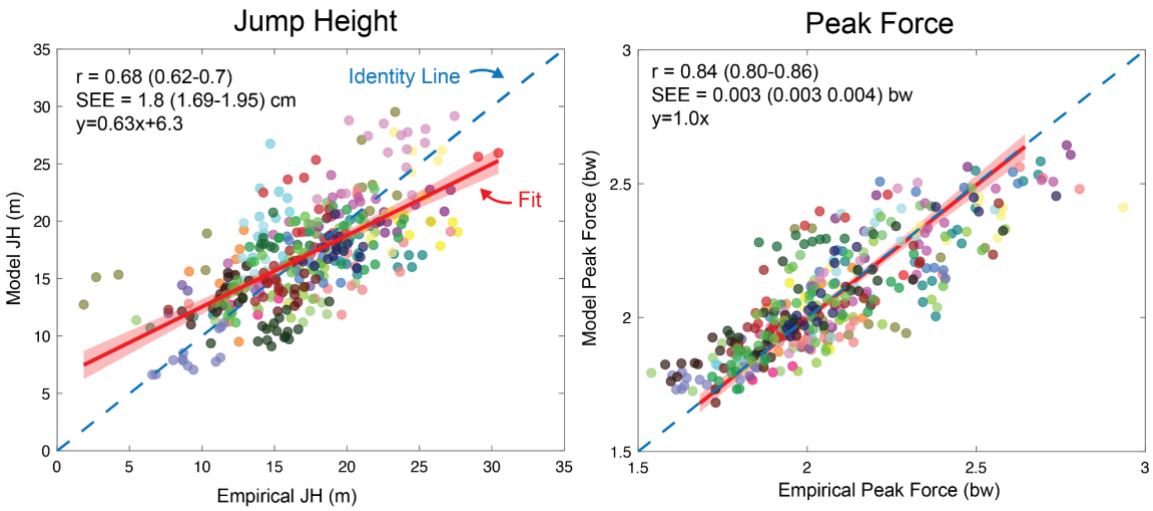

Figure 5-6: Comparison between the vertical jump heights of the empirical data and the model-predicted jump heights (left) and between the peak vertical forces of the empirical data and the model-predicted jump peak vertical forces for all participants (right). These results are for using the front view camera trained on the Core training set. A different colour dot represents each participant. The figure includes the line of identity (dotted line) to demonstrate the ideal scenario where the predicted jump heights or peak force perfectly match the empirical data. The line of best fit (solid red line) is also shown, indicating the trend between the predicted and empirical jump heights. The shading on the best-fit line indicates the 95% confidence interval. The corresponding r-value and standard error of the estimate (SEE) statistically measure the goodness of fit between the predicted and empirical data

5.5. Discussion

We used video data to predict the external ground reaction forces during vertical jumps and investigated the impact of different kinematic inputs on our transformer-based neural network. Our analysis revealed a strong correlation (R^2 values exceeding 0.9) between the predicted and actual vertical ground reaction forces. We observed variations in performance based on the camera perspective, with front-view videos yielding higher accuracy than side-view videos. The superior performance of front-view videos extended to jump height prediction, as the external forces were also better predicted using these videos. In contrast, side-view videos tended to underestimate jump height when trained on the Major marker set and overestimate it when trained on the Reduced set. Nevertheless, both left, and right vertical forces showed consistent predictions with R^2 values ranging from 0.80 to 0.87. The obstruction of landmarks in the side-view videos,

caused by the silhouette of the opposite side, could have contributed to the reduced accuracy. Despite these challenges, our study is the first to use video data to predict each leg's vertical forces during vertical jumps.

Our study has limitations. The first limitation is using OpenPose. While a reliable tool for pose estimation and markerless motion capture, OpenPose may not provide the desired level of accuracy required in biomechanical research. Small discrepancies and inaccuracies in estimating body landmarks could introduce downstream errors in our kinetic measure analysis [92], [93]. One group has sought to improve accuracy by using machine learning to augment OpenPose's predictions of landmarks to better align with those commonly used in biomechanical research [93]. How this would lead to improvements in our study is worth investigating further. Despite any accuracy concerns with OpenPose, pose estimation enabled us to gather and analyze movement data in a way that's both accessible and scalable. However, our dependence on 2D pose estimation limits the complexity of movements we can examine. While 3D motion capture systems might produce more comprehensive kinematic data [220], they generally demand two cameras, which affects practicality. As we refine our methods and benefit from technological advancements, we anticipate improving our approach's accuracy and applicability.

The focus of our study, confined to squat jumps, is a limitation that may restrict the applicability of our findings to other types of jumps or movements. Untrained external forces from different movements could lead to inaccurate predictions [221]. However, our research paves the way for broader exploration. We plan to incorporate diverse locomotive movements in our subsequent work and aspire to develop a comprehensive model that includes several major movements.We acknowledge that the performance of our model largely depends on the quality and diversity of the training data. If the data set does not comprehensively represent the range of variations in human jumping, it could restrict the model's generalization ability. In this study, despite using a relatively small sample of 30 participants, we ensured a wide variety of attributes. The participants varied in age (19-55 years), height (156-195 cm), weight (49.01-91.21 kg), and shoe size (US Size 4.5-12), thereby covering a broad range of human diversity. This diversity, even within a small sample size, strengthens our model's capacity to generalize across a wider population. To further mitigate the limitations of a smaller dataset, we implemented a leave-one-participant-out (LOPO) analysis to evaluate our model's performance. We avoid artificially

inflated accuracy reports by not including the same participant's data in training and testing subsets [219]. This approach led to robust outcomes, enhancing our confidence that our model can yield reliable results when applied to new participants.

Our approach demonstrated encouraging results in predicting vertical ground reaction forces from RGB video, reporting an average R^2 value ranging from 0.83 to 0.94 and an RMSE of 0.12 to 0.20 body weights (bw), depending on the view and training dataset. In the analysis of front-view videos, we observed an R^2 of 0.94±0.05 and an RMSE of 0.12±0.05. We contextualize these results with other studies in the field, each employing their own focus and methods. Research using wearable sensors to estimate external forces during running and walking reported RMSE ranges of 0.21-0.39 body weights [202], [203]. Another study predicting continuous vertical ground reaction forces during running at different slopes indicated an RMSE of 0.12-0.20 body weights [99]. A different study used pressure sensors in shoe insoles to predict vertical forces during running and reported an RMSE of 0.15 body weight [101], [205]. In a comparison with a study that employed an RGB video-based mathematical model to estimate vertical GRF [222], our approach showed correlation coefficients within the same range (R^2 = 0.83 - 0.94 versus R^2 = 0.87-0.92) without the need for an extra mathematical model. Additionally, our model yielded results comparable to a study predicting stance phase ground reaction forces during running directly from RGB video data, which achieved an R^2 of over 0.878 for the vertical GRF component [223]. These comparisons are meant to highlight the performance of our transformer-based neural network in predicting vertical ground reaction forces from video data within the context of current research.

Our jump height estimation results align well with those of other established methods. Commercial software like Kinovea, which estimates jump height from impulse measurements, generated results with a systematic bias of -0.22±2.2cm and mean differences of -0.22 ± 1.15cm. Kinovea had a standard error of estimate (SEE) of 1.15cm [224]. In this context, SEE represents the standard deviation of the error measurements, showing the average variation of the observed error from the mean. In our study, we found group mean differences ranging from -0.63 to 0.14 cm for front-view videos and -1.63 to 1.1 cm for side-view videos. The SEE in the case of front-view videos was 1.8 (range: 1.69-1.95) with a correlation coefficient (r) of 0.68 (95% CI: 0.62-0.70). Previous research using smartphone inertial sensors to estimate jump height reported average accuracies of 4cm with a SEE of 6.3cm [225]. An alternative system based on inertial measurement

units achieved an accuracy of around 1 cm [226]. Studies leveraging smartphones and OpenPose to predict jump height from kinematics found a jump height bias of -2 to 2cm [227]. Commercial mats measuring changes in pressure have reported jump height measurement errors of 1.9cm [228]. Although these comparisons show our method's results are similar to those of existing techniques, it's important to clarify that similarity doesn't imply identical. Different studies have varying focuses and techniques, which may impact the results. Our approach was beneficial in the context of certain metrics (such as the prediction of vertical ground reaction forces from RGB video). At the same time, other methods outperformed ours in different aspects (like bias in jump height estimation Figure 5-6, $y = 0.63x + 6.3$). Recognizing this, we see room for improvement and anticipate that with continuous refinement of our predictive algorithms, we can further enhance our method's precision and utility.

Our work introduces a new approach that harnesses video data and transformer-based neural networks to accurately predict external ground reaction forces. We determined the external vertical forces for each leg separately, enhancing the depth of our biomechanical analysis during vertical jumps. After training our models on a diverse dataset of 30 participants, we found our models matched or surpassed current methodologies' performance. Importantly, we found the camera's perspective impacted prediction accuracy, highlighting the value of strategic camera placement in future applications. Our work not only opens avenues for more in-depth biomechanical studies but also holds promise for several practical applications. This method's adaptability and cost-effectiveness could dramatically improve sports and healthcare injury prevention and rehabilitation strategies by enabling individualized analyses outside of traditional laboratory environments. Additionally, this approach could facilitate performance optimization in athletic training by providing real-time, actionable feedback to athletes and coaches. As technology continues to evolve, we envision a future where our method could be integrated with smartphones bringing professional-level biomechanical analysis into the hands of everyday fitness enthusiasts. By using machine learning and video technology, we could enable access to detailed biomechanical data, revolutionizing the ways people train, recover, and understand their bodies.

Chapter 6.

Concluding Discussion

6.1. Summary

In this thesis, my work focused on leg external forces. I developed new methods, mathematical models, and technologies to study, control and estimate these forces from video.

In **Chapter 2**, "*Characterizing the performance of human leg external force control,*" I used system identification to characterize the control of leg external forces in 14 participants. To achieve this, I designed and implemented a unique apparatus that immobilized participants but allowed them to exert variable but controlled external forces with a single leg onto a ground-embedded force plate. I provided real-time visual feedback of either the leg force-magnitude or position that participants were exerting against the force platform. I instructed participants to best match their real-time signal to prescribed target step functions. I tested target step functions of a range of sizes and quantified the responsiveness and accuracy of the control. My results suggest a high control performance across various conditions, with similar control performance in responsiveness and accuracy across step sizes and between force-magnitude and position control. I found that a second-order model effectively explained the observed control performance. This work enriches our understanding of human agility and provides a valuable reference for comparing animal and engineered systems.

In **Chapter 3**, "*Neuromuscular fatigue reduces responsiveness when controlling leg external forces*," I explored the impact of neuromuscular fatigue on controlling leg external forces. In this study, I conducted experiments with 18 participants, fatiguing their leg and observing the effects of this fatigue on the performance of leg external force control. As hypothesized, the onset of fatigue resulted in a significant reduction in responsiveness, characterized by a 23% increase in rise time and a 25% narrowing of bandwidth. However, interestingly, fatigue did not significantly affect the accuracy of leg force control. These findings provide insights into the role of fatigue in the control of leg external forces and its implications for agility. More importantly, this work lays the foundation for developing

strategies to maintain agility in the face of fatigue and introduces novel metrics for evaluating force control under fatigue conditions.

In **Chapter 4**, "*Studying the limits of vertical jumping using a physics-based model that predicts external ground reaction forces*," I developed a physics-based model to predict vertical jump heights and corresponding external forces across a range of initial starting depths. The model accurately tracked real-life jumping across a range of depths, as demonstrated by high R^2 values when comparing model-predicted and empirical vertical external forces, and showed a strong capability to predict jump heights for a range of jump depths. This work highlights the roles of the force-velocity (F-V) relationship and the maximal force (F_{max}) in determining jump height. Reducing the impact of the F-V relationship or increasing F_{max} most augmented jump height. In contrast, minimizing the force-length (F-L) relationship led to only minor increases in jump height, suggesting that F_{max} and the F-V relationship exert more substantial constraints on jump performance.

I observed a distinct relationship between maximizing jump height and minimizing jump time that closely matched the empirical data. This finding suggests that the nervous system adopts a dual performance objective to balance jump height and duration during vertical jumps. This balance was evident across a diverse range of participants. For example, certain participants experienced a minimal decrease in jump height of approximately 3% while jumping roughly twice as fast. The robustness of my physics-based model provides valuable insights into the biomechanical constraints and strategies underlying vertical jumping. My work illustrates the power of simple models in shedding light on complex physical phenomena. It opens avenues for further exploration of the interplay between biological constraints and motor performance in jumping.

Finally, in **Chapter 5**, "*Estimating ground reaction forces and vertical jump height from video using pose estimation and machine learning*," I introduced a new method for predicting external ground reaction forces during vertical jumps using video data. I recruited 30 participants, capturing their movements on video from front and side views as they performed a series of vertical jumps. Simultaneously, I recorded each leg's ground reaction force using force plates. The transformer-based neural network model I developed predicted vertical ground reaction forces from RGB video with an impressive average R^2 ranging from 0.83 to 0.94 and an RMSE of 0.12 to 0.20 body weights, depending on the view and the training data set. At best, using the front view video, we

achieved an R^2 of 0.94±0.05 and an RMSE of 0.12±0.05. My findings highlight the use of video perspective on prediction accuracy, emphasizing the need to consider camera placement in future applications carefully. Despite limitations and further work, my work provides a groundwork for using video technology in biomechanics for external force prediction. By using the capabilities of machine learning and the ubiquity of video technology, I believe this work can lead to a step forward for laboratory-level biomechanical analysis outside the constrained lab environment.

Each chapter of this thesis represents a contribution to biomechanics and engineering. The insights gained from this work deepen our understanding of human agility, present new technology, and provide a foundation for future research in sports, robotics, and rehabilitative technologies. As I continue this journey, I will keep exploring these areas, leveraging the power of ever-evolving technology to expand our knowledge and capabilities. My work in characterizing, modelling, and predicting leg external forces has the potential to impact our approach to enhancing physical performance and developing new technologies. Each chapter brings us closer to a deeper understanding of biomechanics, setting the stage for potential technological advancements and improved physical performance.

6.2. Limitations

Despite the comprehensive nature of the four studies I presented in this thesis, there are overarching limitations. Inherent in human participant research is a high degree of variability. Individual differences in force control, fatigue response, and jumping performance can influence my findings—the experimental designs and sample sizes used in this work aimed to mitigate these limitations.

I performed the force control and fatigue studies under controlled laboratory conditions, which may not reflect real-world situations. For example, I immobilized participants during the force control experiments, which did not fully mimic the conditions during actual movement or sports performance. While this controlled environment was necessary for the precision and accuracy of the experiments, it's essential to consider how these conditions might differ from real-world scenarios when interpreting the results. While my work provides insights into the control of leg external forces and the effects of fatigue,

translating these findings into dynamic and complex real-world movements should be approached cautiously.

The approach I used to fatigue participants may only reflect some types of fatigue experienced in different sports or physical activities. I focused on acute, experimentally induced fatigue, and the findings may not apply to chronic fatigue or fatigue resulting from other types of exertion, which have been shown to alter performance [162]. My study did not investigate the potential recovery dynamics following fatigue and how they might influence force control. It is possible that participants recovered during bouts outside of the isometric fatigue holds, and this would affect my results [229], [230].

The mathematical models I developed in this research, used to predict external ground reaction forces during vertical jumping, are simplified representations of a complex biomechanical system and may include only some relevant factors. The motor control system's intricacy surpasses current models' capabilities, and simplified representations, such as the Hill-type muscle models used, serve as approximations [231]. Furthermore, the optimization process I used, while rigorous in my approach, may have yet to converge to a globally optimal solution. Despite my best efforts to find a global optimum using known techniques and practices, it is always possible other methods or approaches I should have investigated could yield better performance, such as machine learning or genetic algorithms. However, it is essential to note that the impact of the force-velocity (F-V) relationship and maximal force (F_{max}) was magnitudes greater than that of the force-length (F-L) relationship. Even with potential improvements in optimization, the conclusions regarding the influence of F-V and F_{max} would likely remain the same.

6.3. General Implications

The implications of this thesis extend far beyond the academic ecosystem, reaching various sectors that directly impact the public. The insights from this research can transform our daily lives, from how we exercise to how we interact with technology.

The exploration of agility mechanisms, as presented in this thesis, holds potential for advancing the field of robotics, particularly in developing more agile-legged robots. These robots, which use leg-like appendages for movement, are typically constructed from metal, wires, sensors, microprocessors, and motors and rely on stored energy from batteries.

Despite their advanced construction, they still struggle to match humans' agility and movement capabilities, who have evolved to use bones, nerves, sensory cells, brains, and muscles and derive energy from food [232]. Current state-of-the-art legged robots, including models like Minitaur [233], SpotMini [234], MIT Cheetah [124], HyQ [235], StarlETH [236], and ATRIAS [237], demonstrate impressive abilities such as running, jumping, and backflipping. However, their movements are often limited and need more versatility of human agility. To achieve human-level agile behaviour, a key objective is a precise control of the robot's motion and the external forces the robot's legs apply to the environment [238]. This control requires the integration of force sensors and feedback mechanisms in the robot's controller, enabling the generation of external forces that facilitate desired movements.

The insights gained from studying human biomechanics and external force control, as presented in this thesis, can inform the design of more agile-legged robots. By understanding how humans generate and control external forces during agile movements, researchers can develop improved control strategies and mechanisms for legged robots. These advancements can enhance the robots' ability to rapidly change directions and generate forces with high bandwidth, mirroring the agility seen in human movements. This thesis contributes to the broader field of legged robot design by providing valuable insights into force control mechanisms and their implications for agile locomotion. The approach and data gained from this research can serve as a benchmark for evaluating the performance and capabilities of legged robot systems. By incorporating these findings into future legged robot design endeavours, researchers can strive to create robots that approach humans' remarkable agility and movement capabilities. This work holds significant implications for the future of robotics, potentially leading to the development of robots that can more closely mimic human agility and versatility in movement.

My research represents an innovative step in technology and personal fitness, having developed an approach that uses video to predict external force. The potential implications of these findings could be important for biomechanics. Fitness trackers and wearable devices rely heavily on sensors such as inertial measurement units or insoles to monitor movement. However, I foresee a future where your smartphone could be employed to study your biomechanics, enhancing the accuracy and comprehensiveness of health and fitness data by tracking additional kinematic and kinetic variables. This growing research space may be the future of biomechanics, where research is moved from outside the lab

into the field [93]. My research, merging video technology with machine learning to predict ground reaction forces, is advancement and opens new possibilities for understanding and predicting human movement. I envision a future where high-quality biomechanical analysis is not confined to specialized labs but is accessible to everyone through their smartphones. Such an evolution would herald a new personal fitness and health monitoring era.

6.4. Future Directions

My Ph.D. research lays the foundation for numerous exciting research avenues in biomechanics. I organize these into three idea pillars: 1) fundamental science, 2) modelling integration, and 3) technology development.

The first pillar of future directions is fundamental science. Fatigue is a crucial factor that can change movement biomechanics and lead to injury [239]. Subsequent studies could explore how changes in leg force control due to fatigue increase the injury risk in different situations. These investigations could deepen our grasp on movement physiology. Integral to this pillar is also the development of real-time monitoring technology. I envision creating systems capable of tracking changes in leg force control as they occur. This will enable immediate feedback, adjustment, and intervention, transforming how we study, train for, and perform physical activities. Such technology will bridge the gap between theory and application, making our understanding of biomechanics directly accessible and immediately relevant.

The second pillar, modelling integration, revolves around refining and expanding upon the mathematical model I proposed in Chapter 4 of my research. While promising, these simple models harbour room for further enhancement. By integrating additional factors such as muscle fatigue or individual muscle strength and flexibility variations, I believe I could improve the models' accuracy and applicability, enabling them to cater to a broader spectrum of individuals and movements. In pursuing comprehensive systems, merging these simple mathematical models with machine learning presents an exciting frontier. By weaving together methods from computer vision, mathematical musculoskeletal models, and machine learning, I see a future where we can develop tools that offer real-time feedback on an individual's movement. Such systems could revolutionize how we monitor and improve performance, provide personalized training recommendations, and even

predict and prevent injury. By leveraging models, the data gathered from video and machine learning can be further reinforced to make more personalized predictions about people's movements. Such tools would benefit athletes and those in physically demanding occupations and open new rehabilitation and personal fitness horizons.

The third pillar, technology, involves broadening the video-based approach from Chapter 5. I demonstrated the capacity of video to predict ground reaction forces during vertical jumps. However, the horizon of potential applications extends far beyond this. For example, recently, researchers demonstrated the concept of predicting EMG using computer vision [240]. I plan to expand my approach in Chapter 5 to include other movements or activities in future efforts. This venture may necessitate the development of novel machine-learning models or the exploration of advanced computer vision techniques. Another aspect worth investigating is how various camera types or lighting conditions influence force estimation accuracy. There is also an aspiration to develop open-source tools that provide comprehensive external force monitoring across multiple movements, even in 3D. By doing so, the aim is to open the accessibility of high-level biomechanical analysis, pushing it beyond the boundaries of specialized laboratories and into the hands of athletes, trainers, rehabilitation specialists, and individuals. This vision highlights the transformative potential of this technology, bringing a new level of sophistication to personalized health and performance monitoring.

6.5. Final Remarks

In this Ph.D. thesis, I have explored the intricate domain of biomechanics, focusing on controlling and estimating leg external forces. I shed light on the interaction with the ground beneath us and the complex nature of the external forces. My research characterizes how our neuromechanical system controls the magnitude and application point of externally applied forces beneath our feet, both rapidly and accurately. Although fatigue impacts control, I found that our nervous system is remarkably adaptable and allows us to maintain a high level of performance, even when fatigued. The mathematical models I developed, capable of accurately predicting external ground reaction forces during vertical jumping, highlight the power of merging physics-based principles with empirical optimization. This work broadens our understanding of the limitations and potential enhancements in vertical jumping performance, directly impacting athletic training and performance enhancement. Finally, working with external forces inspired me

to develop innovative methods for predicting these forces using machine learning and video data. One day my work may replace the force plate. I believe these findings could revolutionize how we approach training and rehabilitation in sports science and have significant implications in prosthetics, robotics, and wearable technology.

However, my work has its limitations. Variability among participants, the confines of controlled experimental conditions, and potential shortcomings of the mathematical models and the video-based approach highlight the complex nature of human biomechanics and the inherent challenges in my studies.

Despite these hurdles, the implications of my work span a broad range, potentially impacting diverse fields such as sports science, physical therapy, prosthetics, robotics, wearable technology, computer vision, machine learning, and personal fitness. Each discovery and innovation marks a step forward in our understanding and equips us with new tools to improve human performance and well-being.

The journey of this thesis has been challenging. But it has been fun, exciting, and rewarding. I look forward to seeing how my findings may be applied and built upon to advance our understanding of human movement further. My work is a foundation for future research and development in biomechanics and machine learning. And to the dedicated reader, I commend you for making it this far. I now leave you and this thesis with a quote from Dr. Richard Feynman, "*You can know the name of a bird in all the languages of the world, but when you're finished, you'll know absolutely nothing whatsoever about the bird... So let's look at the bird and see what it's doing -- that's what counts*."

Paweł Kudzia

References

[1] "agility." https://www.oxfordlearnersdictionaries.com/definition/english/agility (accessed Aug. 27, 2020).

[2] J. M. Sheppard and W. B. Young, "Agility literature review: Classifications, training and testing," *J. Sports Sci.*, vol. 24, no. 9, pp. 919–932, Sep. 2006.

[3] D. Chatzopoulos, C. Galazoulas, D. Patikas, and C. Kotzamanidis, "Acute effects of static and dynamic stretching on balance, agility, reaction time and movement time," *J. Sports Sci. Med.*, vol. 13, no. 2, p. 403, 2014.

[4] A. Asadi, "Relationship Between Jumping Ability, Agility and Sprint Performance of Elite Young Basketball Players: A Field-Test Approach," *Braz. J. Kinanthropometry Hum. Performance*, vol. 18, no. 2, p. 177, May 2016.

[5] T. K. K. Wong *et al.*, "Balance control, agility, eye-hand coordination, and sport performance of amateur badminton players: A cross-sectional study," *Medicine* , vol. 98, no. 2, p. e14134, Jan. 2019.

[6] NSCA -National Strength & Conditioning Association, J. Dawes, and M. Roozen, *Developing Agility and Quickness*. Human Kinetics, 2011.

[7] R. G. Lockie, M. D. Jeffriess, T. S. McGann, S. J. Callaghan, and A. B. Schultz, "Planned and reactive agility performance in semiprofessional and amateur basketball players," *Int. J. Sports Physiol. Perform.*, vol. 9, no. 5, pp. 766–771, Sep. 2014.

[8] N. Mullins, "Obstacle Course Challenges: History, Popularity, Performance Demands, Effective Training, and Course Design," *J. Exerc. Physiol. Online*, vol. 15, no. 2, 2012, [Online]. Available: https://static.julinse.com/m/854b9004777a194f.pdf

[9] P. G. Weyand, D. B. Sternlight, M. J. Bellizzi, and S. Wright, "Faster top running speeds are achieved with greater ground forces not more rapid leg movements," *J. Appl. Physiol.*, vol. 89, no. 5, pp. 1991–1999, Nov. 2000.

[10] F. C. Anderson and M. G. Pandy, "A Dynamic Optimization Solution for Vertical Jumping in Three Dimensions," *Comput. Methods Biomech. Biomed. Engin.*, vol. 2, no. 3, pp. 201–231, Jan. 1999.

[11] R. H. Miller, B. R. Umberger, and G. E. Caldwell, "Limitations to maximum sprinting speed imposed by muscle mechanical properties," *J. Biomech.*, vol. 45, no. 6, pp. 1092–1097, Apr. 2012.

[12] T. Spiteri, R. U. Newton, M. Binetti, N. H. Hart, J. M. Sheppard, and S. Nimphius, “Mechanical Determinants of Faster Change of Direction and Agility Performance in Female Basketball Athletes,” *J. Strength Cond. Res.*, vol. 29, no. 8, pp. 2205–2214, Aug. 2015.

[13] R. M. Alexander, “Optimum Take-Off Techniques for High and Long Jumps,” *Philos. Trans. R. Soc. Lond. B Biol. Sci.*, vol. 329, no. 1252, pp. 3–10, 1990.

[14] G. Gautier, R. Thouvarecq, and N. Vuillerme, “Postural control and perceptive configuration: influence of expertise in gymnastics,” *Gait Posture*, vol. 28, no. 1, pp. 46–51, Jul. 2008.

[15] P. Kudzia, S. N. Robinovich, and J. M. Donelan, “Characterizing the performance of human leg external force control,” *Sci. Rep.*, vol. 12, no. 1, p. 4935, Mar. 2022.

[16] K. G. M. Gerritsen, A. J. van den Bogert, M. Hulliger, and R. F. Zernicke, “Intrinsic Muscle Properties Facilitate Locomotor Control—A Computer Simulation Study,” *Motor Control*, vol. 2, no. 3, pp. 206–220, Jul. 1998.

[17] M. Araz, S. Weidner, F. Izzi, A. Badri-Spröwitz, T. Siebert, and D. F. B. Haeufle, “Muscle preflex response to perturbations in locomotion: In vitro experiments and simulations with realistic boundary conditions,” *Front Bioeng Biotechnol*, vol. 11, p. 1150170, Apr. 2023.

[18] I. D. Neveln, A. Tirumalai, and S. Sponberg, “Information-based centralization of locomotion in animals and robots,” *Nat. Commun.*, vol. 10, no. 1, p. 3655, Aug. 2019.

[19] V. M. Zatsiorsky and V. M. Zaciorskij, *Kinetics of Human Motion*. Human Kinetics, 2002.

[20] C.-Y. Hong, L.-Y. Guo, R. Song, M. L. Nagurka, J.-L. Sung, and C.-W. Yen, “Assessing postural stability via the correlation patterns of vertical ground reaction force components,” *Biomed. Eng. Online*, vol. 15, no. 1, p. 90, Aug. 2016.

[21] F. Quijoux *et al.*, “A review of center of pressure (COP) variables to quantify standing balance in elderly people: Algorithms and open-access code,” *Physiol. Rep.*, vol. 9, no. 22, p. e15067, Nov. 2021.

[22] U. Proske and T. Allen, “The neural basis of the senses of effort, force and heaviness,” *Exp. Brain Res.*, vol. 237, no. 3, pp. 589–599, Mar. 2019.

[23] J. C. Dean, “Proprioceptive Feedback and Preferred Patterns of Human Movement,” *Exerc. Sport Sci. Rev.*, vol. 41, no. 1, pp. 36–43, Jan. 2013.

[24] J. C. Gordon, N. C. Holt, A. Biewener, and M. A. Daley, “Tuning of feedforward control enables stable muscle force-length dynamics after loss of autogenic proprioceptive feedback,” *Elife*, vol. 9, Jun. 2020, doi: 10.7554/eLife.53908.

[25] J. S. Petrofsky and C. A. Phillips, “Closed-loop control of movement of skeletal muscle,” *Crit. Rev. Biomed. Eng.*, vol. 13, no. 1, pp. 35–96, 1985.

[26] A. Prochazka, D. Gillard, and D. J. Bennett, “Positive force feedback control of muscles,” *J. Neurophysiol.*, vol. 77, no. 6, pp. 3226–3236, Jun. 1997.

[27] K. Masani, A. H. Vette, N. Kawashima, and M. R. Popovic, “Neuromusculoskeletal torque-generation process has a large destabilizing effect on the control mechanism of quiet standing,” *J. Neurophysiol.*, vol. 100, no. 3, pp. 1465–1475, Sep. 2008.

[28] J. D. Wong and J. M. Donelan, “Principles of energetics and stability in human locomotion,” *Humanoid Robotics: A Reference. Dordrecht: Springer*, 2017, [Online]. Available: https://pdfs.semanticscholar.org/ff1c/1adbbd829ed781158c21fb7bdc17cbdcdf9a.pdf

[29] M. J. Gillespie and R. B. Stein, “The relationship between axon diameter, myelin thickness and conduction velocity during atrophy of mammalian peripheral nerves,” *Brain Res.*, vol. 259, no. 1, pp. 41–56, Jan. 1983.

[30] G. Macefield, S. C. Gandevia, and D. Burke, “Conduction velocities of muscle and cutaneous afferents in the upper and lower limbs of human subjects,” *Brain*, vol. 112 (Pt 6), pp. 1519–1532, Dec. 1989.

[31] H. L. More and J. M. Donelan, “Scaling of sensorimotor delays in terrestrial mammals,” *Proceedings of the Royal Society B: Biological Sciences*, vol. 285, no. 1885, p. 20180613, Aug. 2018.

[32] H. L. More, J. R. Hutchinson, D. F. Collins, D. J. Weber, S. K. H. Aung, and J. M. Donelan, “Scaling of sensorimotor control in terrestrial mammals,” *Proceedings of the Royal Society B: Biological Sciences*, vol. 277, no. 1700, pp. 3563–3568, Dec. 2010.

[33] A. Del Vecchio, A. Úbeda, M. Sartori, J. M. Azorín, F. Felici, and D. Farina, “Central nervous system modulates the neuromechanical delay in a broad range for the control of muscle force,” *J. Appl. Physiol.*, vol. 125, no. 5, pp. 1404–1410, Nov. 2018.

[34] A. A. Biewener and M. A. Daley, “Unsteady locomotion: integrating muscle function with whole body dynamics and neuromuscular control,” *J. Exp. Biol.*, vol. 210, no. Pt 17, pp. 2949–2960, Sep. 2007.

[35] L. L. Andersen and P. Aagaard, “Influence of maximal muscle strength and intrinsic muscle contractile properties on contractile rate of force development,” *Eur. J. Appl. Physiol.*, vol. 96, no. 1, pp. 46–52, Jan. 2006.

[36] A. F. Huxley, “Muscle structure and theories of contraction,” *Prog. Biophys. Biophys. Chem.*, vol. 7, pp. 255–318, 1957.

[37] B. M. Nigg and W. Herzog, *Biomechanics of the musculo-skeletal system*. John Wiley & Sons, 2007.

[38] W. K. Durfee and K. I. Palmer, “Estimation of force-activation, force-length, and force-velocity properties in isolated, electrically stimulated muscle,” *IEEE Trans. Biomed. Eng.*, vol. 41, no. 3, pp. 205–216, Mar. 1994.

[39] F. E. Zajac, “Muscle and tendon: properties, models, scaling, and application to biomechanics and motor control,” *Crit. Rev. Biomed. Eng.*, vol. 17, no. 4, pp. 359–411, 1989.

[40] R. H. Miller, “Hill-Based Muscle Modeling,” in *Handbook of Human Motion*, Cham: Springer International Publishing, 2018, pp. 373–394.

[41] F. García-Pinillos *et al.*, “Does fatigue alter step characteristics and stiffness during running?,” *Gait Posture*, vol. 76, pp. 259–263, Feb. 2020.

[42] S. Benesch, W. Pütz, D. Rosenbaum, and H. Becker, “Reliability of peroneal reaction time measurements,” *Clin. Biomech.* , vol. 15, no. 1, pp. 21–28, Jan. 2000.

[43] J. B. Thorlund, L. B. Michalsik, K. Madsen, and P. Aagaard, “Acute fatigue-induced changes in muscle mechanical properties and neuromuscular activity in elite handball players following a handball match,” *Scand. J. Med. Sci. Sports*, vol. 18, no. 4, pp. 462–472, Aug. 2008.

[44] F. Mohammadi and A. Roozdar, “Effects of fatigue due to contraction of evertor muscles on the ankle joint position sense in male soccer players,” *Am. J. Sports Med.*, vol. 38, no. 4, pp. 824–828, Apr. 2010.

[45] T. Paillard, “Effects of general and local fatigue on postural control: a review,” *Neurosci. Biobehav. Rev.*, vol. 36, no. 1, pp. 162–176, Jan. 2012.

[46] E. Nagy *et al.*, “Postural control in athletes participating in an ironman triathlon,” *Eur. J. Appl. Physiol.*, vol. 92, no. 4–5, pp. 407–413, Aug. 2004.

[47] A. Nardone, J. Tarantola, A. Giordano, and M. Schieppati, “Fatigue effects on body balance,” *Electroencephalogr. Clin. Neurophysiol.*, vol. 105, no. 4, pp. 309–320, Aug. 1997.

[48] J. L. Taylor, M. Amann, J. Duchateau, R. Meeusen, and C. L. Rice, “Neural Contributions to Muscle Fatigue: From the Brain to the Muscle and Back Again,” *Med. Sci. Sports Exerc.*, vol. 48, no. 11, pp. 2294–2306, Nov. 2016.

[49] S. C. Gandevia, “Spinal and supraspinal factors in human muscle fatigue,” *Physiol. Rev.*, vol. 81, no. 4, pp. 1725–1789, Oct. 2001.

[50] G. C. Sieck and Y. S. Prakash, “Fatigue at the Neuromuscular Junction In Fatigue: Neural and Muscular Mechanisms,” *Edited by Gandevia SC, Enoka RM, McComas AJ, Stuart DG, Thomas CK, Pierce PA: Springer US*, pp. 83–100, 1995.

[51] T. J. Carroll, J. L. Taylor, and S. C. Gandevia, “Recovery of central and peripheral neuromuscular fatigue after exercise,” *J. Appl. Physiol.*, vol. 122, no. 5, pp. 1068–1076, May 2017.

[52] M. Nocella, B. Colombini, G. Benelli, G. Cecchi, M. A. Bagni, and J. Bruton, “Force decline during fatigue is due to both a decrease in the force per individual cross-bridge and the number of cross-bridges,” *J. Physiol.*, vol. 589, no. Pt 13, pp. 3371–3381, Jul. 2011.

[53] J. Oliver, N. Armstrong, and C. Williams, “Changes in jump performance and muscle activity following soccer-specific exercise,” *J. Sports Sci.*, vol. 26, no. 2, pp. 141–148, Jan. 2008.

[54] M. F. Bobbert, M. M. Van Der Krogt, H. Van Doorn, and C. J. de Ruiter, “Effects of Fatigue of Plantarflexors on Control and Performance in Vertical Jumping,” *Med. Sci. Sports Exercise*, vol. 43, no. 4, p. 673, Apr. 2011.

[55] A. L. Rodacki, N. E. Fowler, and S. J. Bennett, “Multi-segment coordination: fatigue effects,” *Med. Sci. Sports Exerc.*, vol. 33, no. 7, pp. 1157–1167, Jul. 2001.

[56] J. C. Wilkins, T. C. Valovich McLeod, D. H. Perrin, and B. M. Gansneder, “Performance on the Balance Error Scoring System Decreases After Fatigue,” *J. Athl. Train.*, vol. 39, no. 2, pp. 156–161, Jun. 2004.

[57] T. Finni, H. Kyröläinen, J. Avela, and P. V. Komi, “Maximal but not submaximal performance is reduced by constant-speed 10-km run,” *J. Sports Med. Phys. Fitness*, vol. 43, no. 4, pp. 411–417, Dec. 2003.

[58] W. Schlicht, W. Naretz, D. Witt, and H. Rieckert, “Ammonia and lactate: differential information on monitoring training load in sprint events,” *Int. J. Sports Med.*, vol. 11 Suppl 2, pp. S85–90, May 1990.

[59] A. Mero and E. Peltola, “Neural activation fatigued and non-fatigued conditions of short and long sprint running,” *Biol. Sport*, vol. 6, no. 1, pp. 43–58, 1989.

[60] A. Ross, M. Leveritt, and S. Riek, “Neural influences on sprint running,” *Sports Med.*, vol. 31, no. 6, pp. 409–425, 2001.

[61] E. Zemková and D. Hamar, “The effect of soccer match induced fatigue on neuromuscular performance,” *Kinesiology* , vol. 41, no. 2, 2009, [Online]. Available: https://hrcak.srce.hr/file/70903

[62] K. Hébert-Losier, C. Zinner, S. Platt, T. Stöggl, and H.-C. Holmberg, “Factors that Influence the Performance of Elite Sprint Cross-Country Skiers,” *Sports Med.*, vol. 47, no. 2, pp. 319–342, Feb. 2017.

[63] C. Nicol, P. V. Komi, and P. Marconnet, “Fatigue effects of marathon running on neuromuscular performance,” *Scand. J. Med. Sci. Sports*, vol. 1, no. 1, pp. 10–17, Mar. 1991.

[64] N. Cortes, D. Quammen, S. Lucci, E. Greska, and J. Onate, “A functional agility short-term fatigue protocol changes lower extremity mechanics,” *J. Sports Sci.*, vol. 30, no. 8, pp. 797–805, Mar. 2012.

[65] J. B. Thorlund, P. Aagaard, and K. Madsen, “Rapid muscle force capacity changes after soccer match play,” *Int. J. Sports Med.*, vol. 30, no. 4, pp. 273–278, Apr. 2009.

[66] M. G. Pandy, F. E. Zajac, E. Sim, and W. S. Levine, “An optimal control model for maximum-height human jumping,” *J. Biomech.*, vol. 23, no. 12, pp. 1185–1198, 1990.

[67] A. Seyfarth, R. Blickhan, and J. L. Van Leeuwen, “Take-off techniques and muscle design for long jump,” p. 10.

[68] R. M. Alexander, “Leg Design and Jumping Technique for Humans, other Vertebrates and Insects,” *Philos. Trans. R. Soc. Lond. B Biol. Sci.*, vol. 347, no. 1321, pp. 235–248, 1995.

[69] J. C. Selinger, S. M. O’Connor, J. D. Wong, and J. M. Donelan, “Humans Can Continuously Optimize Energetic Cost during Walking,” *Curr. Biol.*, vol. 25, no. 18, pp. 2452–2456, Sep. 2015.

[70] X. Hu, J. P. Charles, T. Akay, J. R. Hutchinson, and S. S. Blemker, “Are mice good models for human neuromuscular disease? Comparing muscle excursions in walking between mice and humans,” *Skelet. Muscle*, vol. 7, no. 1, p. 26, Nov. 2017.

[71] R. H. Miller, “Summary of muscle parameters for Hill-based muscle modeling in the human lower limb,” p. 090944, Dec. 03, 2016. doi: 10.1101/090944.

[72] R. H. Miller, B. R. Umberger, and G. E. Caldwell, “Sensitivity of maximum sprinting speed to characteristic parameters of the muscle force–velocity relationship,” *J. Biomech.*, vol. 45, no. 8, pp. 1406–1413, May 2012.

[73] J. Aguilar, “Probing the dynamics of a simple jumping robot on hard and soft ground,” Georgia Institute of Technology, 2016.

[74] J. H. Challis, “An investigation of the influence of bi-lateral deficit on human jumping,” *Hum. Mov. Sci.*, vol. 17, no. 3, pp. 307–325, Jun. 1998.

[75] A. K. Gutmann and J. E. A. Bertram, “Metabolic cost of human hopping,” *J. Exp. Biol.*, vol. 220, no. 9, pp. 1654–1662, May 2017.

[76] H. van Werkhoven and S. J. Piazza, “Computational model of maximal-height single-joint jumping predicts bouncing as an optimal strategy,” *J. Biomech.*, vol. 46, no. 6, pp. 1092–1097, Apr. 2013.

[77] A. Rosendo and F. Iida, “Energy efficient hopping with Hill-type muscle properties on segmented legs,” *Bioinspir. Biomim.*, vol. 11, no. 3, p. 036002, Apr. 2016.

[78] T. A. McMahon, *Muscles, Reflexes, and Locomotion*. Princeton University Press, 1984.

[79] M. F. Bobbert and A. J. ???Knoek van Soest, “Why Do People Jump the Way They Do?:,” *Exerc. Sport Sci. Rev.*, vol. 29, no. 3, pp. 95–102, Jul. 2001.

[80] W. S. Selbie and G. E. Caldwell, “A simulation study of vertical jumping from different starting postures,” *J. Biomech.*, vol. 29, no. 9, pp. 1137–1146, Sep. 1996.

[81] J. H. Challis and Z. J. Domire, “Insights to vertical jumping from computer simulations,” *Movement & Sport Sciences - Science & Motricité*, no. 90, pp. 69–78, 2015.

[82] F. E. Zajac, R. W. Wicke, and W. S. Levine, “Dependence of jumping performance on muscle properties when humans use only calf muscles for propulsion,” *J. Biomech.*, vol. 17, no. 7, pp. 513–523, 1984.

[83] A. J. van Soest and M. F. Bobbert, “The contribution of muscle properties in the control of explosive movements,” *Biol. Cybern.*, vol. 69, no. 3, pp. 195–204, Jul. 1993.

[84] M. A. Boswell, Ł. Kidziński, J. L. Hicks, S. D. Uhlrich, A. Falisse, and S. L. Delp, “Smartphone videos of the sit-to-stand test predict osteoarthritis and health outcomes in a nationwide study,” *NPJ Digit Med*, vol. 6, no. 1, p. 32, Mar. 2023.

[85] W. J. Choi, J. M. Wakeling, and S. N. Robinovitch, “Kinematic analysis of video-captured falls experienced by older adults in long-term care,” *J. Biomech.*, vol. 48, no. 6, pp. 911–920, Apr. 2015.

[86] S. N. Robinovitch *et al.*, “Video capture of the circumstances of falls in elderly people residing in long-term care: an observational study,” *Lancet*, vol. 381, no. 9860, pp. 47–54, Jan. 2013.

[87] T. Nath, A. Mathis, A. C. Chen, A. Patel, M. Bethge, and M. W. Mathis, “Using DeepLabCut for 3D markerless pose estimation across species and behaviors,” *Nat. Protoc.*, vol. 14, no. 7, pp. 2152–2176, Jul. 2019.

[88] D. Tuia *et al.*, “Perspectives in machine learning for wildlife conservation,” *Nat. Commun.*, vol. 13, no. 1, pp. 1–15, Feb. 2022.

[89] J. Lauer *et al.*, “Multi-animal pose estimation, identification and tracking with DeepLabCut,” *Nat. Methods*, vol. 19, no. 4, pp. 496–504, Apr. 2022.

[90] Z. Cao, G. Hidalgo Martinez, T. Simon, S.-E. Wei, and Y. A. Sheikh, “OpenPose: Realtime Multi-Person 2D Pose Estimation using Part Affinity Fields,” *IEEE Trans. Pattern Anal. Mach. Intell.*, Jul. 2019, doi: 10.1109/TPAMI.2019.2929257.

[91] L. Needham *et al.*, “Human Movement Science in The Wild: Can Current Deep-Learning Based Pose Estimation Free Us from The Lab?,” *bioRxiv*, p. 2021.04.22.440909, Apr. 23, 2021. doi: 10.1101/2021.04.22.440909.

[92] J. Stenum, C. Rossi, and R. T. Roemmich, “Two-dimensional video-based analysis of human gait using pose estimation,” *PLoS Comput. Biol.*, vol. 17, no. 4, p. e1008935, Apr. 2021.

[93] S. D. Uhlrich *et al.*, “OpenCap: 3D human movement dynamics from smartphone videos,” *bioRxiv*, p. 2022.07.07.499061, Jul. 10, 2022. doi: 10.1101/2022.07.07.499061.

[94] K. Greff, R. K. Srivastava, J. Koutnik, B. R. Steunebrink, and J. Schmidhuber, “LSTM: A Search Space Odyssey,” *IEEE Trans Neural Netw Learn Syst*, vol. 28, no. 10, pp. 2222–2232, Oct. 2017.

[95] E. Rapp, S. Shin, W. Thomsen, R. Ferber, and E. Halilaj, “Estimation of kinematics from inertial measurement units using a combined deep learning and optimization framework,” *J. Biomech.*, vol. 116, p. 110229, Feb. 2021.

[96] M. Mundt *et al.*, “Prediction of lower limb joint angles and moments during gait using artificial neural networks,” *Med. Biol. Eng. Comput.*, vol. 58, no. 1, pp. 211–225, Jan. 2020.

[97] M. Mundt, W. R. Johnson, W. Potthast, B. Markert, A. Mian, and J. Alderson, “A Comparison of Three Neural Network Approaches for Estimating Joint Angles and Moments from Inertial Measurement Units,” *Sensors* , vol. 21, no. 13, Jul. 2021, doi: 10.3390/s21134535.

[98] “Deep learning based ground reaction force estimation for stair walking using kinematic data,” *Measurement*, vol. 198, p. 111344, Jul. 2022.

[99] R. S. Alcantara, W. Brent Edwards, G. Y. Millet, and A. M. Grabowski, “Predicting continuous ground reaction forces from accelerometers during uphill and downhill running: a recurrent neural network solution,” *PeerJ*, vol. 10, p. e12752, Jan. 2022.

[100] J. Kim, H. Kang, S. Lee, J. Choi, and G. Tack, “A Deep Learning Model for 3D Ground Reaction Force Estimation Using Shoes with Three Uniaxial Load Cells,” *Sensors* , vol. 23, no. 7, Mar. 2023, doi: 10.3390/s23073428.

[101] M. Hajizadeh, A. L. Clouthier, M. Kendall, and R. B. Graham, “Predicting vertical and shear ground reaction forces during walking and jogging using wearable plantar pressure insoles,” *bioRxiv*, p. 2023.02.19.529141, Feb. 21, 2023. doi: 10.1101/2023.02.19.529141.

[102] S. Siami-Namini, N. Tavakoli, and A. S. Namin, “The Performance of LSTM and BiLSTM in Forecasting Time Series,” in *2019 IEEE International Conference on Big Data (Big Data)*, Dec. 2019, pp. 3285–3292.

[103] A. Vaswani *et al.*, “Attention is all you need,” *Adv. Neural Inf. Process. Syst.*, vol. 30, 2017, [Online]. Available: https://proceedings.neurips.cc/paper/7181-attention-is-all

[104] S. Ahmed, I. E. Nielsen, A. Tripathi, S. Siddiqui, G. Rasool, and R. P. Ramachandran, “Transformers in Time-series Analysis: A Tutorial,” *arXiv [cs.LG]*, Apr. 28, 2022. [Online]. Available: http://arxiv.org/abs/2205.01138

[105] J. Sun, B. Zhou, M. J. Black, and A. Chandrasekaran, “LocATe: End-to-end Localization of Actions in 3D with Transformers,” *arXiv [cs.CV]*, Mar. 21, 2022. [Online]. Available: http://arxiv.org/abs/2203.10719

[106] L. Ferariu and A. Ţucaş, “Using Hand-Crafted and Learned EEG Features for the Detection of Epileptic Seizures,” in *2021 International Conference on e-Health and Bioengineering (EHB)*, Nov. 2021, pp. 1–4.

[107] A. Mathis *et al.*, “DeepLabCut: markerless pose estimation of user-defined body parts with deep learning,” *Nat. Neurosci.*, vol. 21, no. 9, pp. 1281–1289, Sep. 2018.

[108] Y. Zhu, D. Xia, and H. Zhang, “Using Wearable Sensors to Estimate Vertical Ground Reaction Force Based on a Transformer,” *NATO Adv. Sci. Inst. Ser. E Appl. Sci.*, vol. 13, no. 4, p. 2136, Feb. 2023.

[109] H. C. Howland, “Optimal strategies for predator avoidance: the relative importance of speed and manoeuvrability,” *J. Theor. Biol.*, vol. 47, no. 2, pp. 333–350, Oct. 1974.

[110] R. J. Full, T. Kubow, J. Schmitt, P. Holmes, and D. Koditschek, “Quantifying dynamic stability and maneuverability in legged locomotion,” *Integr. Comp. Biol.*, vol. 42, no. 1, pp. 149–157, Feb. 2002.

[111] J. Hwangbo *et al.*, “Learning agile and dynamic motor skills for legged robots,” *Sci Robot*, vol. 4, no. 26, Jan. 2019, doi: 10.1126/scirobotics.aau5872.

[112] J. D. Vescovi and M. R. Mcguigan, “Relationships between sprinting, agility, and jump ability in female athletes,” *J. Sports Sci.*, vol. 26, no. 1, pp. 97–107, Jan. 2008.

[113] W. B. Young, B. Dawson, and G. J. Henry, “Agility and Change-of-Direction Speed are Independent Skills: Implications for Training for Agility in Invasion Sports,” *Int. J. Sports Sci. Coach.*, vol. 10, no. 1, pp. 159–169, Feb. 2015.

[114] L. Stirling, C. Eke, and S. M. Cain, “Examination of the perceived agility and balance during a reactive agility task,” *PLoS One*, vol. 13, no. 6, p. e0198875, Jun. 2018.

[115] T. Garland, “The relation between maximal running speed and body mass in terrestrial mammals,” *J. Zool.*, vol. 199, no. 2, pp. 157–170, Jan. 1983.

[116] G. P. Sutton *et al.*, “Why do Large Animals Never Actuate Their Jumps with Latch-Mediated Springs? Because They can Jump Higher Without Them,” *Integr. Comp. Biol.*, p. icz145, Aug. 2019.

[117] A. M. Wilson, J. C. Lowe, K. Roskilly, P. E. Hudson, K. A. Golabek, and J. W. McNutt, “Locomotion dynamics of hunting in wild cheetahs,” *Nature*, vol. 498, no. 7453, pp. 185–189, Jun. 2013.

[118] D. L. Jindrich, N. C. Smith, K. Jespers, and A. M. Wilson, “Mechanics of cutting maneuvers by ostriches (Struthio camelus),” *J. Exp. Biol.*, vol. 210, no. Pt 8, pp. 1378–1390, Apr. 2007.

[119] L. M. Rogers, D. A. Brown, and K. G. Gruben, “Foot force direction control during leg pushes against fixed and moving pedals in persons post-stroke,” *Gait Posture*, vol. 19, no. 1, pp. 58–68, Feb. 2004.

[120] V. Zordan, D. Brown, A. Macchietto, and K. Yin, “Control of Rotational Dynamics for Ground and Aerial Behavior,” *IEEE Trans. Vis. Comput. Graph.*, vol. 20, no. 10, pp. 1356–1366, Oct. 2014.

[121] W. Herzog, “Muscle properties and coordination during voluntary movement,” *J. Sports Sci.*, vol. 18, no. 3, pp. 141–152, Mar. 2000.

[122] A. Santuz, A. Ekizos, Y. Kunimasa, K. Kijima, M. Ishikawa, and A. Arampatzis, “Lower complexity of motor primitives ensures robust control of high-speed human locomotion,” *Heliyon*, vol. 6, no. 10, p. e05377, Oct. 2020.

[123] P. D. Cha, J. J. Rosenberg, and C. L. Dym, *Fundamentals of Modeling and Analyzing Engineering Systems*. Cambridge University Press, 2000.

[124] P. M. Wensing, A. Wang, S. Seok, D. Otten, J. Lang, and S. Kim, “Proprioceptive Actuator Design in the MIT Cheetah: Impact Mitigation and High-Bandwidth Physical Interaction for Dynamic Legged Robots,” *IEEE Trans. Rob.*, vol. 33, no. 3, pp. 509–522, Jun. 2017.

[125] H.-W. Park, P. M. Wensing, and S. Kim, “High-speed bounding with the MIT Cheetah 2: Control design and experiments,” *Int. J. Rob. Res.*, vol. 36, no. 2, pp. 167–192, Feb. 2017.

[126] V. L. Chiu, A. S. Voloshina, and S. H. Collins, “An Ankle-Foot Prosthesis Emulator Capable of Modulating Center of Pressure,” *IEEE Trans. Biomed. Eng.*, vol. 67, no. 1, pp. 166–176, Jan. 2020.

[127] BERTEC Corporation, “Bertec Force Plates,” Mar. 2012.

[128] R. K. Fukuchi, C. A. Fukuchi, and M. Duarte, “A public dataset of running biomechanics and the effects of running speed on lower extremity kinematics and kinetics,” *PeerJ*, vol. 5, p. e3298, May 2017.

[129] M. T. Thompson, “Review of Signal Processing Basics,” in *Intuitive Analog Circuit Design*, Elsevier, 2014, pp. 15–52.

[130] P. Sedgwick, “Multiple significance tests: the Bonferroni correction,” *BMJ*, vol. 344, Jan. 2012, doi: 10.1136/bmj.e509.

[131] J. Duysens and H. W. A. A. Van de Crommert, “Neural control of locomotion; Part 1: The central pattern generator from cats to humans,” *Gait Posture*, vol. 7, no. 2, pp. 131–141, Mar. 1998.

[132] S. Grillner and P. Wallén, “Central Pattern Generators for Locomotion, with Special Reference to Vertebrates,” Nov. 2003, doi: 10.1146/annurev.ne.08.030185.001313.

[133] R. Toyoshima and S. Sakurai, “Kinematic Characteristics of High Step Frequency Sprinters and Long Step Length Sprinters at Top Speed Phase,” *International Journal of Sport and Health Science*, vol. 14, pp. 41–50, 2016.

[134] S. Rossignol, R. Dubuc, and J.-P. Gossard, “Dynamic sensorimotor interactions in locomotion,” *Physiol. Rev.*, vol. 86, no. 1, pp. 89–154, Jan. 2006.

[135] K. Häkkinen and P. V. Komi, “Electromyographic and mechanical characteristics of human skeletal muscle during fatigue under voluntary and reflex conditions,” *Electroencephalogr. Clin. Neurophysiol.*, vol. 55, no. 4, pp. 436–444, Apr. 1983.

[136] C. Ertekin, B. Mungan, and M. Ertaş, “Human root and cord potentials evoked by Achilles tendon tap,” *Electromyogr. Clin. Neurophysiol.*, vol. 35, no. 5, pp. 259–271, Aug. 1995.

[137] W. F. Brechue, D. M. Koceja, and J. M. Stager, “Acetazolamide reduces peripheral afferent transmission in humans,” *Muscle Nerve*, vol. 20, no. 12, pp. 1541–1548, Dec. 1997.

[138] A. A. Faisal, L. P. J. Selen, and D. M. Wolpert, “Noise in the nervous system,” *Nat. Rev. Neurosci.*, vol. 9, no. 4, pp. 292–303, Apr. 2008.

[139] R. J. van Beers, P. Haggard, and D. M. Wolpert, “The role of execution noise in movement variability,” *J. Neurophysiol.*, vol. 91, no. 2, pp. 1050–1063, Feb. 2004.

[140] K. E. Jones, A. F. de C. Hamilton, and D. M. Wolpert, “Sources of signal-dependent noise during isometric force production,” *Neurophysiology*, vol. 88, pp. 1533–1544, 2002.

[141] S. Kalouche, “DESIGN FOR 3D AGILITY AND VIRTUAL COMPLIANCE USING PROPRIOCEPTIVE FORCE CONTROL IN DYNAMIC LEGGED ROBOTS,” 2016.

[142] V. L. Chiu, M. Raitor, and S. H. Collins, “Design of a Hip Exoskeleton with Actuation in Frontal and Sagittal Planes,” *IEEE Transactions on Medical Robotics and Bionics*, vol. 3, no. 3, pp. 773–782, 2021.

[143] G. Boccia *et al.*, “Decrease of muscle fiber conduction velocity correlates with strength loss after an endurance run,” *Physiol. Meas.*, vol. 38, no. 2, pp. 233–240, Feb. 2017.

[144] D. A. Jones, “Changes in the force-velocity relationship of fatigued muscle: implications for power production and possible causes,” *J. Physiol.*, vol. 588, no. Pt 16, pp. 2977–2986, Aug. 2010.

[145] C. N. Cooper, N. C. Dabbs, J. Davis, and N. M. Sauls, “Effects of Lower-Body Muscular Fatigue on Vertical Jump and Balance Performance,” *J. Strength Cond. Res.*, vol. 34, no. 10, pp. 2903–2910, Oct. 2020.

[146] J. L. R. Jayalath, M. de Noronha, N. Weerakkody, and R. Bini, “Effects of fatigue on ankle biomechanics during jumps: A systematic review,” *J. Electromyogr. Kinesiol.*, vol. 42, pp. 81–91, Oct. 2018.

[147] J. L. Taylor and S. C. Gandevia, “A comparison of central aspects of fatigue in submaximal and maximal voluntary contractions,” *J. Appl. Physiol.*, vol. 104, no. 2, pp. 542–550, Feb. 2008.

[148] R. M. Enoka and J. Duchateau, “Muscle fatigue: what, why and how it influences muscle function,” *J. Physiol.*, vol. 586, no. 1, pp. 11–23, Jan. 2008.

[149] A. D. Kuo, “The relative roles of feedforward and feedback in the control of rhythmic movements,” *Motor Control*, vol. 6, no. 2, pp. 129–145, Apr. 2002.

[150] A. F. Azocar, L. M. Mooney, L. J. Hargrove, and E. J. Rouse, “Design and Characterization of an Open-Source Robotic Leg Prosthesis,” in *2018 7th IEEE International Conference on Biomedical Robotics and Biomechatronics (Biorob)*, Aug. 2018, pp. 111–118.

[151] A. Phinyomark, S. Thongpanja, H. Hu, P. Phukpattaranont, and C. Limsakul, “The usefulness of mean and median frequencies in electromyography analysis,” *Computational intelligence in electromyography analysis-A perspective on current applications and future challenges*, vol. 81, p. 67, 2012.

[152] S. Nagata, A. B. Arsenault, D. Gagnon, G. Smyth, and P. A. Mathieu, “EMG power spectrum as a measure of muscular fatigue at different levels of contraction,” *Med. Biol. Eng. Comput.*, vol. 28, no. 4, pp. 374–378, Jul. 1990.

[153] J. R. Potvin and L. R. Bent, “A validation of techniques using surface EMG signals from dynamic contractions to quantify muscle fatigue during repetitive tasks,” *J. Electromyogr. Kinesiol.*, vol. 7, no. 2, pp. 131–139, Jun. 1997.

[154] F. B. Stulen and C. J. DeLuca, “Frequency parameters of the myoelectric signal as a measure of muscle conduction velocity,” *IEEE Trans. Biomed. Eng.*, vol. 28, no. 7, pp. 515–523, Jul. 1981.

[155] S. E. Salomoni and T. Graven-Nielsen, “Muscle fatigue increases the amplitude of fluctuations of tangential forces during isometric contractions,” *Hum. Mov. Sci.*, vol. 31, no. 4, pp. 758–771, Aug. 2012.

[156] N. B. Singh, A. Arampatzis, G. Duda, M. O. Heller, and W. R. Taylor, “Effect of fatigue on force fluctuations in knee extensors in young adults,” *Philosophical Transactions of the Royal Society A: Mathematical, Physical and Engineering Sciences*, vol. 368, no. 1920, pp. 2783–2798, Jun. 2010.

[157] G. Boccia *et al.*, “Neuromuscular Fatigue Does Not Impair the Rate of Force Development in Ballistic Contractions of Submaximal Amplitudes,” *Front. Physiol.*, vol. 9, p. 1503, Oct. 2018.

[158] B. L. Tracy and R. M. Enoka, “Older adults are less steady during submaximal isometric contractions with the knee extensor muscles,” *J. Appl. Physiol.*, vol. 92, no. 3, pp. 1004–1012, Mar. 2002.

[159] B. C. M. Smits-Engelsman, Y. Westenberg, and J. Duysens, “Children with developmental coordination disorder are equally able to generate force but show more variability than typically developing children,” *Hum. Mov. Sci.*, vol. 27, no. 2, pp. 296–309, Apr. 2008.

[160] M. A. Oliveira, A. M. Rodrigues, R. M. S. Caballero, R. D. S. Petersen, and J. K. Shim, “Strength and isometric torque control in individuals with Parkinson’s disease,” *Experimental Brain Research*, vol. 185, no. 3. pp. 533–533, 2008. doi: 10.1007/s00221-008-1290-3.

[161] R. M. Enoka and J. Duchateau, “Translating Fatigue to Human Performance,” *Med. Sci. Sports Exerc.*, vol. 48, no. 11, pp. 2228–2238, Nov. 2016.

[162] F. Skala and E. Zemková, “Effects of Acute Fatigue on Cognitive Performance in Team Sport Players: Does It Change the Way They Perform? A Scoping Review,” *NATO Adv. Sci. Inst. Ser. E Appl. Sci.*, vol. 12, no. 3, p. 1736, Feb. 2022.

[163] F. Ranieri and V. Di Lazzaro, “The role of motor neuron drive in muscle fatigue,” *Neuromuscul. Disord.*, vol. 22 Suppl 3, pp. S157–61, Dec. 2012.

[164] B. Bigland-Ritchie, “Muscle fatigue and the influence of changing neural drive,” *Clin. Chest Med.*, vol. 5, no. 1, pp. 21–34, Mar. 1984.

[165] E. Azim and K. Seki, “Gain control in the sensorimotor system,” *Curr Opin Physiol*, vol. 8, pp. 177–187, Apr. 2019.

[166] Franklin, *Feedback Control of Dynamic Systems*. Pearson Education, 2008.

[167] R. Sigrist, G. Rauter, R. Riener, and P. Wolf, “Augmented visual, auditory, haptic, and multimodal feedback in motor learning: a review,” *Psychon. Bull. Rev.*, vol. 20, no. 1, pp. 21–53, Feb. 2013.

[168] P. Aagaard, “Training-induced changes in neural function,” *Exerc. Sport Sci. Rev.*, vol. 31, no. 2, pp. 61–67, Apr. 2003.

[169] M. S. Ashtiani, A. Aghamaleki Sarvestani, and A. Badri-Spröwitz, “Hybrid Parallel Compliance Allows Robots to Operate With Sensorimotor Delays and Low Control Frequencies,” *Front Robot AI*, vol. 8, p. 645748, Jun. 2021.

[170] B. Katz, J. D. Carlo, and S. Kim, “Mini Cheetah: A Platform for Pushing the Limits of Dynamic Quadruped Control,” in *2019 International Conference on Robotics and Automation (ICRA)*, May 2019, pp. 6295–6301.

[171] R. D. Johnston, T. J. Gabbett, and D. G. Jenkins, “Influence of an intensified competition on fatigue and match performance in junior rugby league players,” *Journal of Science and Medicine in Sport*, vol. 16, no. 5. pp. 460–465, 2013. doi: 10.1016/j.jsams.2012.10.009.

[172] S.-H. Chen and L.-S. Chou, “Gait balance control after fatigue: Effects of age and cognitive demand,” *Gait Posture*, vol. 95, pp. 129–134, Jun. 2022.

[173] P. C. R. D. Santos, F. A. Barbieri, I. Zijdewind, L. T. B. Gobbi, C. Lamoth, and T. Hortobágyi, “Effects of experimentally induced fatigue on healthy older adults’ gait: A systematic review,” *PLoS One*, vol. 14, no. 12, p. e0226939, Dec. 2019.

[174] National Collegiate Athletic Association, “Men’s soccer Injuries NCAA.” [Online]. Available: https://www.datalyscenter.org/sites/datalyscenter.org/files/NCAA_M_Soccer_Injuries_HiRes.pdf

[175] N. P. Linthorne, “Analysis of standing vertical jumps using a force platform,” *Am. J. Phys.*, vol. 69, no. 11, pp. 1198–1204, Nov. 2001.

[176] D. A. Winter, “Biomechanics and Motor Control of Human Movement.” 2009. doi: 10.1002/9780470549148.

[177] E. W. Hawkes *et al.*, “Engineered jumpers overcome biological limits via work multiplication,” *Nature*, vol. 604, no. 7907, pp. 657–661, Apr. 2022.

[178] J. P. Van Zandwijk, M. F. Bobbert, M. Munneke, and P. Pas, “Control of maximal and submaximal vertical jumps:,” *Med. Sci. Sports Exercise*, vol. 32, no. 2, p. 477, Feb. 2000.

[179] S. Faraji, A. R. Wu, and A. J. Ijspeert, “A simple model of mechanical effects to estimate metabolic cost of human walking,” *Sci. Rep.*, vol. 8, no. 1, p. 10998, Jul. 2018.

[180] A. D. Kuo, “A simple model of bipedal walking predicts the preferred speed-step length relationship,” *J. Biomech. Eng.*, vol. 123, no. 3, pp. 264–269, Jun. 2001.

[181] M. Srinivasan and A. Ruina, “Computer optimization of a minimal biped model discovers walking and running,” *Nature*, vol. 439, no. 7072, pp. 72–75, Jan. 2006.

[182] A. Seyfarth, R. Blickhan, and J. L. Van Leeuwen, “Optimum take-off techniques and muscle design for long jump,” *J. Exp. Biol.*, vol. 203, no. Pt 4, pp. 741–750, Feb. 2000.

[183] Y. Blache and K. Monteil, “Effect of arm swing on effective energy during vertical jumping: Experimental and simulation study: Influence of arm swing during vertical jumping,” *Scand. J. Med. Sci. Sports*, vol. 23, no. 2, pp. e121–e129, Mar. 2013.

[184] K. A. Inkol, C. Brown, W. McNally, C. Jansen, and J. McPhee, “Muscle torque generators in multibody dynamic simulations of optimal sports performance,” *Multibody Syst. Dyn.*, Jun. 2020, doi: 10.1007/s11044-020-09747-9.

[185] Z. J. Domire and J. H. Challis, “Maximum height and minimum time vertical jumping,” *J. Biomech.*, vol. 48, no. 11, pp. 2865–2870, Aug. 2015.

[186] S. Weisberg, *Applied Linear Regression*. John Wiley & Sons, 2013.

[187] M. G. Pandy and F. E. Zajac, “Optimal muscular coordination strategies for jumping,” *J. Biomech.*, vol. 24, no. 1, pp. 1–10, 1991.

[188] M. F. Bobbert and G. J. van Ingen Schenau, “Coordination in vertical jumping,” *J. Biomech.*, vol. 21, no. 3, pp. 249–262, 1988.

[189] A. J. van Soest, A. L. Schwab, M. F. Bobbert, and G. J. van Ingen Schenau, “The influence of the biarticularity of the gastrocnemius muscle on vertical-jumping achievement,” *J. Biomech.*, vol. 26, no. 1, pp. 1–8, Jan. 1993.

[190] J. L. van Leeuwen and C. W. Spoor, “On the role of biarticular muscles in human jumping,” *Journal of biomechanics*, vol. 25, no. 2. pp. 207–209, Feb. 1992.

[191] M. F. Bobbert, L. J. Richard Casius, and D. A. Kistemaker, “Humans make near-optimal adjustments of control to initial body configuration in vertical squat jumping,” *Neuroscience*, vol. 237, pp. 232–242, May 2013.

[192] L. Wade, G. Lichtwark, and D. J. Farris, “Movement Strategies for Countermovement Jumping are Potentially Influenced by Elastic Energy Stored and Released from Tendons,” *Sci. Rep.*, vol. 8, no. 1, p. 2300, Feb. 2018.

[193] R. Mandic, O. M. Knezevic, D. M. Mirkov, and S. Jaric, “Control strategy of maximum vertical jumps: The preferred countermovement depth may not be fully optimized for jump height,” *J. Hum. Kinet.*, vol. 52, no. 1, pp. 85–94, Sep. 2016.

[194] A. Albright and J. Vaughan, “Learning Energy Efficient Jumping Strategies for Flexible-Legged Systems,” *IFAC-PapersOnLine*, vol. 54, no. 20, pp. 443–448, Jan. 2021.

[195] T. Finni, P. V. Komi, and V. Lepola, “In vivo human triceps surae and quadriceps femoris muscle function in a squat jump and counter movement jump,” *Eur. J. Appl. Physiol.*, vol. 83, no. 4–5, pp. 416–426, Nov. 2000.

[196] K. Kubo, Y. Kawakami, and T. Fukunaga, “Influence of elastic properties of tendon structures on jump performance in humans,” *J. Appl. Physiol.*, vol. 87, no. 6, pp. 2090–2096, Dec. 1999.

[197] J. M. Gabriel, “The effect of animal design on jumping performance,” *J. Zool.* , vol. 204, no. 4, pp. 533–539, Dec. 1984.

[198] S. J. Longo *et al.*, “Beyond power amplification: latch-mediated spring actuation is an emerging framework for the study of diverse elastic systems,” *J. Exp. Biol.*, vol. 222, no. Pt 15, Aug. 2019, doi: 10.1242/jeb.197889.

[199] P. Cormie, J. M. McBride, and G. O. McCaulley, “Power-time, force-time, and velocity-time curve analysis of the countermovement jump: impact of training,” *J. Strength Cond. Res.*, vol. 23, no. 1, pp. 177–186, Jan. 2009.

[200] P. Kudzia, J. M. Wakeling, S. N. Robinovitch, and J. Maxwell Donelan, “Neuromuscular fatigue reduces responsiveness when controlling leg external forces,” *bioRxiv*, p. 2023.05.24.541485, May 25, 2023. doi: 10.1101/2023.05.24.541485.

[201] B. M. Nigg, “Biomechanics, load analysis and sports injuries in the lower extremities,” *Sports Med.*, vol. 2, no. 5, pp. 367–379, Sep-Oct 1985.

[202] F. J. Wouda *et al.*, “Estimation of Vertical Ground Reaction Forces and Sagittal Knee Kinematics During Running Using Three Inertial Sensors,” *Front. Physiol.*, vol. 9, p. 218, Mar. 2018.

[203] E. Dorschky, M. Nitschke, C. F. Martindale, A. J. van den Bogert, A. D. Koelewijn, and B. M. Eskofier, “CNN-Based Estimation of Sagittal Plane Walking and Running Biomechanics From Measured and Simulated Inertial Sensor Data,” *Front Bioeng Biotechnol*, vol. 8, p. 604, Jun. 2020.

[204] K. J.-H. Ngoh, D. Gouwanda, A. A. Gopalai, and Y. Z. Chong, “Estimation of vertical ground reaction force during running using neural network model and uniaxial accelerometer,” *J. Biomech.*, vol. 76, pp. 269–273, Jul. 2018.

[205] E. C. Honert, F. Hoitz, S. Blades, S. R. Nigg, and B. M. Nigg, “Estimating Running Ground Reaction Forces from Plantar Pressure during Graded Running,” *Sensors* , vol. 22, no. 9, p. 3338, Apr. 2022.

[206] S. R. Donahue and M. E. Hahn, “Estimation of ground reaction force waveforms during fixed pace running outside the laboratory,” *Front Sports Act Living*, vol. 5, p. 974186, Feb. 2023.

[207] E. Dorschky *et al.*, “Comparing sparse inertial sensor setups for sagittal-plane walking and running reconstructions,” *bioRxiv*, p. 2023.05.25.542228, May 25, 2023. doi: 10.1101/2023.05.25.542228.

[208] J. Heikenfeld *et al.*, “Wearable sensors: modalities, challenges, and prospects,” *Lab Chip*, vol. 18, no. 2, pp. 217–248, Jan. 2018.

[209] H. L. Cornman, J. Stenum, and R. T. Roemmich, “Video-based quantification of human movement frequency using pose estimation: A pilot study,” *PLoS One*, vol. 16, no. 12, p. e0261450, Dec. 2021.

[210] V. Kosourikhina, D. Kavanagh, M. J. Richardson, and D. M. Kaplan, “Validation of deep learning-based markerless 3D pose estimation,” *PLoS One*, vol. 17, no. 10, p. e0276258, Oct. 2022.

[211] L. Needham *et al.*, “The accuracy of several pose estimation methods for 3D joint centre localisation,” *Sci. Rep.*, vol. 11, no. 1, p. 20673, Oct. 2021.

[212] M. Goldacre *et al.*, “Predicting ground reaction forces from 2d video: Bridging the lab to field nexus.” https://commons.nmu.edu/cgi/viewcontent.cgi?article=2281&context=isbs (accessed Apr. 25, 2022).

[213] N. Louis, J. J. Corso, T. N. Templin, T. D. Eliason, and D. P. Nicolella, “Learning to Estimate External Forces of Human Motion in Video,” in *Proceedings of the 30th ACM International Conference on Multimedia*, in MM ’22. New York, NY, USA: Association for Computing Machinery, Oct. 2022, pp. 3540–3548.

[214] “Masking layer.” https://keras.io/api/layers/core_layers/masking/ (accessed Jun. 25, 2023).

[215] “Introduction to the keras tuner,” *TensorFlow*. https://www.tensorflow.org/tutorials/keras/keras_tuner (accessed Jun. 29, 2023).

[216] B. Lejdel, E. Clementini, and L. Alarabi, *Artificial Intelligence and Its Applications: Proceeding of the 2nd International Conference on Artificial Intelligence and Its Applications (2021)*. Springer Nature, 2022.

[217] T. M. Khan, M. Alhussein, K. Aurangzeb, M. Arsalan, S. S. Naqvi, and S. J. Nawaz, “Residual Connection-Based Encoder Decoder Network (RCED-Net) for Retinal Vessel Segmentation,” *IEEE Access*, vol. 8, pp. 131257–131272, 2020.

[218] E. Halilaj, A. Rajagopal, M. Fiterau, J. L. Hicks, T. J. Hastie, and S. L. Delp, “Machine learning in human movement biomechanics: Best practices, common pitfalls, and new opportunities,” *J. Biomech.*, vol. 81, pp. 1–11, Nov. 2018.

[219] E. Chaibub Neto *et al.*, “Detecting the impact of subject characteristics on machine learning-based diagnostic applications,” *NPJ Digit Med*, vol. 2, p. 99, Oct. 2019.

[220] N. Nakano *et al.*, “Evaluation of 3D Markerless Motion Capture Accuracy Using OpenPose With Multiple Video Cameras,” *Front Sports Act Living*, vol. 2, p. 50, May 2020.

[221] M. F. Bobbert, K. G. Gerritsen, M. C. Litjens, and A. J. Van Soest, “Why is countermovement jump height greater than squat jump height?,” *Med. Sci. Sports Exerc.*, vol. 28, no. 11, pp. 1402–1412, Nov. 1996.

[222] H. Jeong and S. Park, “Estimation of the ground reaction forces from a single video camera based on the spring-like center of mass dynamics of human walking,” *J. Biomech.*, vol. 113, p. 110074, Dec. 2020.

[223] M. Mundt, Z. Born, M. Goldacre, and J. Alderson, “Estimating Ground Reaction Forces from Two-Dimensional Pose Data: A Biomechanics-Based Comparison of AlphaPose, BlazePose, and OpenPose,” *Sensors* , vol. 23, no. 1, Dec. 2022, doi: 10.3390/s23010078.

[224] B. Pueo, A. Penichet-Tomas, and J. M. Jimenez-Olmedo, “Validity, reliability and usefulness of smartphone and kinovea motion analysis software for direct measurement of vertical jump height,” *Physiol. Behav.*, vol. 227, p. 113144, Dec. 2020.

[225] G. Mascia, B. De Lazzari, and V. Camomilla, “Machine learning aided jump height estimate democratization through smartphone measures,” *Front Sports Act Living*, vol. 5, p. 1112739, Feb. 2023.

[226] S. Marković, M. Dopsaj, S. Tomažič, A. Kos, A. Nedeljković, and A. Umek, “Can IMU Provide an Accurate Vertical Jump Height Estimate?,” *NATO Adv. Sci. Inst. Ser. E Appl. Sci.*, vol. 11, no. 24, p. 12025, Dec. 2021.

[227] T. B. Aderinola, H. Younesian, D. Whelan, B. Caulfield, and G. Ifrim, “Quantifying Jump Height Using Markerless Motion Capture with a Single Smartphone,” *IEEE Open J Eng Med Biol*, vol. 4, pp. 109–115, May 2023.

[228] B. Pueo, P. Lipinska, J. M. Jiménez-Olmedo, P. Zmijewski, and W. G. Hopkins, “Accuracy of Jump-Mat Systems for Measuring Jump Height,” *Int. J. Sports Physiol. Perform.*, vol. 12, no. 7, pp. 959–963, Aug. 2017.

[229] B. Skof and V. Strojnik, “Neuromuscular fatigue and recovery dynamics following prolonged continuous run at anaerobic threshold,” *Br. J. Sports Med.*, vol. 40, no. 3, pp. 219–22; discussion 219–22, Mar. 2006.

[230] F. Ashtiani, V. S. M. Sreedhara, A. Vahidi, R. Hutchison, and G. Mocko, “Experimental Modeling of Cyclists Fatigue and Recovery Dynamics Enabling Optimal Pacing in A Time Trial,” in *2019 American Control Conference (ACC)*, Jul. 2019, pp. 5083–5088.

[231] S.-H. Yeo, J. Verheul, W. Herzog, and S. Sueda, “Numerical instability of Hill-type muscle models,” *J. R. Soc. Interface*, vol. 20, no. 199, p. 20220430, Feb. 2023.

[232] N. Hogan and D. Sternad, “Dynamic primitives in the control of locomotion,” *Front. Comput. Neurosci.*, vol. 7, p. 71, Jun. 2013.

[233] J. Tan *et al.*, “Sim-to-Real: Learning Agile Locomotion For Quadruped Robots,” *arXiv [cs.RO]*, Apr. 27, 2018. [Online]. Available: http://arxiv.org/abs/1804.10332

[234] E. Ackerman, “Boston Dynamics’ SpotMini Is All Electric, Agile, and Has a Capable Face-Arm,” *IEEE Spectrum*, 2016.

[235] C. Semini, N. G. Tsagarakis, E. Guglielmino, M. Focchi, F. Cannella, and D. G. Caldwell, “Design of HyQ – a hydraulically and electrically actuated quadruped robot,” *Proc Inst Mech Eng Part I J Syst Control Eng*, vol. 225, no. 6, pp. 831–849, Sep. 2011.

[236] M. Hutter, C. D. Remy, M. A. Hoepflinger, and R. Siegwart, *HIGH COMPLIANT SERIES ELASTIC ACTUATION FOR THE ROBOTIC LEG SCARL ETH*. WORLD SCIENTIFIC, 2011.

[237] C. Hubicki *et al.*, “ATRIAS: Design and validation of a tether-free 3D-capable spring-mass bipedal robot,” *Int. J. Rob. Res.*, vol. 35, no. 12, pp. 1497–1521, Oct. 2016.

[238] P.-B. Wieber, R. Tedrake, and S. Kuindersma, “Modeling and Control of Legged Robots,” in *Springer Handbook of Robotics*, B. Siciliano and O. Khatib, Eds., Cham: Springer International Publishing, 2016, pp. 1203–1234.

[239] R. B. Johnston 3rd, M. E. Howard, P. W. Cawley, and G. M. Losse, “Effect of lower extremity muscular fatigue on motor control performance,” *Med. Sci. Sports Exerc.*, vol. 30, no. 12, pp. 1703–1707, Dec. 1998.

[240] M. Chiquier and C. Vondrick, “Muscles in Action,” *arXiv [cs.CV]*, Dec. 05, 2022. [Online]. Available: http://arxiv.org/abs/2212.02978

Appendix

Table 2-A: The determined modelling predictions using a second-order system

Force-magnitude						
Step (x bodyweight)	**Rise time (ms)**	**Bandwidth(Hz)**	**SSE (%)**	**SSV (%)**	**Settling Time (ms)**	**Overshoot (%)**
x0.25	179 ± 65	2.0 ± 0.5	4.8 ± 4.4	0.0 ± 0.0	1941.1 ± 352.7	21.3 ± 8.5
x0.45	190 ± 53	1.9 ± 0.4	2.4 ± 2.4	0.0 ± 0.0	1693.3 ± 192.5	14.3 ± 7.1
x0.85	210 ± 72	1.8 ± 0.5	1.8 ± 1.2	0.0 ± 0.0	1588.6 ± 88.9	8.7 ± 4.3
x1.25	233 ± 73	1.6 ± 0.4	2.2 ± 2.5	0.0 ± 0.0	1555.8 ± 210.1	5.6 ± 2.5
rAnova (p-value)	1.61e-05	1.18e-05	0.05		8.02e-05	5.37e-09
Force-position						
Step (cm)	**Anterior (+) / Posterior (-)**					
-1.0	186 ± 31	1.9 ± 0.3	8.1 ± 8.4	0.0 ± 0.0	2399.0 ± 671.7	25.8 ± 7.3
-2.5	216 ± 55	1.7 ± 0.4	4.5 ± 2.4	0.0 ± 0.0	1754.1 ± 315.4	14.0 ± 6.4
2.5	194 ± 35	1.8 ± 0.3	5.0 ± 2.7	0.0 ± 0.0	1857.0 ± 308.5	17.5 ± 6.4
4.0	217 ± 38	1.6 ± 0.3	3.6 ± 2.4	0.0 ± 0.0	1800.3 ± 389.3	13.9 ± 7.0
rAnova (p-value)	6.67e-03	2.93e-03	0.04		7.54e-03	1.57e-05
Step (cm)	**Medial (+) / Lateral (-)**					
0.5	194 ± 38	1.8 ± 0.3	7.8 ± 7.6	0.0 ± 0.0	2067.1 ± 502.5	20.4 ± 6.1
-0.5	183 ± 34	1.9 ± 0.3	7.4 ± 6.4	0.0 ± 0.0	1851.5 ± 254.5	20.7 ± 6.8
-1	207 ± 32	1.7 ± 0.2	3.6 ± 2.3	0.0 ± 0.0	1573.6 ± 202.5	10.4 ± 4.6
1	222 ± 40	1.6 ± 0.3	4.5 ± 4.0	0.0 ± 0.0	1780.1 ± 490.0	12.5 ± 9.0
rAnova (p-value)	0.027139	0.031862	0.077315		4.73e-04	9.35e-07